PROCEEDINGS OF THE 24TH INTERNATIONAL APPLIED GEOCHEMISTRY SYMPOSIUM

FREDERICTON, NEW BRUNSWICK, CANADA

JUNE 1ST-4TH, 2009

EDITED BY

DAVID R. LENTZ, KATHLEEN G. THORNE, & KRISTY-LEE BEAL

VOLUME I

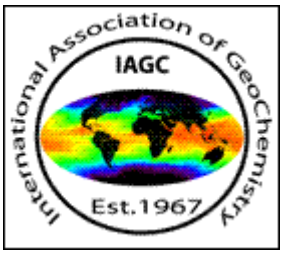

ISBN 978-1-55131-136-4

PROCEEDINGS OF THE 24TH INTERNATIONAL APPLIED GEOCHEMISTRY SYMPOSIUM

FREDERICTON, NEW BRUNSWICK
CANADA
JUNE 1ST-4TH, 2009

EDITED BY

DAVID R. LENTZ
KATHLEEN G. THORNE
KRISTY-LEE BEAL

VOLUME I

TECHNICAL EDITORS

(Listed in alphabetical order)

Mark Arundell
U. Aswathanarayana
Roger Beckie
Chris Benn
Robert Bowell
Charles Butt
Bill Coker
Hugh deSouza
Sara Fortner
David Gladwell
Wayne Goodfellow
Eric Grunsky
William Gunter
Gwendy Hall
Jacob Hanley
Russell Harmon
David Heberlein
Brian Hitchon
Andrew Kerr
Dan Kontak
Kurt Kyser
David Lentz
Ray Lett
Matthew Leybourne
Steven McCutcheon
Beth McClenaghan
Nancy McMillan
Paul Morris
Lee Ann Munk
Dogan Paktunc
Roger Paulen
Ernie Perkins
David Quirt
Andy Rencz
David Smith
Cliff Stanley
Gerry Stanley
Nick Susak
Bruce Taylor
Ed Van Hees
James Walker
Lawrence Winter

RECENT DEVELOPMENTS IN LITHOGEOCHEMICAL METHODS WITH EXPLORATION APPLICATIONS

EDITED BY:

JAMES WALKER
CLIFF STANLEY
NICK SUSAK

Lithogeochemistry of central Victorian orogenic gold deposits, Australia

Dennis Arne[1], Emily House[2], & Vladimir Lisitsin[2]
[1]*ioGlobal, 469 Glen Huntley Road, Elsternwick, VIC 3185 AUSTRALIA (e-mail: dennis.arne@ioGlobal.net)*
[2]*Geoscience Victoria, Department of Primary Industries, GPO Box 4440, Melbourne,VIC 3001 AUSTRALIA*

ABSTRACT: Whole-rock geochemical data from almost 900 fresh drill core and underground samples taken from seven central Victorian orogenic gold deposits confirm the presence of distinct alteration haloes around the deposits. Using carbonate C analyses, thin section petrography, carbonate staining methods and TIR-NIR-SWIR hyperspectral imaging, primary ferroan carbonate alteration can be traced for up to several hundred metres away from gold mineralisation in meta-sedimentary rocks that are unaffected by post-mineralization metamorphism. A narrower and less distinct phyllic alteration zone can be identified using geochemical molar ratios in fresh samples or SWIR analysis. This zone extends from 70 m to 100 m beyond gold mineralisation. The phyllic halo generally overlaps a primary sulfidic alteration halo characterised by disseminated pyrite in areas distal to mineralized structures and arsenopyrite in areas proximal to mineralized structures. The extent of the sulfidic halo can be traced for up to 70 m – 90 m away from gold mineralization using low-level analysis of pathfinder elements, such as S, Au, As and Sb. A preliminary assessment of a further 650 whole-rock analyses of weathered rock suggests that secondary dispersion of chalcophile indicator elements exceeds that defined by primary dispersion haloes.

KEYWORDS: *lithogeochemistry, orogenic gold, central Victoria*

INTRODUCTION

A major study of primary and secondary geochemical dispersion around seven central Victorian gold deposits has been conducted by Geoscience Victoria as part of the 3-year, $9 million Developing Gold Undercover initiative of the Victorian government. The major purpose of this work is to document the style and extent of wallrock alteration associated with central Victorian gold deposits to aide mineral explorers drilling through Cenozoic sedimentary cover in the Gold Undercover initiative area (Fig. 1). The study has been broken into two components: primary alteration and secondary dispersion effects. This paper mainly summarise the results of the investigation into primary alteration haloes at Bendigo, Ballarat, Castlemaine, Costerfield, Maldon, Fosterville and Wildwood. Preliminary results from a study of secondary dispersion using outcrop and soil samples will also be presented, along with a summary of hyperspectral analysis of representative diamond drill core.

GEOLOGICAL SETTING

The geochemical study covers selected gold deposits and occurrences in the western Lachlan Fold Belt. Most of the gold deposits studied in this report lie within the Bendigo Zone of the western Lachlan Fold Belt (Bendigo, Ballarat, Castlemaine, Maldon and Fosterville). A recent assessment of undiscovered gold endowment of the Bendigo and Stawell structural zones is provided by Lisitsin *et al.* (2007, 2009). Overviews of the regional geology, including summaries on gold metallogeny, are provided in VandenBerg *et al.* (2000) and Birch (2003). A recent detailed description of gold deposit models relevant to this study is provided by Moore (2007).

GEOCHEMICAL INVESTIGATIONS

Methodology

Nearly 900 fresh diamond drill core samples were collected from multiple drill holes along two or more cross sections through each of the deposits under investigation. Field determinations for ferroan carbonate were made on all fresh

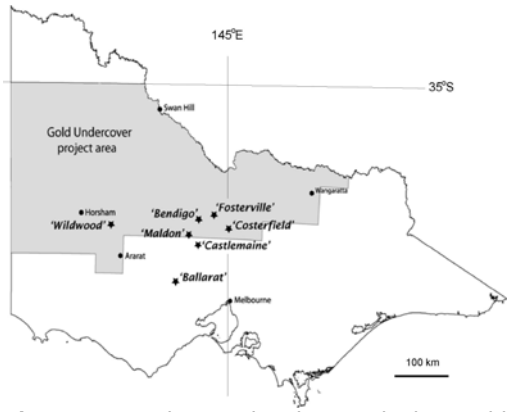

Fig. 1. Geoscience Victoria Developing Gold Undercover initiative area (shaded) showing the locations of the gold deposits discussed in this report.

samples. An additional 650 outcrop, shallow diamond drill core, aircore, soil auger (C-horizon only) and open pit samples were also collected from around the deposits, with the exception of Maldon. All samples were submitted for analysis of Al, Ca, Fe, K, Mg, Mn, Na, P, S, Zn, Au, Ag, As, Bi, Co, Cu, Mo, Ni, Pb, Rb, Sb, Se, Sr, Te (fresh samples only), Ba, Ti, W, Zr and, in a limited number of fresh samples, carbonate C, Hg, Pd & Pt.

Analytical and quality control details are summarised in Arne *et al* (2008). Gold was determined by fire assay, and major elements by ICP-OES following a four-acid digestion, with the exception of fresh drill core samples from Wildwood, which were analysed by lithium borate fusion and XRF. Trace elements were determined by ICP-MS. Refractory elements (W, Zr, Ba and Ti) were analysed by pressed powder XRF.

Jaw crusher splits were returned for hyperspectral analysis and were placed into plastic chip trays and sent to the CSIRO Hylogging Group in North Ryde, New South Wales, for analysis using HyChips™. Representative drill core from each of the study areas was scanned in its entirety using a Hylogger™. Diamond drill core from Ballarat was also scanned using thermal infrared radiation (TIR) in order to assess the potential for mapping ferroan carbonate alteration patterns. The initial interpretation of the hyperspectral results was undertaken by AusSpec International.

RESULTS

The results of this investigation generally support previous descriptions of primary wallrock alteration surrounding central Victorian gold deposits but, in addition, provide estimates of the lateral extent of alteration as well as practical geochemical threshold values. With the exception of deposits within the Stawell corridor that are associated with basaltic structural domes (i.e., Wildwood), primary geochemical dispersion around sediment-hosted central Victorian gold deposits can be characterized in terms of three overlapping alteration haloes:

(1) A sulfidic halo is characterized mostly by elevated S, Au, As and Sb. It extends further than suggested by previous alteration studies, and is defined by the development of disseminated hydrothermal pyrite and, to a lesser extent, arsenopyrite. Gold deposits of the Costerfield stibnite domain (i.e., Fosterville and Costerfield) can be differentiated from Au–As orogenic deposits by a greater primary dispersion of anomalous As and higher threshold values for Sb, as well as by the presence of slightly elevated concentrations of Hg (>0.01 ppm). Other chalcophile elements at variably elevated levels within the sulfidic alteration halo include Mo, Se, Bi, Pb and Cu.

(2) A poorly defined zone of phyllic alteration, which is characterized by a drop in the albite saturation index and an increase in the muscovite saturation index (when normalized to the Al content of the sample), either coincides with or lies within the sulfidic alteration halo. Absolute changes in K and Na concentrations in meta-sedimentary host rocks are dominated by lithological changes, and so the use of molar ratios is required to adequately define this zone by lithogeochemistry. This zone is not recognized in contact-metamorphosed deposits such as Maldon.

(3) Ferroan carbonates define the largest alteration halo associated with orogenic gold mineralization in central Victoria. They are most abundant adjacent to

mineralized structures, but can be detected up to 200 m away from mineralised structures, where the ferroan carbonate co-exists with regional metamorphic chlorite. The easiest method of detecting this halo in fresh core is by the use of carbonate staining techniques. Ferroan carbonate alteration can also be detected using carbonate C analyses, allowing the halo to be defined using the carbonate saturation index or Pearce Element Ratios, as well as through the use of thin-section petrography. Carbonate alteration appears to be accompanied by enrichments in Mn and Sr, and, at some deposits, Ca. The carbonate zone is also absent at contact-metamorphosed deposits.

The interpretation of lithogeochemical data from basaltic structural domes is complicated by lithological changes associated with the transition from basalt to overlying siliciclastic rocks, as well as by the polydeformed nature of the host sequence. Ferroan carbonate alteration is well developed, and low-level Au enrichment extends for a considerable distance away from zones of economic interest. Arsenic and Sb/Al anomalies are restricted to within approximately 10 m of mineralized zones. Sericite alteration is indicated by Na depletion and K enrichment in basalt within 20 to 40 m of mineralized zones. A number of other elements, including Mn, P, S, Zn, Mo, Cu, Se and Ba, are variably enriched within the rocks hosting Au mineralization, but it is not clear whether elevated concentrations of these elements are a product of syn-sedimentary exhalative activity or result from later hydrothermal alteration.

A preliminary interpretation of both new and historical surface rock and soil geochemical data suggests that Au, As and Sb are the most effective pathfinder elements in the supergene environment and that extensive secondary dispersion haloes can be recognized. Base metals, which are only rarely enriched in wallrocks within primary alteration haloes (Arne *et al.* 2008), correlate with Fe and Mn in weathered material due to scavenging.

Hyperspectral data

The phyllic alteration zone coincides with a subtle but consistent shift in the dominant AlOH peak in the short-wave infrared spectrum (~2210 nm) to slightly lower wavelengths, consistent with an inner white mica–ferroan carbonate mineral assemblage. A preliminary analysis of hyperspectral data over the visible to near infrared range suggests that ferroan carbonates may be detected but not reliably quantified. However, TIR data allow calcite and ferroan carbonate to be distinguished, and may also detect increasing Fe content in ferroan dolomite as mineralized structures are approached.

CONCLUSIONS

Recognition of the alteration haloes surrounding orogenic gold deposits in central Victoria provides a vector toward mineralized structures. The largest halo is defined by minor amounts of ferroan carbonate co-existing with regional metamorphic chlorite. Both the amount of ferroan carbonate and its iron content increases with proximity to the mineralized structures, whereas chlorite decreases to create a bleached appearance in fresh diamond drill core. Levels of Mn and Sr become elevated approaching gold mineralization while low-level elevated concentrations of S, Au, As and Sb accompany ferroan carbonate alteration. Levels of Au, As and Sb increase dramatically close to mineralization, and are accompanied by a drop in the albite saturation index and an increase in the ratio of the muscovite saturation index to Al. The presence of ferroan carbonate and changes in white mica composition can be determined by hyperspectral methods. Major deposits are associated with broad secondary dispersion haloes characterized by elevated Au, As and Sb.

ACKNOWLEDGEMENTS

It would not be possible to carry out a project of this scope without the assistance of the Victorian mineral exploration and mining industry. The following companies have provided access to diamond drill core material:

AGD Operations, Alliance Resources, Ballarat Goldfields (now Lihir Gold), Bendigo Mining, Castlemaine Goldfields, and Perseverance Corporation (now Northgate Minerals). This paper is published with the permission of the Director, GeoScience Victoria.

REFERENCES

ARNE, D.C., HOUSE, E., & LISITSIN, V. 2008. Lithogeochemical haloes surrounding central Victorian gold deposits: Part 1 – Primary alteration systems, *Geoscience Victoria Gold Undercover Report* **4**. Department of Primary Industries, Victoria

BIRCH, W.D. (ed.). 2003. *Geology of Victoria*, Geological Society of Australia (Victorian Division) Special Publication **23**, 842 p.

LISITSIN, V., OLSHINA, A., MOORE, D.H., & WILLMAN, C.E. 2007. Assessment of undiscovered mesozonal orogenic gold endowment under cover in the northern part of the Bendigo Zone. *Geoscience Victoria Gold Undercover Report* **2**, Department of Primary Industries, Victoria.

LISITSIN, V.A., OLSHINA, A., MOORE, D.H., & WILLMAN, C.E. 2009. Assessment of undiscovered mesozonal orogenic gold endowment under cover in the northern part of the Stawell Zone (Victoria). *Geoscience Victoria Gold Undercover Report* **13**. Department of Primary Industries, Victoria.

MOORE, D.H. 2007. Classifying gold deposits in central and western Victoria. *Geoscience Victoria Gold Undercover Report* **1**, Department of Primary Industries, Victoria.

VANDENBERG, A.H.M. *et al.* 2000. The Tasman Fold Belt System in Victoria – Geology and mineralisation of Proterozoic to Carboniferous rocks. *Geological Survey of Victoria Special Publication*. Department of Natural Resources and Environment.

Immobile Element Lithogeochemistry of felsic volcanic rocks hosting the Restigouche Volcanogenic Massive Sulfide Deposit, Bathurst Mining Camp, New Brunswick, Canada

Amanuel Bein[1] & David R. Lentz[1]

[1]Department of Geology, University of New Brunswick, 2 Bailey Drive, Fredericton, NB,, E3B 5A3 CANADA
(email: u3x30@unb.ca)

ABSTRACT: Altered volcanic rocks that host the Restigouche volcanogenic massive sulfide deposit in the Bathurst Mining Camp (BMC) consist of effusive and volcaniclastic rhyodacitic-dacitic volcanic rocks of tholeiitic–transitional, transitional, transitional-calc-alkaline magmatic nature. The rocks are characterized by evenly distributed volcanic facies and moderate to intense hydrothermal sericite, chlorite, carbonate, and silica alteration types. Lithogeochemical techniques such as binary plots of immobile elements and immobile element ratios are used to classify the various volcanic rocks into 7 groups and geological data from core logging confirmed that the geochemical classification is consistent and geologically meaningful. The study characterized geochemically unique units A, B, C, D, E, F, and G with distinctive Zr/TiO_2, Zr/Nb, Nb/Y, Zr/Th, TiO_2/Y, and TiO_2/Nb ratios. Temporal evolution of dominantly felsic volcanism from tholeiitic-transitional (unit B) to calc-alkaline (unit C) is demonstrated on the basis of Zr/Y ratio plot and chemostratigraphic relationships between the units.

KEYWORDS: *Restigouche, massive sulfide, immobile elements, binary plot, Zr/TiO_2*

INTRODUCTION

The Restigouche massive sulfide deposit is located in the northwestern part of the Bathurst Mining Camp (BMC), 60 km west of the city of Bathurst, northern New Brunswick. The property is currently controlled by Blue Note Mining and the company reports show that the deposit has an estimated reserve of 1.3 Mt grading 6.53% Zn, 5.05% Pb, and 99.6g/t Ag as of 2007 (Art Hamilton, Pers. Communication).

The present study was commenced in September 2008 in order to define the geological and lithogeochemical characteristics of the volcanic rocks hosting the Restigouche deposit. Geological mapping at 1:500 scale and drill core logging were performed at the Restigouche open pit mine site and the provincial drill core storage facility in Madran. Preliminary petrographic data from 8 diamond drill cores in combination with lithogeochemical data have been utilized to discern the volcano-stratigraphy characteristics and the effects of alteration overprinting due to hydrothermal activity associated with formation of the deposit.

GEOLOGICAL SETTING

Regional Geology

The Bathurst Super Group comprises tectonically juxtaposed and internally imbricated nappes of the Fournier, California Lake, Tetagouche, and Sheephouse Brook groups. Collectively these units are interpreted to represent remnants of the Middle Ordovician ensialic-ensimatic Tetagouche–Exploits back-arc basin which formed by rifting of the Arenig-Caradoc Popelogan arc.

In the BMC the majority of the massive sulfide deposits occur in Late-Middle Ordovician volcano-sedimentary units of the California Lake and Tetagouche groups that disconformably overlie Cambro-Ordovician sedimentary rocks of the Miramichi Group (van Staal *et al.* 2003). Mineralized horizons of the California Lake and Tetagouche groups are dominantly made up of consanguineous calc-alkaline felsic volcanic rocks that were produced by melting of old, possibly sialic, infracrustal

rocks (Whalen *et al.* 1998).

The California Lake Group consists dominantly of volcanic rocks that occur in three major nappes, which are referred as the Canoe Landing Lake, Spruce Lake, and Mount Brittain, each off these nappes contains rocks assigned to formations of the same name (Rogers *et al*. 2003). The Restigouche volcanogenic massive sulfide deposit is hosted in the Mount Brittain Formation (MB) that according to Rogers *et al*. (2003) predominantly composed of feldspar- and minor quartz-porphyritic dacitic to rhyolitic rocks that are divided into MB1 and MB2 suites on the basis of petrographic and geochemical differences. Gower (1996) reported that the Mount Brittain Formation dominantly consists of felsic feldspar-crystal, lithic tuffs that conformably (?) overlie sedimentary rocks of the Miramichi Group on a northern limb of a regional anticlinorium. The Restigouche deposit occurs at the contact between feldspar crystal-poor (footwall) and feldspar crystal-rich (hanging wall) sequences. The apparent absence of feldspars in the crystal-poor footwall rocks might be attributed to pervasive feldspar-destructive hydrothermal alteration of the footwall (Gower 1996).

Local Geology

The Restigouche deposit is hosted by a sequence of effusive massive felsic flows and related autoclastic felsic breccias, volcaniclastic material (tuffaceaous sedimentary) and feldspar-quartz-lithic lapilli tuffs. Intense chlorite alteration and accompanying silica alteration are well developed in footwall rocks immediately below massive sulfides, whereas pervasive sericitic and subordinate chloritic alteration, characterize the hanging wall. The strong silica alteration is characterized by relatively hard siliceous volcanic units with 5-30cm chert layers. Siderite occurring as rims on feldspar grains and on felsic lithic fragments, and siderite spots (<1-4mm in diameter) are common. The volcanic rocks that host the massive sulfide lens are strongly pyritiferous with disseminated <1-3mm anhedral to euhedral pyrite grains as well as veins and veinlets and 0.5-10 cm aggregated pyrite patches. Fine-grained (<1mm) disseminated sphalerite and galena in both the hanging wall and footwall rocks are spatially associated with the massive sulfide. Minor chalcopyrite occurs in pyrite-rich stockwork below the sulfide lens and is associated with intense silica-altered zones below the exhalative massive sulfides.

Lithogeochemical Analysis

Lithogeochemical study of the volcanic sequence at the Restigouche deposit is based on XRF analysis of 123 diamond drill core samples, of these 80 are from 4 cores that were sampled to assess unit-controlled chemo-stratigraphic variation. Binary plots and ratios of immobile elements are used to discriminate the altered volcanic units. On the basis of Zr/TiO_2, Zr/Nb, Zr/Y, Nb/Y, Zr/Th, TiO_2/Y, and TiO_2/Nb the rhyodacitic-dacitic with subordinate rhyolitic and minor andesitic–trachy-andesitic volcanic rocks that host the Restigouche deposit are classified into seven geochemically distinct units of A, B, C, D, E, F, and G (Table 1). Units of A, B, C, D, E, and F are in ascending stratigraphic order whereas the stratigraphic position of unit G is yet to be defined. The Restigouche massive sulfide horizon occurs between units A-D and A-E.

Based on TiO_2/Al_2O_3 vs. Zr/Al_2O_3 plot, 5 separate populations; A, B, C, D and E with average Zr/TiO_2 = 0.041, 0.083, 0.110, 0.048, and 0.042 are recognized (Fig. 1). This classification is supported by other immobile-element ratios used in this study (Table 1; Figs. 2 to 4).

On the basis of Nb/Al_2O_3 vs. Y/Al_2O_3 unit A has Nb/Y=0.3 (Fig. 2). On Zr/Al_2O_3 vs. Nb/Al_2O_3 plot characterization of another unit G with Zr/Nb ratio of 8.19 is made (Fig. 3). The discrete grouping of samples from unit F is observed on TiO_2/Al_2O_3 vs. Nb/Al_2O_3, TiO_2/Al_2O_3 vs. Y/Al_2O_3 and Zr/Al_2O_3 vs. Th/Al_2O_3 diagrams. The clustering of unit F on the TiO_2/Al_2O_3 vs. Zr/Al_2O_3 plot (Fig. 1) is interpreted to be a primary feature of this unit (Fig. 4).

On the Zr/Al_2O_3 vs. Y/Al_2O_3

Table 1. Selected immobile element ratios of volcanic units (A-G) recognized at the Restigouche deposit.

		A	B	C	D	E	F	G
Zr/TiO_2	*Average*	0.0414	0.0830	0.1100	0.0483	0.0423	0.0610	0.0715
	STD	0.0015	0.0070	0.0287	0.0032	0.0013	0.0022	0.0192
Zr/Nb	*Average*	14.23	14.77	19.01	15.07	14.22	15.13	8.19
	STD	0.77	1.43	2.31	0.79	0.66	1.12	0.78
Zr/Y	*Average*	12.11	4.45	7.98	6.80	8.72	4.48	4.98
	STD	26.76	0.73	1.36	2.86	3.89	0.88	1.19
Nb/Y	*Average*	0.912	0.300	0.420	0.457	0.613	0.299	0.616
	STD	2.152	0.031	0.052	0.216	0.273	0.066	0.167
Zr/Th	*Average*	9.64	10.56	32.30	13.03	12.84	10.60	7.94
	STD	2.43	2.53	8.45	4.09	4.45	2.07	1.91
TiO_2/Y	*Average*	299.56	54.29	82.16	140.11	206.46	73.58	87.77
	STD	679.78	11.39	41.14	52.34	93.02	14.64	77.25
TiO_2/Nb	*Average*	343.79	179.38	200.69	313.47	336.42	248.01	140.62
	STD	15.52	24.72	119.53	27.59	16.50	15.74	110.61

STD=standard deviation.

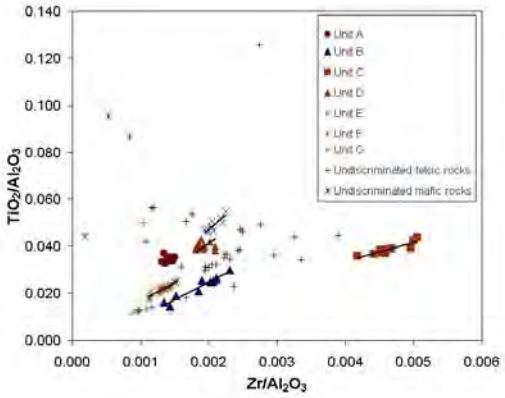

Fig. 1. TiO_2/Al_2O_3 vs. Zr/Al_2O_3 plot showing distinct clusters of the geochemically distinct volcanic units A, B, C, D, and E.

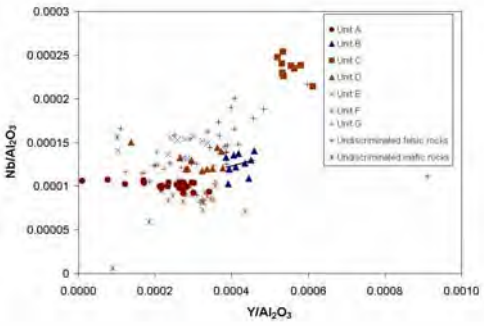

Fig. 2. Nb/Al_2O_3 vs. Y/Al_2O_3 plot marks that unit B represents a group of geochemically related volcanic rocks. Average Nb/Y ratio for units A, B, C, D, E, F and G is 0.912, 0.3, 0.42, 0.457, 0.613, 0.3, and 0.616, respectively.

discrimination diagram tholeiitic-transitional, transitional and transitional-calc-alkaline magmatic nature of the volcanic rocks is demonstrated, showing

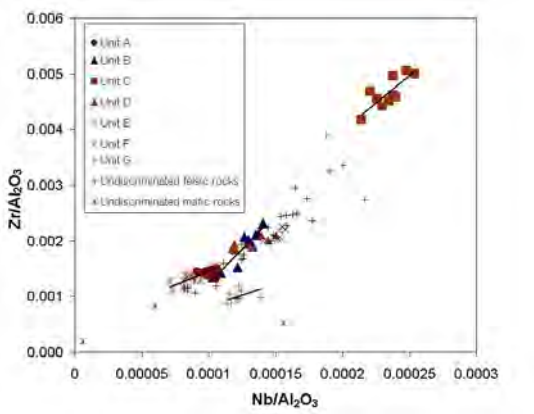

Fig. 3. Zr/Al_2O_3 vs. Nb/Al_2O_3 plot confirms that unit G is separate and geochemically unique. Trend lines for units B, C, F, and G are shown in figure. Zr/Nb ratios for units B, C, D, E, and G are 14.77, 19.01, 15.07, 14.22, 15.13, 14.23, and 8.19 respectively.

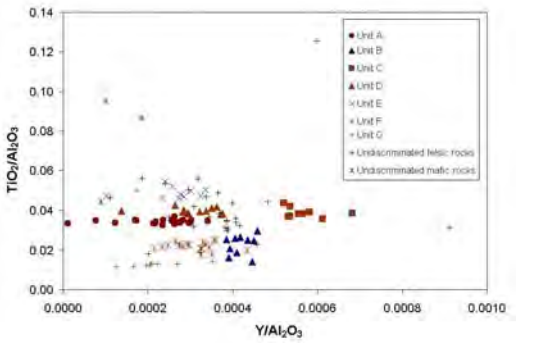

Fig. 4. TiO_2/Al_2O_3 vs. Y/Al_2O_3 plot showing geochemical association of unit F rocks. TiO_2 /Y ratio for unit F is 73.58.

that tholeiitic-transitional unit B is overlain by calc-alkaline unit C (Fig. 5).

Several samples labelled as "undiscriminated samples" on the binary plots are widely scattered on figure 1. Most of these samples were collected from areas adjacent to chemostratigraphic contacts. The spurious nature of these data may reflect the effect of mixed-source sampling.

CONCLUSIONS

This study has revealed that;

(1) The altered volcanic sequence that hosts the Restigouche deposit is dominantly made up of rhyodacitic/dacitic massive flows and related autoclastic breccias and volcaniclastic ash (tuffaceos

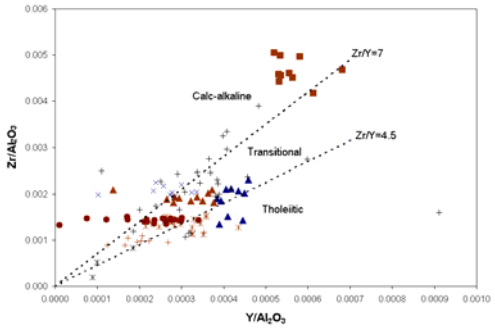

Fig. 5. Zr/Al_2O_3 vs. Y/Al_2O_3 plot showing tholeiitic-transitional, transitional, and transitional-calc-alkaline nature of the volcanic rocks that host the Restigouche massive sulfide deposit. Zr/Y boundary ratios for the trends that divide the tholeiitiic-transitional and transitional-calc-alkaline fields are 4.5 and 7, respectively.

sedimentary rock) and quartz-feldspar-lithic tuff. Within this package seven geochemically distinct units are recognized.

(2) The Mount Brittain Formation is made up of tholeiitic-transitional, transitional, and transitional-calc-alkaline dominantly felsic volcanic units and have similar magmatic nature that is recognized elsewhere in felsic volcanic rocks of the BMC.

(3) Temporal evolution of felsic volcanism from transtional (unit B) to calc-alkaline (unit C) is supported by chemostratigraphic relationships between units A and B. Thus, the processes responsible for formation of the volcanic rocks hosting the Restigouche deposit are associated with episodic felsic volcanism that produced volcanologically similar, but geochemically distinct rocks.

ACKNOWLEDGEMENTS

We acknowledge Blue Note Mining and NB Department of Natural Resources for their assistance and support during the course of the study.

REFERENCES

GOWER, S.J. 1996. Geology, lithogeochemistry and mineral occurrences in the Portage Brook area, northwestern Bathurst Mining Camp, New Brunswick. New Brunswick Department of Natural Resources and Energy, Minerals and Energy Division, *Mineral Resource Report* **96-1**, 13-43.

ROGERS, N., VAN STAAL, C.R., MCNICOLL, V. & THERIAULT, R. 2003. Volcanology and tectonic setting of the northern Bathurst Mining Camp: Part 1. Extension and rifting of the Popelogan Arc. *Economic Geology Monograph*, **11**, 157-179.

VAN STAAL, C.R., WILSON, R.A., ROGERS, N., *et al.* 2003. Geology and tectonic history of the Bathurst Supergroup, Bathurst Mining Camp, and its relationships to coeval rocks in southwestern New Brunswick and adjacent Maine: a synthesis. *Economic Geology Monograph*, **11**, 37-60.

WHALEN, J.B., ROGERS, N., VAN STAAL, C.R., LONGSTAFFE, F.J., JENNER, G.A., & WINCHESTER, J.A. 1998. Geochemical and isotopic (Nd, O) data from Ordovician felsic plutonic and volcanic rocks of the Miramichi highlands: petrogenetic and metallogenic implications for the Bathurst Mining Camp. *Canadian Journal of Earth Sciences*, **3**, 237-252.

Geological and geochemical evolution of the San Miguel skarn, Tandilia Belt, Buenos Aires Province, Argentina

Raúl de Barrio[1], Mabel Lanfranchini[1]*, Ricardo Etcheverry[1,2], Agustín Martín-Izard[3], Mario Tessone[1], & María Paz[1]

[1]Instituto de Recursos Minerales (INREMI), FCNyM-UNLP, calle 64 N° 3, (1900), La Plata ARGENTINA (e-mail: debarrio@inremi.unlp.edu.ar)
[2]Consejo Nacional de Investigaciones Científicas y Técnicas (CONICET) ARGENTINA
[3]Departamento de Geología, Universidad de Oviedo SPAIN

ABSTRACT: The San Miguel skarn deposit is located in the Tandilia Belt, in the southern part of the Buenos Aires province in Argentina. It has developed in an igneous metamorphic complex, which exhibits a long geological evolution and is associated with a Proterozoic granitic magmatism.

The main mineral assemblages identified in the San Miguel deposit are: (1) Plagioclase ± clinopyroxene ± garnet formed during prograde metasomatic endoskarn development, (2) clinopyroxene ± garnet ± wollastonite ± vesuvianite, formed by metasomatic processes in marbles, and (3) amphibole > epidote ± quartz ± chlorite ± titanite, resulting from hydrous retrograde alteration of skarn.

The San Miguel deposit is classified as calcic skarn. Sulfide mineral deposition was not recognized in surface exposures.

KEYWORDS: *San Miguel Skarn, Buenos Aires Province, Argentina.*

INTRODUCTION

The San Miguel skarn is located 43km south of Tandil city, Buenos Aires Province, eastern Argentina (Fig. 1). It represents an isolated occurrence within the Tandilia Belt.

Previous geological work is scarce. The San Miguel skarn was discovered by Villar Fabre (1956). During the sixties, Villar Fabre & Quartino (1966), and Quartino & Villar Fabre (1967) conducted petrological studies of this deposit, defining skarn mineral facies.

The present study is part of a regional investigation program for the characterization of hydrothermal alteration processes in the Tandilia Belt, carried out by the research group of the Instituto de Recursos Minerales of the University of La Plata. As a result of that work, a magmatic-hydrothermal system with interesting geological features is recognized at the San Miguel skarn.

GEOLOGICAL SETTING

Regional Geology

The Tandilia Belt constitutes the southern sector of the Río de La Plata Craton, together with Martín García Island and the western border of Uruguay. It comprises a complex igneous metamorphic association, which exhibits an extensive evolution during two main regional geotectonic events in southern South America: The Transamazonian Cycle (Paleoproterozoic ≈2200-1800 Ma) and the Brazilian Cycle (Neoproterozoic ≈900-570 Ma).

The Precambrian basement represented by the Buenos Aires Complex (Marchese & Di Paola 1975) comprises the oldest rocks in the Tandilia Belt. It is made up of tonalitic gneisses, granitic migmatites, amphibolites and scarce marbles, all of which are intruded by Proterozoic granitic bodies. These rocks form extensive hills of low relief, where lithological contacts are hardly ever observed due to the extensive Quaternary cover. Nevertheless, numerous quarries were developed in the region with the purpose of rock exploitation, allowing us to observe stratigraphic relationships between the different units. A Proterozoic-Lower

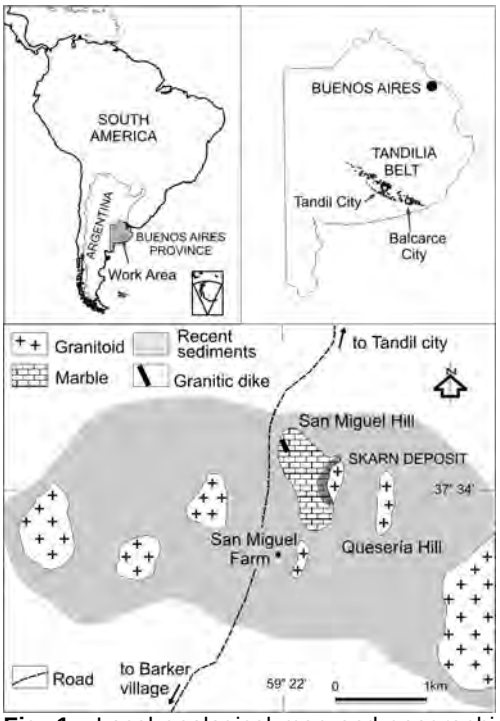

Fig. 1. Local geological map and geographic location of the San Miguel area.

Paleozoic sedimentary sequence (limestones, quarzites, and pelites), and a Quaternary cover complete the stratigraphic column.

Precambrian carbonate rocks were only recognized in two places: San Miguel quarry, located between the cities of Tandil and Barker, and Punta Tota quarry (Delpino & Dristas 2007), near Balcarce city, 100 km southeast of San Miguel. The San Miguel skarn was developed by the intrusion of granites and Punta Tota skarn is related to pegmatites that were segregated from garnet migmatite. Carbonate rocks at San Miguel skarn are mainly calcitic in composition. By contrast the marbles of Punta Tota are dolomitic in composition and form thin beds intercalated in amphibolites, constituting the upper part of a stratified basement sequence.

No geochronological data is available for the San Miguel granitic rocks; nevertheless, granitoids of similar mineralogical and petrological features, outcropping in neighboring areas, were dated by the SHRIMP method and indicated a Paleoproterozoic age (Cingolani *et al.* 2002). They form part of a granitic series formed by several isolated bodies. This multiple granitic complex seems to correspond to the same tectonic event, syn-to-post tectonic with respect to the Transamazonian Cycle. They form a collisional belt where crust thickening linked with anatectic processes occurred, which in turn generated local acid volcanism and relevant milonitic zones (Dalla Salda *et al*. 2005).

LOCAL GEOLOGY

Surface exposures of the San Miguel skarn deposit occur isolated over a 4000 m^2 area, surrounded by intruding Proterozoic granitoid outcrops. The San Miguel skarn is mainly hosted by the Precambrian marbles of the Buenos Aires Complex.

Marbles are whitish grey in colour. They occur in the form of irregular elongated bodies, several metres in length. The grain size varies from a few millimetres to 7cm, representing different recrystallization stages. Dark green diopside crystals are abundantly disseminated within the marble. Also, scarce tremolite, epidote, and other accessory minerals were recognized.

Granitoids are tonalitic to granitic in composition; they have granular hypidiomorphic to saccharoid microgranular texture. They are composed of plagioclase (An_{32-38}), microcline, quartz, diopside, tremolite, titanite, and apatite. Granitoids develop sub-horizontal lenses, and irregular elongated bodies, up to 1m wide which are intercalated within the marbles. In addition, granitic veins and veinlets a few millimetres to 10cm thick, cut the marble, following a chaotic pattern.

MINERAL GEOCHEMISTRY

Electron microprobe analyses were performed using a Cameca Camebax SX-100 at the Departamento de Geología, Universidad de Oviedo, Spain. Operating conditions were a 15 to 20 kV accelerating voltage, beam current of 15 to 20 mA, and beam size of 1 to 2 µm. Natural standards were certificated by MAC (Micro Analysis

Consultants Ltd., United Kingdom). The analyses were performed on pyroxene and garnet crystals of exoskarn facies. Microprobe data obtained from pyroxene shows a wide composition variation that fluctuates between 53-80 wt.% Di, 20-47 wt.% Hd, and minor amounts of Jo (0.05-0.36 wt.%). Furthermore, mineral garnet composition ranges between 68-99 wt.% Grs, 0-20 wt.% Ad, 0-8 wt.% Alm, and 0-0.75 wt.% Prp. These significant changes are mainly linked to the variations in the magmatic fluid composition of the system, where Fe, Mg, Al, and Si contents show an erratic behaviour, whereas Ca values remain constant.

GEOLOGICAL AND GEOCHEMICAL EVOLUTION

According to mineralogical textures, alteration mineral assemblages, geochemical analysis, structural relationships, and field observations, a sequential magmatic-hydrothermal evolution was defined at San Miguel Skarn.

1-Marble was firstly intruded by numerous pinkish, small granite veins, up to 2cm thick, developing an initial metasomatic stage represented by incipient reaction along cleavage and fissure planes of large calcite crystals. The calc-silicate mineral assemblage developed in marble is constituted by diopsidic clinopyroxene ± wollastonite, during which Ca enrichment began in the plagioclase of igneous rocks.

2- The increasing size of granitic intrusions, up to 1m thick, caused calcareous xenolith digestion, and a stronger reaction with the marble, generating magma hybridization (Fig. 2). Compositional and textural changes took place in igneous rocks, allowing endoskarn formation. This process was induced by high contents of CO_2 in the system that provoked some depletion in the aqueous phase activity of the granitic magma. Thus, the incorporation of a large amount of carbonate material in this magma allowed anhydrous calc-silicate mineral formation (pyroxene-garnet).

Fig. 2. Granitic intrusion in marble of San Miguel skarn.

Tonalitic-granodioritic facies subsequently show an increase of CaO of between 9.1 and 10.9 wt.%, and a depletion of SiO_2, reaching 56.4-58.8 wt.% (after Villar Fabre & Quartino 1966) towards the contact zone. Petrographically, a depletion of modal quartz and an increase of Ca contents in plagioclase are observed in an endoskarn mineral assemblage consisting of plagioclase ± diopside ± garnet ± titanite.

In addition, metasomatism of the marbles produced an exoskarn mineral association within the xenoliths, and also towards the contact with granitic rocks (several centimetres thick). This exoskarn paragenesis represents an advanced metasomatic stage. It is constituted by massive aggregates of diopside ± grossular ± wollastonite ± vesuvianite. It comprises < 1cm long, dark green prismatic clinopyroxene crystals, up to 4cm in length, isotropic reddish brown garnet, and 2cm long, white fibrous wollastonite that forms reaction rims surrounding garnet cores (Fig. 3).

3- Retrograde metamorphic processes, linked to hydrothermal fluid circulation, finally produced a new mineral assemblage constituted mainly by tremolite-actinolite> epidote ± chlorite ± quartz ± sericite ± titanite ± hematite. The amphibole appears as green fibrous crystals over clinopyroxene and other anhydrous minerals.

CONCLUSIONS

(1) The singular occurrence of

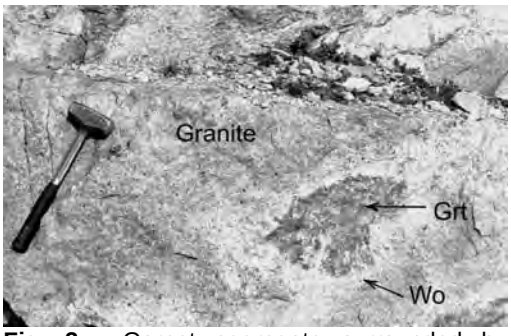

Fig. 3. Garnet aggregate surrounded by wollastonite rim, within granitic rocks.

Precambrian carbonate rocks in the San Miguel area allowed the formation of an isolated skarn deposit related to the Proterozoic magmatic hydrothermal activity and associated with the granite intrusions. Similar processes occurred at the Punta Tota skarn. These deposits at the present time constitute the only two skarns recognized in the Tandilia Belt of Buenos Aires Province.

(2) The San Miguel deposit is classified as calcic skarn (Ca and Ca-Mg (-Fe)-silicates). Sulfide mineral deposition was not recognized in the retrograde alteration facies, at least not in surface exposures.

REFERENCES

CINGOLANI, C.A., HARTMANN, L.A., SANTOS, J.O.S., & MCNAUGHTON, N.J. 2002. U-Pb SHRIMP dating of zircons from the Buenos Aires Complex of the Tandilia Belt, Río de La Plata Craton, Argentina. *XV Congreso Geológico Argentino*, La Plata, **1**,149-154.

DALLA SALDA, L., DE BARRIO, R.E., ECHEVESTE, H.J., & FERNÁNDEZ, R.R., 2005. El basamento de las Sierras de Tandilla. In: DE BARRIO, R.E., ETCHEVERRY, R.O., CABALLÉ, M.F., & LLAMBÍAS, E. (eds), *Geología y Recursos Minerales de la Provincia de Buenos Aires. XVI Congreso Geológico Argentino*, La Plata, Relatorio, **31-50**.

DELPINO, S.H. & DRISTAS, J.A. 2007. Dolomitic marbles and associated calc-silicates, Tandilia belt, Argentina: Geothermobarometry, metamorphic evolution, and P-T path. *Journal of South American Earth Sciences*, **23**, 147-175.

MARCHESE, H.G. & DI PAOLA, E.C. 1975. Reinterpretación estratigráfica de la perforación Punta Mogotes N° 1, provincia de Buenos Aires. *Revista de la Asociación Geológica Argentina*, **30**, 17-44.

QUARTINO, B. & VILLAR FABRE, J. 1967. Geología y petrología del basamento de Tandil y Barker, provincia de Buenos Aires, a la luz del estudio de localidades críticas. *Revista de la Asociación Geológica Argentina*, **22**, 223-251.

VILLAR FABRE, J. 1956. Descripción geológica de la Hoja 33q, Barker (provincia de Buenos Aires). *Dirección Nacional de Minería. Unpublished report.*

VILLAR FABRE, J. & QUARTINO, B. 1966. Exomorphic and endomorphic effects from marble-contaminated granite contacts in the "San Miguel" quarry, Barker, Province of Buenos Aires, Argentina. *American Journal of Science*, **264**, 310-320.

Geochemistry of auriferous banded iron formation, northeastern Saharan metacraton, Egypt

Ahmed M. El Mezayen[1], Talaat M. Ramadan[2], & Atef O. Abu Salem[3]

1Geology Dept, Al Azhar Univ., Cairo, EGYPT
2National Authority for Remote Sensing and Space Sciences, Cairo, EGYPT
(e-mail: ramadan_narss2002@yahoo.com)
3The Geological Survey of Egypt, Cairo, EGYPT

ABSTRACT: The present article presents and discusses the results of geochemical studies on the Archean banded iron formation (BIF) and their host rocks in East Oweinat district. The study area lies in the southern part of the Western Desert of Egypt and is underlain by the north eastern part of Saharan metacraton. Detailed mapping reveals intercalation of the Archean gneisses with thick (0.5-100 m) layers of BIF. Lithogeochemical analyses of the BIF for major- and trace-elements show that: SiO_2 and Fe_2O_3 are the two most abundant oxides, varying from 37.02 to 60.3% and 32.5 to 61.06% respectively. Also, 20 bedrock samples from the BIF were analyzed for gold using Atomic Absorption. The results of these analyses revealed that gold contents range from 3.75 up to 6.18 g/t. The Atomic Absorption data were confirmed by Fire Assay that returned gold values from 0.3 up to 3.47 g/t. The recognition of gold-bearing BIF makes the southern and southeastern parts of the study area promising territories for further exploration.

KEYWORDS: *Owienat, Archean, Early Proterozoic, Banded Iron Formation, felsic granulites*

INTRODUCTION

The East Oweint district is located in the southwestern part of the Western Desert of Egypt and is bounded by Latitudes 22°00' and 22°15' N and by Longitudes 25°35' and 26°05' E (Fig. 1). The area is underlain by the north eastern part of Saharan metacraton of Abdelsalam *et al.* (2002). Several authors stated that the high grade gneiss and migmatite terrane in the basement, west of the Nile, are part of a Pre-Pan- African continental plate (Richter & Schandelmeier 1990, Khattab *et al.* 2002). Several authors discussed the gold mineralization associated with the Banded Iron Formation (BIF) in the central Eastern Desert of Egypt.

El Shimi & Soliman (2002) were the first recognize gold mineralization in association with BIF in the central Eastern Desert of Egypt. Botros (2004) classified the gold deposits of Egypt into three types, i.e., I) stratabound deposits, II) non-stratabound deposits hosted in igneous metamorphic rocks and III) placer gold deposits. He subdivided the stratabound deposits into three main types: gold-bearing Algoma-type BIF, gold-bearing tuffaceous sedimentary rocks and gold-bearing volcanogenic massive sulfide deposits.

This study focuses on the geochemistry of the BIF. This work also attempts to document the lithologic and structural controls of the BIF in East Oweinat district using Landsat ETM+ and Radarsat imagery complimented by field studies (Figs. 2 to 4).

GEOLOGICAL SETTING

The study district is mainly underlain by metamorphic Archean to Early Proterozoic and Neoproterozoic rocks. These are intruded by Late Precambrian granodiorites and biotite granites that have sharp intrusive contacts with host rocks and are uncomfortably overlain by the Gilf Formation (Paleozoic), Abu Ras Formation (Mesozoic) and Quaternary sediments (Fig. 4). The Archean to Early Proterozoic rocks are medium- to high-grade metamorphic rocks that include felsic granulites, garnet-quartz-feldspathic gneisses and quartzo-

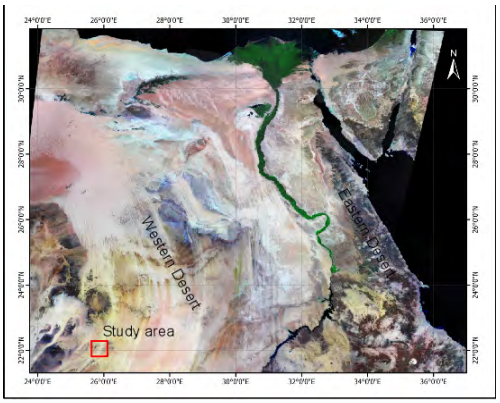

Fig. 1. Landsat TM image showing the study area (red box in southwest corner is the study area), western Desert Egypt.

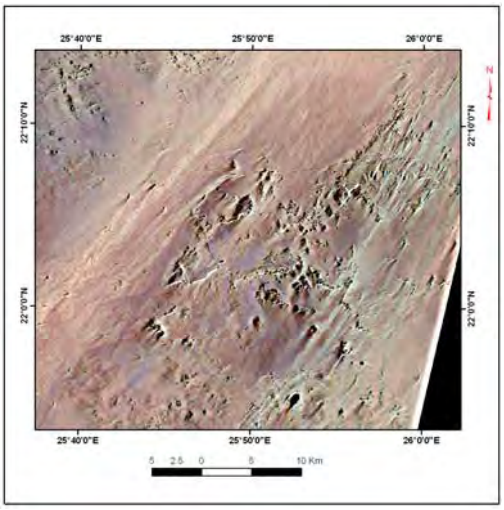

Fig. 2. Landsat TM image (Bands 7,4,2) for the study area outlined in Fig. 1

feldspathic gneisses. Detailed mapping shows that the gneisses are intercalated with thick (≤100 m) horizons of BIF.

MINERALIZATION

The southern part of the study area (Fig. 4) is characterized by a large volume of BIF and associated gold mineralization. Here the BIF is hosted in the gneissic rocks and form ridges and isolated hills. The BIF horizons are strongly folded and faulted. These units generally strike E-W or NE-SW with dips of N 45° to NW 60°. Locally, some bands strike NNE-SSW and NW-SE with dips of NNW 40° and NE 60°, respectively. Generally, the thickness of

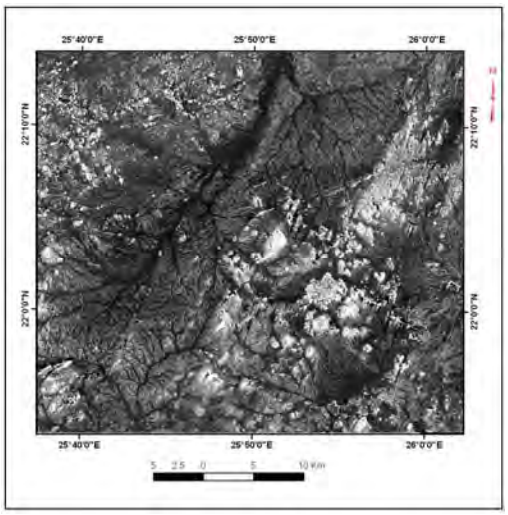

Fig. 3. RADARSAT-1 image for the study area outlined in Fig. 1

these beds ranges from 0.5 to 100 m and strike lengths have been traced for up to approximately 4 km. The BIF in NNE-SSW is generally thinner (average 5 m) than that of the other trends. The beds end abruptly by fault displacement or are obscured by thick sand sheets. Radarsat images reveal subsurface structures such as folds and faults that control the distribution of the BIF in the study area (Fig. 3).

Microscopically, the BIF is composed mainly of iron oxide rich bands that alternate with microcrystalline silica bands, quartz, chert and jasper. The ratios of these constituents are different from one sample to another. Occasionally, the samples contain sulfides, garnet and graphite.

Complete chemical analyses for major oxides and trace elements of 6 representative samples of BIF were carried out using XRF technique. The analyses reveal the following:

- SiO_2 and Fe_2O_3 are the two most abundant oxides. They vary from 37.02 to 60.3% and 32.5 to 61.06% respectively.
- (K_2O+Na_2O), MnO and P_2O_5 occur in very low concentrations.

The graphical representation of the average chemical composition for the trace elements of the BIF in this study are

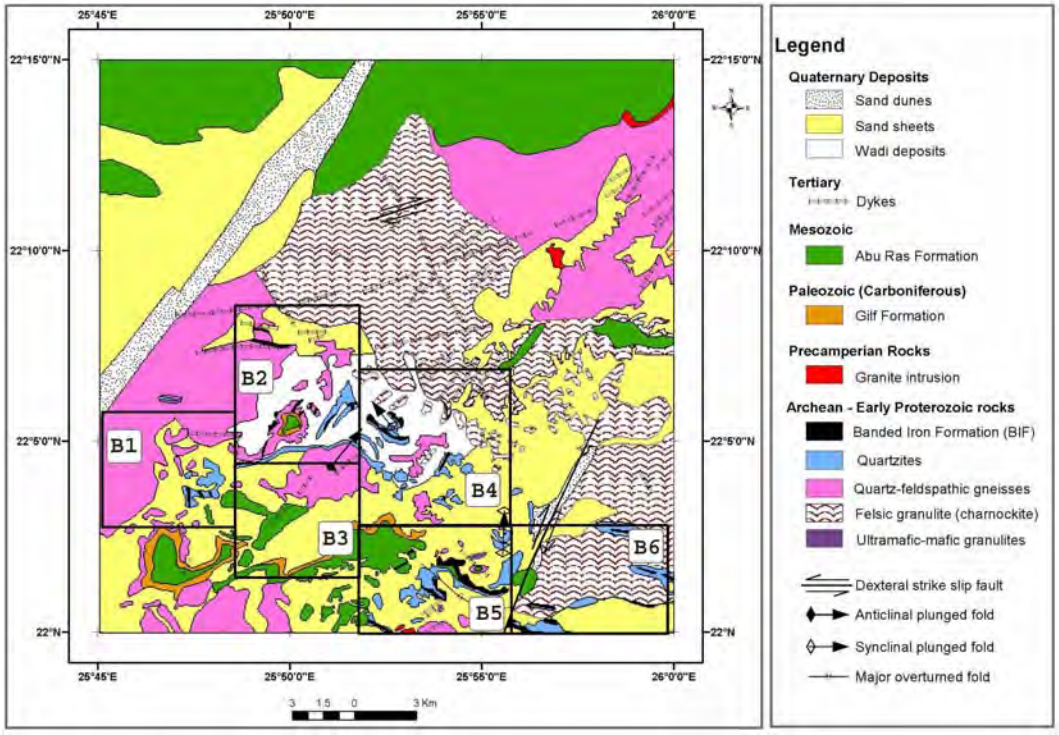

Fig. 4. Geological map for the study area (Modified after Khattab *et al.* 2002), B1 - B6 are promising areas

compared to typical Algoma type and Lake Superior type BIFs (Fig. 5) and shows that the samples in this study are similar to Superior type BIF. It is of particular interest to note that although the BIF in the study area have significant strike length and thicknesses, other field relations particularly the host rocks make them akin to the Lake Superior BIF. Twenty samples from the investigated BIF (areas B1-B6 on Fig. 4) were analyzed for gold, silver and other trace elements using Atomic Absorption. The results of these analyses revealed that gold contents range from 3.75 to 6.18 g/t. The Au is associated with arsenic and silver, where As and Ag contents range from 5.67 to 84 ppm and from 5.58 to 20.9 g/t respectively. The anomalous gold results were checked by Fire Assay analysis which confirmed that gold contents range from 0.3 to 3.47 g/t.

CONCLUSIONS

The study area is underlain by metamorphic Archean to Early Proterozoic and Neoproterozoic rocks. The Archean to Early Proterozoic rocks are represented by medium- to high-grade metamorphic rocks, including felsic granulites, garnet quartz-feldspathic gneisses and quartzo-feldspathic gneisses. Detailed mapping reveals intercalation of these gneisses with thick (up to 100 m), horizons of BIF. Radarsat imagery reveals subsurface structures such as folds and faults control the distribution of the BIF in the study area. The chemical analyses for major oxides and trace elements of the studied BIF reveal that: SiO_2 and Fe_2O_3 are the two most abundant oxides and vary from 37.02 to 60.3% and 32.5 to 61.06% respectively. Fire Assay analysis confirms the elevated gold content of the BIF returning values between 0.3 and 3.47 g/t. Therefore, the southern and southeastern parts of the region located in areas B1, B2, B3, B4, B5,

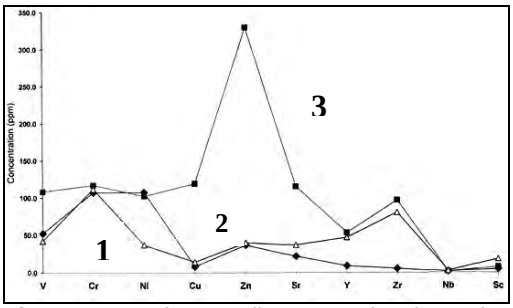

Fig. 5. Binary diagram showing the concentration of the average trace elements of the BIFs in the studied area (1), Lake Superior type (2) and Algoma type (3).

and B6 (Fig. 4) are promising for further Au exploration.

REFERENCES

ABDELSALAM, M.G., LIEGEOIS, J.P., & STERN, R.J. 2002. *T*he Sahara Metacraton. *Journal of African Earth Sciences,* **34**, 119-136.

BOTROS, N. S. 2004. A new classification of the gold deposits of Egypt. *Ore Geology Reviews*, **25**, 1-37

EL SHIMI, K.A. & SOLIMAN, A.A. 2002. Gold mineralization associated the banded iron formation in the central Eastern Desert of Egypt; first record. *Annals of the Geological Survey, Egypt,* **25**, 281-299.

KHATTAB, M.M, *et al.* 2002. Al Oweinat Banded Iron Formation (SW Egypt) distribution and related gold mineralization. *Annals of Geological Survey, Egypt,* **25**, 343-364

RICHTER, A. & SCHANDELMIEIR, H. 1990. Precambrian basement Inliers of Western Desert, Geology, Petrology and Structural Evolution. In: SAID, R. (ed.), *The Geology of Egypt,* A. A. Balkema, 1990, 185-200.

Gold depletion and enrichment in basalt-covered areas in Central Victoria, Australia: key for mineral exploration

I. Goldberg[1], G. Abramson[1], & V. Los[2]
[1]*Interesources Pty Ltd, Level 2, 49-51 York St, Sydney, NSW 2000 AUSTRALIA*
(e-mail: igoldberg@ionex.com.au)
[2]*Academy of Mineral Resources, Nasarbaya Batyra, 146/11. Almaty KAZAKHSTAN*

ABSTRACT: The problem of exploration for gold and other mineral deposits hidden under basalt in the Central Victoria gold province is part of the general problem of searching for concealed deposits. For bedrock areas we have demonstrated the effectiveness of identifying conjugate zones of ore element depletion and enrichment. Collectively, the enrichment and depletion zones constitute a unified ore geochemical system. A good correlation exists between the dimensions of the zone depleted in the ore-forming elements and the amount of those elements in the associated enrichment zone. Structurally similar geochemical systems have been identified by us in regions overlapped uncomformably by basalts such as the southern part of Central Victoria. Here, a regional geochemical survey (over an area of 12 000 km^2) using registration of metal-organic forms of gold and other metals in soil by the selective extraction of fulvate-humate (MPF method), we have identified geochemical systems similar to those in the Bendigo gold field. Mapping of geochemical systems, including enrichment and depletion zones of mobile forms of metals could be a key criterion for assessing the favourability of a region, in particular areas covered by basalt.

KEYWORDS: *Gold, depletion, enrichment, cover basalt area*

INTRODUCTION

Geochemical exploration in areas covered by blankets of consolidated or unconsolidated material is difficult at best. The Central Victoria gold province, Australia is a typical example. In the northern part of this province, where Ordovician host rocks crop out a considerable number of gold deposits are known, including the two largest goldfields at Bendigo and Ballarat (Fig. 1). No gold deposits are known in the southern part of the Central Victoria gold province where Ordovician host-rocks are unconformably overlain by post mineralization basalts.

Currently, an evaluation of the basalt covered area is being carried out by the geochemical group "Interesources Pty Ltd" using IONEX technology. This technology is based on mapping polar geochemical systems of various scales (Goldberg *et al.* 2003). Such systems include zones enriched and zones depleted in ore-forming elements. There is a linear relationship between the size of the depletion zone and the quantity of ore metals in the deposit. This correlation is the principal criterion for assessing the potential of enrichment zones.

In covered areas IONEX technology involves investigating the distribution of mobile metals in soil. Depending on the environment, various geoelectrochemical methods are used: CHIM, selective extraction of fulvate-humate (MPF), TMGM and MDE (Antropova *et al.* 1992).

The present paper provides new data for the distribution of organic forms of gold in soil (MPF method) in the southern part of the Bendigo-Ballarat zone. The study area covers 12 000 km^2, most of which is covered by Tertiary basalts (Fig. 1).

GEOCHEMICAL SYSTEMS OF BENDIGO GOLDFIELD

The Bendigo-Ballarat zone is notable as the most productive gold mining region in Victoria, and includes the giant Bendigo goldfield as well as the large goldfields of Maldon, Castlemaine, and Fosterville.

The Bendigo-Ballarat zone lies between the Avoca and Mount William faults and

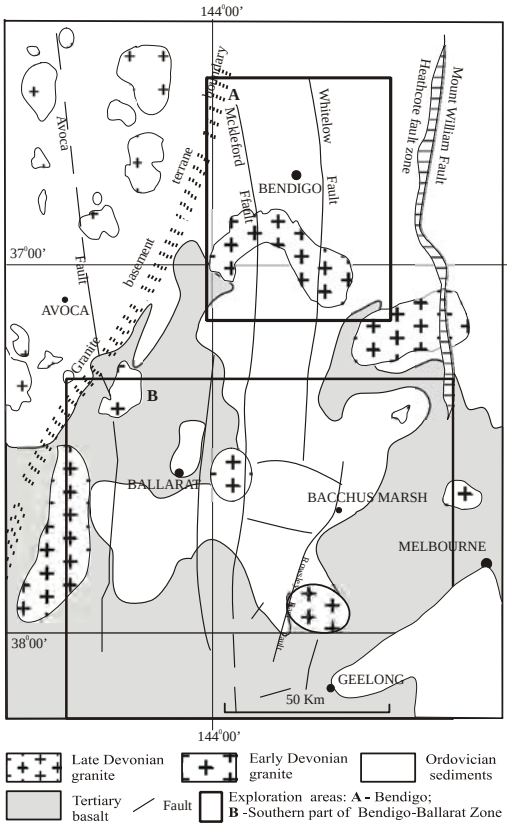

Fig. 1. Simplified geological map of Bendigo - Ballarat Zone. Victoria. Australia (Geology after Morand *et al.* 1995)

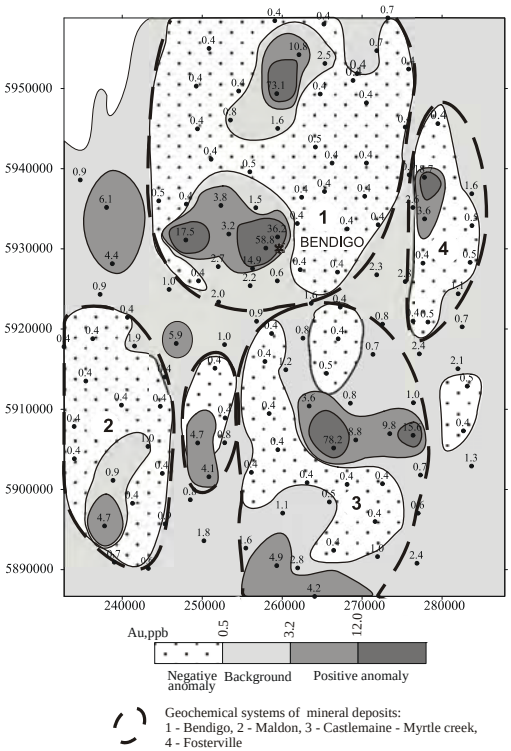

Fig. 2. Distribution of gold in rock and geochemical systems in Bendigo region Victoria. The area of this figure is outlined by box A on Fig. 1.

has a width averaging about 100 km (Vandenberg *et al.* 2000). The zone is characterized by north-south regional structural grain (Fig. 1).

The northern part of the Bendigo-Ballarat zone consists of an Ordovician flysch sequence which has been complexly deformed and intruded by late Devonian granitoids. In the south-western part of the study area Tertiary basalt overlies much of the Ordovician sedimentary sequence. Practically all known goldfields and mineralized zones have been discovered in areas where Ordovician sedimentary rocks crop out.

In the Bendigo area the distribution of gold and associated elements was studied in bedrock samples over an area of 3,750 km^2 (Fig.2).

The Bendigo goldfield is located within an enrichment zone of approximately 100 km^2 that has an average of 14 ppb Au. To the north a depletion zone underlying an area of some 700-800 km^2, has an average gold content of less than 0.5 ppb. Together, the enrichment and depletion zones constitute a geochemical system which covers an area of more than 1000 km^2 (Goldberg *et al.* 2007).

A key criterion for the evaluation of a promising area is the approximately linear relationship between the area of the depletion zone and the amount of gold contained in the deposit (Fig. 3).

THE GEOCHEMICAL SYSTEM IN BASALT-COVERED AREAS

The 586 soil samples analyzed by the MPF method were collected in the southern part of the Bendigo-Ballarat zone a 12 000 km^2 area predominantly covered by Tertiary basalt (Figs. 1 and 4). The MPF method involves an extraction of mobile metal from soil where the concentration of the trace element is described relative to the amount of organic carbon (% C) as Me/C.

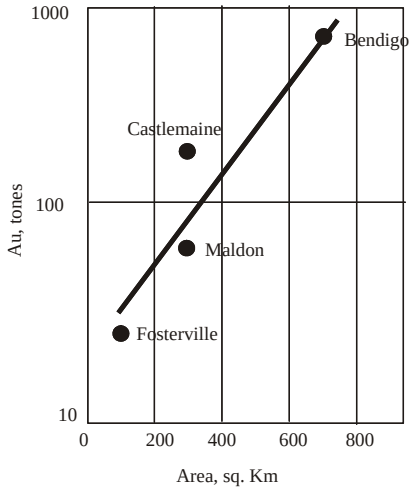

Fig. 3. Correlation between area of depletion zones in sq. km and proven resources of Au in tones for deposits in Bendigo region. Victoria. Australia.

The cumulative curve of Au/C% identifies 3 populations: I) < $0.04*10^{-4}$% (constitutes a depletion zone), II) > $0.04*10^{-4}$% and < $0.2*10^{-4}$% corresponds to background and III) >$0.2*10^{-4}$% to $1.35*10^{-4}$% corresponds to a zone of enrichment. The distribution of Au/C% in the area is characterized by a clear zoning, represented by spatially related zones of depletion and enrichment. There are two large geochemical systems in the area, namely Ballarat and Mount Rothwell (I and II, respectively on Fig. 4). The Mount Rothwell geochemical system covers approximately 2300 km^2 with an enrichment zone (nucleus of the system) covering an area of 150 km^2. The size of the Mount Rothwell geochemical system is comparable to the geochemical depletion and enrichment zones in the Bendigo area (Fig. 2). Spatially these anomalies, according to the model of geochemical polar systems, could be united in single systems.

CONCLUSIONS

Regional geochemical surveying with a sampling density of 1 point per 25 km^2 was carried out in the gold-ore province of Victoria over an area of 12 000 km^2. The distribution of mobile organic forms of gold in soils was investigated using the MPF method.

The aim of the investigation was to outline the most promising areas for gold exploration in Ordovician host rock lying under more recent basalts. According to preliminary data, the thickness of the basalt cover is between 100 and 300 m.

Using the phase geochemistry method, areas were identified in the soils with anomalously high concentrations of gold (enrichment zones). It has been shown in many works, including our own data (Antropova *et al.* 1972, Goldberg *et al.* 1997), that such anomalies of mobile forms of metals at the surface largely reflect the distribution of ore metals in underlying host rocks. This is so even when the apparent source is deeply buried, or concealed under very thick overburden be it consolidated or unconsolidated.

For the first time, in the case of this territory, areas have been identified with anomalously low concentrations of gold (depletion zones) which stand out clearly on the cumulative statistical gold-distribution graphs. Anomalous areas of low gold concentrations are spatially associated with areas of high concentrations. As can be seen from the data presented, the structure of such systems is polar and similar to the structure of geochemical systems in host rocks and akin to the geochemical systems identified in rocks hosting the gold-ore deposits of Bendigo and other deposits.

Mapping of geochemical systems, including enrichment and depletion zones of metals mobile forms in covered areas, could be a key criterion for assessing a favourable region.

Nevertheless, the genesis of such geochemical systems superimposed onto surfical sediment is still not well enough understood; therefore, the interpretation of the geochemical mapping data remains complicated.

REFERENCES

ANTROPOVA, L.V., GOLDBERG I.S., VOROSHILOV N.A., & RYSS JU.S. 1992. New methods of regional exploration for blind mineralisation:

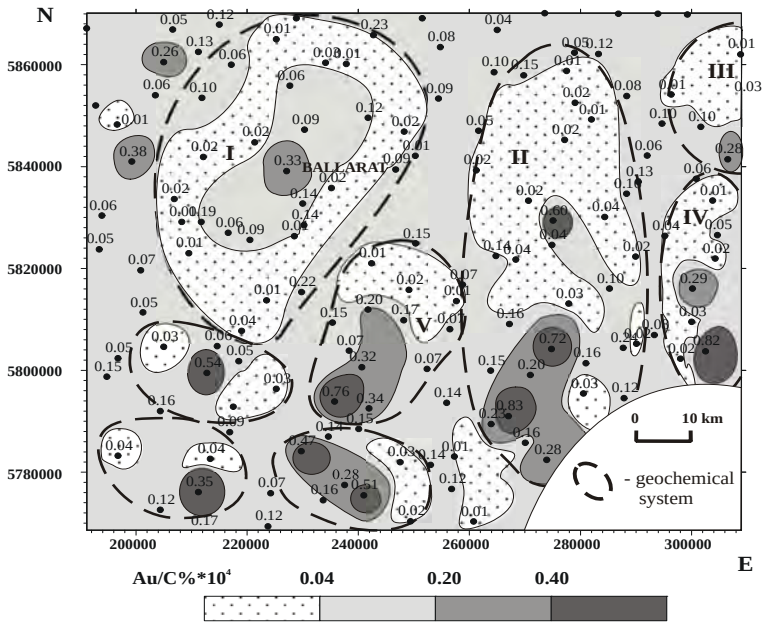

Fig. 4. Distribution of gold in soil (MPF) and geochemical systems in southern part of Bendigo–Ballarat Zone. Victoria, Australia. The area of this figure is outlined by box B on Fig.1.

application in the USSR. *Journal Geochemical Exploration,* **43**, 157-166.

GOLDBERG, I.S., ABRAMSON, G.J., & LOS, V.L. 2003. Depletion and enrichment of *primary* haloes: their importance in the genesis of and exploration for mineral deposits: *Geochemistry: Exploration, Environment, Analysis,* **3**, 281-293.

GOLDBERG, I.S. ABRAMSON, G.Y., HASLAM, C.O., & Los, V.L.. 1997. Mobile form of elements: their use in geochemical mapping and exploration: *Proceeding of Exploration 97:Fourth Decennial International Conference on Mineral Exploration, 365-370.*

GOLDBERG, I.S. ABRAMSON, G.Y., HASLAM, C.O., & Los, V.L. 2007. Depletion and enrichment zones in the Bendigo gold field. A possible source of gold and implications for exploration: *Economic Geology,* **102**, 745-753.

MORAND, V.J., RAMSAY, W.R.H., HUGHES, M., & STANLEY, J.M. 1995. The southern Avoca Fault Zone: site of newly identified 'greenstone' belt in western Victoria. *Australian Journal of Earth Sciences,* **42**, 133-143.

VANDENBERG, A. 1974. Melbourne Sheet S1 55-1. Geological Map. Scale: 1:63,360. Lower half of Melbourne (7822) 30x30 minute Quadrangle. *Geological Survey of Victoria.*

The application of quantitative automated mineralogy in enhancing geochemical data interpretation in mineral exploration and metallurgical processes

Chris Gunning[1], Hugh de Souza[1], & Tassos Grammatikopoulos[1],
[1]*Advanced Mineralogy Facility, SGS Minerals Services, 185 Concession Street, Lakefield, ON, K0L 2H0 CANADA*
(e-mail: chris.gunning@sgs.com)

ABSTRACT: Complete mineralogical and geochemical analyses of rocks have always been a key to improve understanding of the mineral deposits, their genesis and evolution. Furthermore, mineralogy can be applied to predict metallurgical and environmental responses of the ore. Advances in methods of geochemical analysis have had a distinct advantage over mineralogical studies in that they generate high volumes of data for a wide range of elements at low cost. However, over the past few years, significant technical developments in instrumentation for mineralogical analysis can now produce large amounts of mineralogical data quickly. Although these instruments still cannot match the throughput of commercial XRF or ICP-MS, these advances have made significant strides in providing high volume, unbiased, reproducible, and cost effective mineralogical analyses, which yield reliable data on ore samples with relatively low mineral/elemental concentrations.

Mineralogical data can improve interpretation of geochemical data, thus adding value to mineral exploration programs. Combined geochemical and mineralogical analyses can lead to ore delineation, resource estimation and definition of geological domains characterized by specific metallurgical parameters.

KEYWORDS: *automated mineralogy, QEMSCAN™, geometallurgy, Explomin™*

INTRODUCTION

The new generation of automated mineralogy instruments is based on a fully automated Scanning Electron Microscope (SEM) platform, with high speed Energy Dispersive Spectrometers (EDS) and sophisticated software – fully integrated systems available on the market include the QEMSCAN™ (Butcher *et al.* 2007, Reid 2007) and the Mineral Liberation Analyzer (MLA) (Gu 2003). Equipped with large SEM chambers that accommodate up to 16 sections for unattended sample analysis, along with digital control and monitoring of electron beam functions, these systems allow a higher volume of samples to be analyzed at lower cost. In general, only the backscattered electron (BSE) image is used as it allows phases to be discriminated on the basis of their average atomic number. The latest EDS systems are Peltier-cooled, high speed detectors that are capable of high count rates (c. 100 000 cps) with minimal dead time. This is critical because it permits the real time collection of higher resolution X-ray based mineralogical maps and phase chemistry to complement the BSE image. The technological core of the system is the image acquisition and analysis software that, in addition to fully controlling the instruments, allows rapid image acquisition and processing and graphical output of data. The mineralogist's input is critical in setting the criteria for mineral recognition (on the basis of BSE signal and phase chemistry) and for interpretation of the output.

The advantages of using SEM based automated mineralogy instruments over conventional mineralogical techniques are three-fold. (1) Ten to hundreds of thousands (on average) of data points (or X-Ray chemistries) are collected within a single sample. This is in order of magnitudes greater than traditional optical microscopy. (2) The detection limits for low concentration minerals are superior compared to X-Ray Diffraction (XRD) analysis (cf. Berry *et al*. 2008). XRD will

likely not discern the Cu-bearing minerals for a 0.5% Cu sample, especially if there are more than two Cu phases, but QEMSCAN™ will be able to resolve this with relative ease. (3) Low level deleterious elements, e.g., Pb and As, can be mineralogically speciated, that is As can occur as arsenopyrite and/or, lollingite etc, or Pb as galena or cerrusite.

Over the past decade SGS has utilized QEMSCAN™ to focus primarily on the mineral processing sector for plant optimization, flow sheet development, and prefeasibility and feasibility studies which required High Definition Mineralogy™. Samples types used in these studies include drill-core, hand specimens, crushed reject material, feeds, concentrates, leached and smelter products. However, exploration programs do not require all of the detail associated with these studies - the Explomin™ analysis uses a standardized methodology to provide modal data (including deleterious & advantageous minerals at trace levels), mineral associations & liberation, particle & grain sizes, and elemental deportment. For these programs it is advisable to sample the coarsely crushed reject portion of the drill core for QEMSCAN™ analysis for best correlation with the geochemical data. The Explomin™ output replaces classical petrographic descriptions with mineral and textural maps of the entire section that are more complete and easier to comprehend.

CASE STUDIES

The QEMSCAN™ mineralogical applications, in conjunction with geochemistry can be applied to a variety of different ore bodies and commodities as illustrated below.

Case-1: Porphyry-type: Cu assays and mineral abundances were measured at 3 meter intervals through a Cu–Au porphyry. Figure 1 displays the sample depth vs. the total clay content vs. the Cu-Sulfide content (chalcopyrite and secondary Cu-sulfides such as bornite and covellite). Based on the mineral abundances, three distinct zones are recognized; leached, supergene and hypogene zones, each

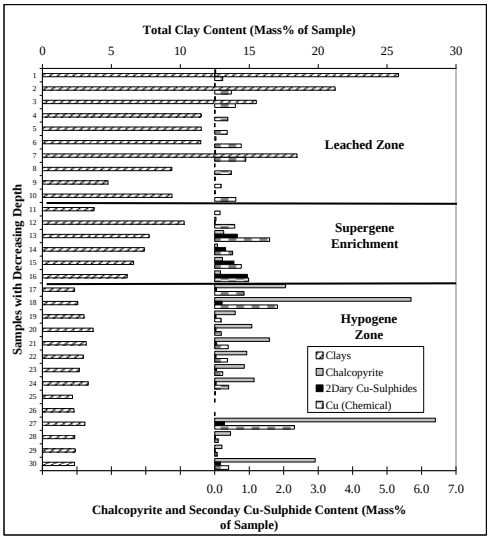

Fig. 1. An example of a Cu-Porphyry defining the leached, supergene and hypogene enriched zone from the mineral abundances of a typical figure.

geometallurgically distinct. There is a significant increase in clay content from the hypogene to the leached zone. The supergene zone is characterized by a greater abundance of secondary Cu-Sulfides to chalcopyrite. Clay content in the hypogene zone is generally less than 4% and chalcopyrite is the predominant Cu mineral. It should be noted that Cu occurs in low concentrations within clay minerals.

Case-2: Iron oxide copper gold deposits (IOCG): Tables 1 and 2 display a geochemical and mineralogical comparison, respectively, of composite samples from two different IOCG ores. The data are based on the analysis of hundreds of samples, necessary to understand the variability of each deposit. The comparison illustrates the obvious geochemical and mineralogical differences in major element chemistry that are reflected in the mineral distributions. Thus, the high LOI in IOCG-A is attributed to the higher abundance of hydrous minerals and carbonates. IOCG-A is composed predominately of Fe-oxides, and olivine and serpentine, whereas IOCG-B is composed of Fe-oxides, pyroxene, amphibole, quartz and

Table 1. Major element geochemistry for IOCG A & B.

Assay	IOCG Deposit A	IOCG Deposit B
SiO_2 %	*10.4*	*28.2*
Al_2O_3 %	*1.00*	*4.20*
Fe_2O_3 %	*65.4*	*50.3*
MgO %	*15.70*	*4.46*
CaO %	*0.62*	*9.20*
Na_2O %	*<0.05*	*1.26*
K_2O %	*0.03*	*0.42*
TiO_2 %	*0.11*	*0.19*
P_2O_5 %	*0.14*	*0.12*
MnO %	*0.14*	*0.20*
Cr_2O_3 %	*<0.01*	*0.01*
V_2O_5 %	*<0.01*	*0.01*
LOI %	*5.42*	*0.64*
Sum %	*99.0*	*99.2*
S %	*2.56*	*2.71*
Cu %	*0.15*	*0.26*
Au g/t	*0.03*	*0.21*
Fe %	*45.7*	*35.2*

feldspars.

The two IOCG ores have similar S and Cu contents, but different mineralogical expression (Table 2). Vallerite is the main Cu-bearing mineral within IOCG A, and chalcopyrite within IOCG-B. Additionally, the pyrrhotite content has mineral processing implications. Thus, if pyrrhotite is monoclinic (magnetic), it would significantly elevate the S content during magnetic separation of the magnetite concentrate, and therefore affect its saleability. Although QEMSCAN™ cannot distinguish between monoclinic and hexagonal pyrrhotite, the pyrrhotite to pyrite ratio can be used to help determine the maximum S content from the pyrrhotite in a concentrate (assuming all of the pyrrhotite is monoclinic). Based on the mineral distributions, IOCG-A will be more problematic than IOCG-B because pyrrhotite is more abundant in the former. Pyrrhotite and pyrite account for ~6% and 7%, of the total Fe, in IOCG-A and B, respectively. However, there is a significant difference in gangue Fe distribution whereby IOCG-B has significantly more Fe bearing silicate.

Case-3: Rare Earth Mineral (REE) Deposits. The Thor Lake rare metals deposits are hosted by the peralkaline Blachford Lake intrusion, an Aphebian ring complex emplaced in Archean-supracrustal rocks of the Yellowknife

Table 2. Mineral distribution between IOCG A & B.

Mineral Abundances	IOCG Deposit A	IOCG Deposit B
Fe-Oxides	**66.2**	**48.4**
Pyrite	**1.22**	**2.29**
Pyrrhotite	**4.26**	**3.22**
Chalcopyrite	**0.02**	**0.77**
Valleriite	**0.81**	**N/A**
Other Sulphides	0.04	0.27
Quartz	0.11	**2.18**
Feldspar	0.03	**6.93**
Pyroxene	0.33	**21.7**
Amphiboles	3.02	9.19
Serpentine	**13.57**	**N/A**
Olivine	6.27	0.64
Chlorite	2.02	1.02
Epidote	0	0.25
Mica/Clays	0.16	2.40
Other Silicates	0	0.06
Carbonates	1.36	0.18
Apatite	0.15	0.18
Other	0.48	0.31
Total	**100**	**100**
Py/Po Ratio	**3.5**	**1.4**

Supergroup. The principal rock-types in the intrusion are syenites, granites and gabbros, and associated pegmatitic bodies hosting rare metal mineralization. Five distinct zones of rare metal mineralization have been identified as potentially economic. The Lake Zone is one of them and is characterized by its enrichment in the more valuable HREE (Eu, Tb, and Dy), relative to light rare earths (LREE, i.e., La and Ce) (Palmer & Broad 2007).

Geochemical data can generally provide little quantitative information on the mineralogical distribution of the host REE minerals in any deposit. Many REE deposits can contain a number of REE phases with significant variations in light REE (LREE) and the heavy REE (HREE). Understanding this is important for mineral processing and estimating mineral resources. A combination of QEMSCAN™ on drill core samples, reject material and size by size analysis, and electron microprobe analyses of a large number of samples have quantified the REM (rare earth minerals) and the REE distribution among the REM. Thus, Figure 2 illustrates an example of the distribution of LREE and HREE and Y. The diagram shows that zircon ($ZrSiO_4$) and fergusonite ((Y, HREE)NbO_4) account for most of the

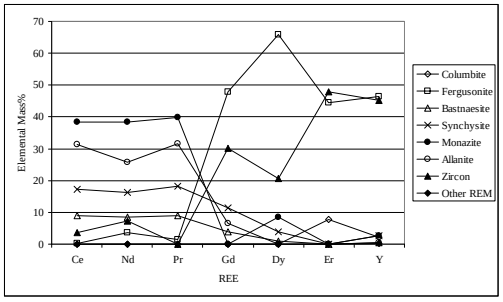

Fig. 2. LREE and HREE and Y distribution within the Lake Zone REM.

HREE & Y, whereas monazite, allanite, synchysite and bastnaesite contain most of the LREE. Based on quantitative data approximately half of the fergusonite mass% is associated mainly with zircon, and <2% of the zircon with fergusonite (i.e., reflecting mass distribution differences in the samples). Therefore, in order to recover the HREE, both minerals must be processed and recovered together. The LREE carriers can be recovered as a group.

CONCLUSIONS

The value of basic geological and geochemical information from mapping, sampling and assaying, and, diverse drillhole-logging methods is enhanced if accompanied by quantitative mineralogical data on mineralization as can be provided by automated mineralogy (QEMSCAN™).

The geological work coupled with the quantitative, statistically representative and complete mineralogical data and input into a geometallurgical framework provides a strong foundation for the development of any project.

Mineralogical variations, among the different ore zones in deposits, are critical in establishing a detailed geological context for delineating the limits of the deposits and for bulk metallurgical testing.

QEMSCAN™ studies are performed according to the needs of the project at different stages and it is currently the sole avenue for quantitative mineralogical studies. They can help in the recognition of the lithology, petrography, and alteration assemblages, that can define geometrical patterns and dimensions of exploration targets and mineralization, but most importantly that can provide metallogenic and metallurgical information.

ACKNOWLEDGMENTS

We thank SGS Lakefield Research for logistical support for this paper. We thank Volta Resources Inc, Northland Resources Inc., Avalon Ventures Ltd., and Rare Metals Inc. for permission to publish parts of data.

REFERENCES

BERRY, R.F., HUNT, J.A., & MCKNIGHT S.W. 2008. Estimating mineralogy in bulk samples. *GeM^{III} (Amira P843) Technical Report 1 - February*.

BUTCHER, A. BENEDICTUS, A. CROPP, A., & GOTTLIEB, P. 2007. Improving Process Efficiencies by Linking Macro-, Meso-, and Micro-Features Obtained from Automated Mineralogical Techniques. *SME '07, Denver, Colorado, Feb 26-28*.

GU, Y. 2003. Automated scanning electron microscope based mineral liberation analysis. An introduction to JKMRC/FEI mineral liberation analyzer. *Journal of Minerals & Materials Characterization & Engineering*, **2**, 33-41.

PALMER, K. & BROAD, P. 2007. Avalon Ventures Ltd, Technical Report on the Thor Lake Rare Metals Project, NT. *Wardrop,* 97 p.

REID, A. 2007. QEM*SEM® to QEMSCAN® 1974 – 2007. *iUG07, September 2007, Brisbane Australia.*

Provenance of the Upper Carboniferous sedimentary rocks, Maritime Basin, New Brunswick, Canada: a sedimentary geochemical approach

M.M.N. Islam, David R. Lentz, & David G. Keighley
University of New Brunswick, 2 Bailey Dr., Box 4400, Fredericton, NB, E3B 5A3 CANADA
(e-mail: z1x61@unb.ca)

ABSTRACT: A sedimentary geochemical approach is adopted to assess provenance in the Upper Carboniferous of New Brunswick. Data for this study is compiled from the mineral occurrence database of the provincial Department of Natural Resources. Studied drill core is composed of sandstone and claystone with minor conglomerate and coal. Mainly grey to red, very fine- to coarse-grained sandstone can be classified as litharenite based on major oxide analysis. Chemical Index of Alteration (CIA) values range from 63.91 to 73.77, suggesting a moderate to relatively high degree of alteration (weathering) in the source area. Major- and trace-element concentrations in the rocks of the studied sandstone indicate that sediments were derived from felsic to mixed felsic/basic and quartzose sedimentary source.

KEYWORDS: *Carboniferous Sedimentary Rock, Litharenite, Provenance, Weathering, New Brunswick*

INTRODUCTION

The chemical composition of clastic sedimentary rocks is a function of a multifaceted association of a number of variables, including the nature of the source rocks, source area weathering, and diagenesis (McLennan *et al*. 1993). However, the provenance of the sedimentary basins has been considered as the dominant control on the composition of sedimentary rocks (McLennan *et al*. 2003). Though weathering and diagenesis can alter the composition of basin sediments, there often remains a potent geochemical signature of the original source terrain which reflects the nature of the exposed continental crust (Roser & Korsch 1988). Literature provides many examples of the use of discrimination diagrams based on the relationship of major- and trace-elements to interpret sedimentary rock provenance (e.g., Roser & Korsch 1988; Amstrong-Altrin *et al.* 2004). As the major elements can be mobile under conditions of diagenesis (Zimmermann & Bahlburg 2003), less mobile elements (i.e., Ti, Cr, Co, Th, Y, Th, Zr, Hf, Nb, and Sc), are more reliable for discrimination of provenance (Taylor & McLennan 1985; Bhatia & Crook 1986; Asiedu *et al.* 2000).

The study area is located within in the eastern tip of the Indian Mountain Deformed Zone, southeastern New Brunswick, Canada. The area is underlain by Upper Carboniferous sedimentary rock and bounded by the Smith Creek and Berry Mills faults to the north and south, respectively (St. Peter 2006). These sedimentary rocks are dominantly grey to red, very fine- to coarse-grained sandstone, and variable red grey/green claystone with minor conglomerate and coal fragments. The study was conducted, based on MacDougall SB-3 (W 64˚ 39' 25.0", N 46˚ 16' 28.7) drill core samples. The geochemical data for this investigation was taken from a New Brunswick Department of Natural Resources Minerals Policy and Planning Division, Mineral Assessment Report (# 476200).

CLASSIFICATION OF SANDSTONE

For geochemical classification of sandstone, most of the recent literature (Armstrong-Altrin *et al.* 2004; Spalletti 2008) uses the classification schemes of Pettijohn (1972) and Herron (1988). The geochemical classification diagram presented in Fig. 1 shows that samples used in this study (Table 1) fall in the

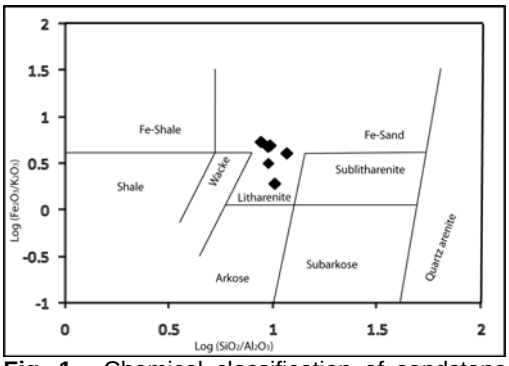

Fig. 1. Chemical classification of sandstone samples from the MacDougall SB-3 drill hole (Table 1). Field boundaries are from Herron 1988).

Table 1. Chemical composition of the selected samples.

Sample No.	S-1	S-2	S-3	S-4	S-8
Major Oxide (wt%)					
SiO_2	80.19	81.68	73.83	75.22	73.74
Al_2O_3	6.84	7.95	7.56	7.88	8.35
Fe_2O_3	5.08	2.81	7.3	6.85	7.41
MgO	0.42	0.77	0.6	0.57	0.81
CaO	1.29	0.88	0.27	1.36	0.57
Na_2O	1.23	1.31	1.25	1.71	1.07
K_2O	1.21	1.43	1.43	1.38	1.33
TiO_2	0.23	0.78	0.44	0.34	0.51
P_2O_3	0.06	0.08	0.07	0.07	0.11
MnO	0.08	0.08	0.04	0.09	0.08
Cr_2O_3	0.002	0.004	0.003	0.003	0.005
Trace elements (ppm)					
La	18.6	27.8	25.5	22.1	29.4
Th	4.1	8.3	5.8	7.1	5.5
Sc	4	7	5	5	7
Hf	2.8	8.4	5.9	6.1	4.8
Co	5.4	7.3	11.6	7.8	19.5

litharenite class, reflecting the mineralogical submaturity of these sediments.

SOURCE AREA WEATHERING

The most common method of measuring the degree of chemical weathering is to calculate the chemical index of alteration (CIA = $[Al_2O_3/(Al_2O_3 + CaO + Na_2O + K_2O) \times 100]$; Nesbitt & Young 1982). High CIA values (64.7, 68.7, 71.9, 63.9, and 73.8) indicate a high degree of alteration of the source rocks. The average CIA values for the samples used in this study are 68.6. Most of the data used in this study plot between idealized plagioclase (CIA = 50) and shale (CIA = 70-75), indicating that the weathering is dominantly the conversion of plagioclase to clay (Fig. 2). Yet, the high value of CIA suggests transportation and recycling from sources located distal to the depositional basin (Nesbitt & Young 1982), which is consistent with a provenance from the stable craton interior or recycled orogen (Dickinson *et al.*1983). Also, the SiO_2/Al_2O_3 ratios for the samples are high (average 10.0), and indicate a high degree of maturity of the sediments (Asiedu *et al.* 2000).

PROVENANCE

In order to determine the source composition of sediments using trace elements, it is necessary to ascertain that the element is immobile under conditions of diagenesis and weathering (Spalletti 2008). Several ratios and plots may be used to define the source rocks. The felsic source rock compositions are found in the Co/Th vs. La/Sc diagram (Fig. 3; Table 1). Other trace element characteristics of sedimentary rocks also place some constrains on the nature of the source rock. Floyd & Leveridge (1987) used a La/Sc vs. Hf plot to discriminate between different source compositions. In this plot, most data fall in the felsic source to mixed felsic/basic source field (Fig. 4; Table 1).

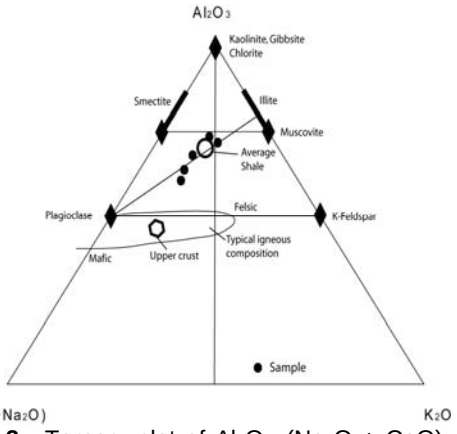

Fig. 2. Ternary plot of Al_2O_3–(Na_2O + CaO)–K_2O (CIA) for the studied sample (after Gu *et al.* 2002).Black filled circles are samples used in this study.

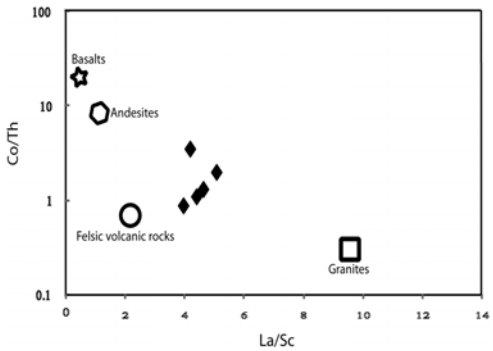

Fig. 3. Co/Th vs. La/Sc source rock discrimination diagram (after Gu *et al.* 2002) illustrating the distribution of samples from MacDougall SB-3 (black diamond symbol).

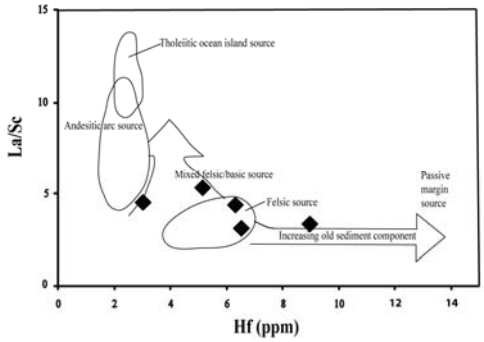

Fig. 4. La/Sc vs. Hf source rock discrimination diagram (after Floyd and Leveridge 1987) illustrating the distribution of samples from MacDougall SB-3 (black diamond symbol).

High contents of Fe_2O_3 and high Al_2O_3/TiO_2 ratios indicate continentally derived sediments (Fyffe & Pickerill 1993). Presences of greater than 70% SiO_2 implies the sandstones are rich in quartz from quartz-rich crystalline provenance (Potter 1978). In the discrimination diagrams for sedimentary provenance, samples used in this study plot in the quartzose recycled fields (Fig. 5).

CONCLUSIONS

The geochemical classification using major oxides shows that the samples used in this study plot in the litharenite field, and, implies that they are mineralogically submature. Major-element concentrations point to significant weathering effect in the source area of the sample set. Provenance analyses, based on major- and trace-element compositions suggest

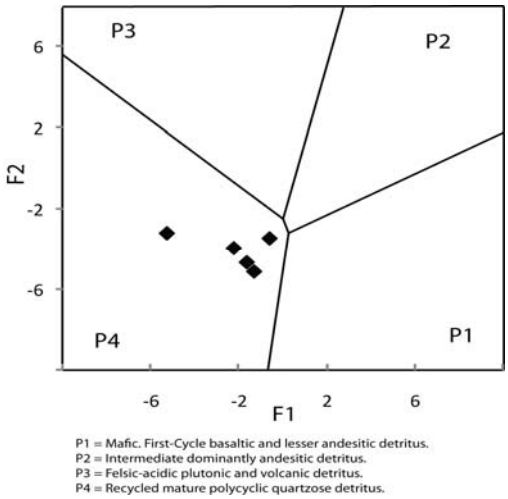

Fig. 5. Provenance discriminant function diagram from Roser & Korsch (1988). F1=-1.773 TiO_2+0.607 Al_2O_3+ 0.76 Fe_2O_3-1.5 MgO+ 0.616 CaO+ 0.509 Na_2O- 1.224 K_2O-9.09; F2=0.445 TiO_2+ 0.07 Al_2O_3- 0.25 Fe_2O_3-1.142 MgO+ 0.438 CaO+ 1.475 Na_2O+1.426 K_2O-6.861.

the sandstones were derived from felsic to mixed felsic/basic and quartzose sedimentary source.

ACKNOWLEDGEMENTS

The authors would like to thank ValeInco for the funding of this research. Thanks are also extended to New Brunswick Department of Natural Resources-Minerals, Policy and Planning Division.

REFERENCES

ARMSTRONG-ALTRIN, J.S., YONG, I.L., VERMA, S.P., & RAMASAMY, S. 2004. Geochemistry of sandstones from the Upper Miocene kudankulam formation, southern india: implications for provenance, weathering, and tectonic setting. *Journal of Sedimentary Research,* **74**, 285-297.

ASIEDU, D.K., SUZUKI, S., & SHIBATA, T. 2000. Provenance of sandstones from the Lower Cretaceous Sasayama Group, Inner Zone of Southwest Japan. *Sedimentary Geology,* **131**, 9-24.

BHATIA, M.R. & CROOK, K.A.W. 1986. Trace element characteristics of graywackes and tectonic setting discrimination of sedimentary basins. *Contributions to Mineralogy and Petrology,* **92**, 181-193.

DICKINSON, W.R. *et al*. 1983. Provenance of North American Phanerozoic sandstone in

relation to tectonic setting, *Geological Society of America Bulletin*, **94**, 222-235.

FLOYD, P.A. & LEVERIDGE, B.E. 1987. Tectonic environment of the Devonian Gramscatho basin, south Cornwall: framework mode and geochemical evidence from turbiditic sandstones. *Journal of the Geological Society of London,* **144**, 531-542.

FYFFE, L.R. & PICKERILL, R.K. 1993. Geochemistry of Upper Cambrian – Lower Ordovician black shale along a northeastern Appalachian transect. *Geological Society of America Bulletin*, **105**, 897-910.

GU, X.X., LIU, J.M., ZHENG, M.H., TANG, J.X., & QI, L. 2002. Provenance and tectonic setting of the Proterozoic turbidites in Hunan, South China: Geochemical Evidence. *Journal of Sedimentary Research*, **72**, 393-407.

HERRON, M.M. 1988. Geochemical classification of terrigenous sands and shales from core or log data. *Journal of Sedimentary Petrology,* **58**, 820-829.

MCLENNAN, S.M., BOCK, B., HEMMING, S.R., HUROWITZ, J.A., LEV, S.M., & MCDANIEL, D.K. 2003. The role of provenance and sedimentary processes in the geochemistry of sedimentary rock. In: Lentz, D.R. (ed.), *Geochemistry of Sediments and Sedimentary Rocks: Evolutionary Considerations to Mineral Deposits-Forming Environments:* Geological Association of Canada, Geotext, **4**, 121-133

MCLENNAN, S.M., HEMMING, S., MCDANIEL, D.K., & HANSON, G. N. 1993. Geochemical approaches to sedimentation, provenance, and tectonics. In: JOHNSON, M.J.& BASU, A. (eds.), *Processes Controlling the Composition of Clastic Sediments*. Geological Society of America. Special Paper, **284**, 21-40.

NESBITT, H.W. & YOUNG, G.M. 1982. Early Proterozoic climates and plate motions inferred from major element chemistry of lutites. *Nature*, **299**, 715-717.

PETTIJOHN, F.J., POTTER, P.E., & SIEVER, R. 1972. *Sand and Sandstone.* Springer-Verlag, New York.

POTTER, P.E. 1978. Petrology and chemistry of modern Big River sands. *Journal of Geology,* **86**, 423-449.

ROSER, B.P. & KORSCH, R.J. 1988. Provenance signatures of sandstone-mudstone suites determined using discriminant function analysis of major-element data. *Chemical Geology,* **67**, 119-139.

SPALLETTI, L.A., MERODIO, J.C., & MATHEOS, S.D. 2008. Sedimentary petrology and geochemistry of siliciclastic rocks from the upper Jurassic Tordillo Formation (Neuque´n Basin, western Argentina): Implications for provenance and tectonic setting. *Journal of South American Earth Sciences,* **25**, 440-463.

ST. PETER, C. 2006. Geological relationship between the Cocagne Subbasin and Indian Mountain Deformed Zone, Maritime Basin, New Brunswick. In: MARTIN, G.L. (ed.), *Geological Investigations in New Brunswick for 2005.* New Brunswick Department of Natural Resources, Mineral ,Policy and Planning Division, Mineral Resource Report **2006-3**, 103-183.

TAYLOR S.R. & MCLENNAN S.M. 1985. *The Continental Crust: Its Composition and Evolution.* Blackwell Science Publisher, Oxford.

ZIMMERMANN, U. & BAHLBURG, H. 2003. Provenance analysis and tectonic setting of the Ordovician clastic deposits in the southern Puna Basin, NW Argentina. *Sedimentology,* **50**, 1079-1104.

Spatial geochemical trends of beach and dune sands from the Northeastern coast of Mexico: implications for provenance

Juan Jose Kasper-Zubillaga[1], John S. Armstrong-Altrin[1], & Arturo Carranza Edwards[1]

1 Instituto de Ciencias del Mar y Limnologia, Universidad Nacional Autonoma de Mexico, Circuito Exterior s/n, Coyoacan, México DF, MÉXICO 04510 (e-mail: kasper@icmyl.unam.mx)

ABSTRACT: A geochemical analysis of major, trace and rare earth elements was carried out in beach sands collected from the Northeastern coast of Mexico in order to observe the spatial trends along three different beaches. Results show that major elements patterns along the beaches are controlled by heavy minerals and plutonic and sedimentary input towards the coast. In addition, trace elements tendencies indicate that the beach sands are influenced by the presence of magnetite. Finally, the differences in Eu anomalies indicate a mix of felsic to mafic and intermediate rocks and feldspar weathering.

KEYWORDS: *beach, sand, provenance, Mexico*

INTRODUCTION

Beach and dune sediments are compositionally controlled by physical, chemical and mechanical factors such as waves, wind, and long shore currents, climate, relief, source composition, transport and river discharges among others (Folk 1974, Ibbeken & Schleyer, 1991; Carranza-Edwards *et al*. 1994; Critelli *et al.* 1997; Carranza-Edwards *et al*. 1998; Armstrong-Altrin *et al*. 2003; Armstrong-Altrin *et al*. 2004; Kasper-Zubillaga & Carranza-Edwards 2005; Kasper-Zubillaga *et al*. 2008a). A wide range of techniques are used for geochemical determinations to investigate the compositional differences of the beach and dune sediments. Such techniques are defined by major, trace and rare earth elements analyses. Furthermore, these techniques allow to understanding the multi-factorial roles that control the composition of coastal sediments. In this paper we focus our attention in showing the spatial trends of geochemical data obtained during the dry season in the northeastern coast of the Gulf of Mexico to discuss the provenance implications.

STUDY AREA

The study area is located in the coastal area of the state of Tamaulipas, Mexico ($22^{o}10'$ $24^{o}00'$W; $98^{o}00'$N). The sampling was carried out in three main localities: Playa Miramar, Boca del Tordo and La pesca (Figs. 1 & 2). Main rivers discharging in each site are Panuco, Carrizal and Soto La Marina.

The geology of the study area comprises mainly: limestones, shales, alluvial deposits, and basic extrusive and intrusive rocks.

MATERIALS AND METHODS

Sand samples were dried at 110 ^{o}C and treated with lithium meta- and tetraborate to make pressed powder pellets. They were analysed using an X-ray fluor-escence Siemens SRS 3000 equipment for major and trace elements. For major and trace elements precision is valuated in terms of relative standard deviation being $<$ 1% (Sutarno & Steger 1985).

The REE analysis was carried out in 22 sand samples by using 0.1 g of dried sample (mesh 200) and digested with strong acid. Digestion was performed in teflon vessels using 4 ml of HCl O_4 and 10 ml HF. This mixture was heated and residue dissolved in distilled water.

Residue was incorporated to a volumetric flask. Determinations of REE

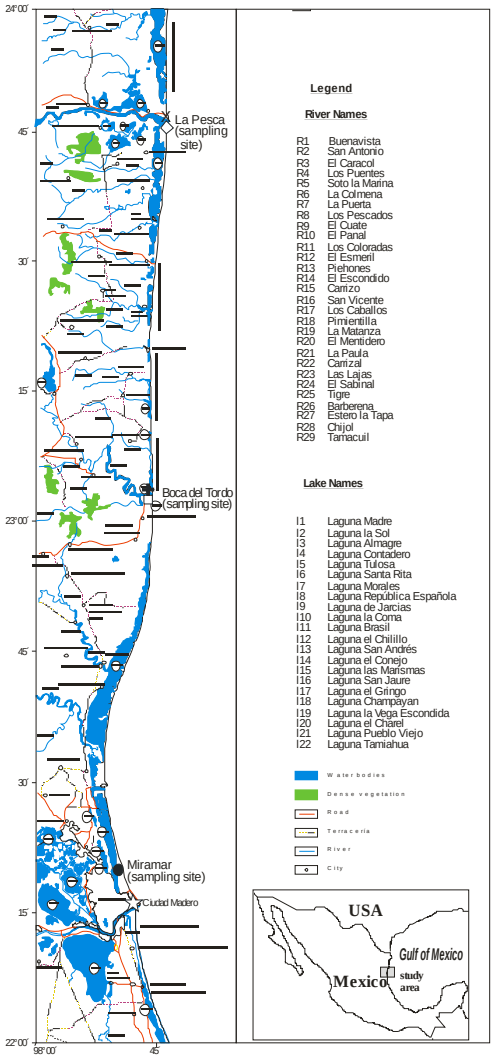

Fig. 1. Study area and sampling sites.

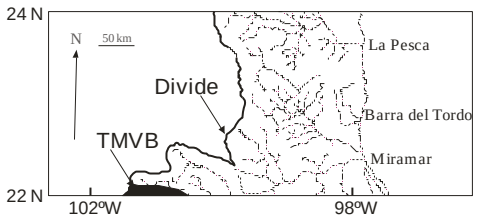

Fig. 2. Map showing the Trans-Mexican Volcanic Belt (TMVB) near to the study area.

were carried out with an ICP mass spectrometer VG Elemental model PQ3. Detection limits were calculated as the concentration equivalent to three times the standard deviation of five replicates of the blank solution. It was better than 200 ppt for all elements determined. Calibration of the apparatus was done with a 0.1, 1 10 and 100 ppb multi elemental standard solution (SPEX- High Purity) and a blank solution of de-ionized water all containing HNO_3 at 2%. Results were observed for international standards (JG-2). The validity of the analytical procedure was assessed by means of accuracy and precision tests. They were calculated by comparing measured and reference values (JA-2). All elements determined had a better than 10 % relative standard deviation (RSD) precision. Data resulted for BCU-3 or "in house standard indicated good agreement with the certified values.

Chondrite-normalized REE patterns were based on values by Evensen *et al*. (1978) averaging the samples firstly determined in ppm for each site.

RESULTS & DISCUSSION

From Figure 3 it can be observed that among the major element trends Ti shows various peaks from localities 10 to 22 that correspond to some beach areas from Playa Miramar, the whole area of Boca del Tordo and one sample from the La Pesca This suggests that this area might have influenced by heavy minerals and plutonic and sedimentary outcrops as it has previously reported in dune sands from Mexico (Kasper-Zubillaga *et al*. 2008a). The rest of the major elements do not show differences in their trends along the coast. However, Ca shows a dynamic behavior represented by oscillations along the coast probably produced by the amount of biogenic debris.

Trace elements show that V exhibit high peaks in Boca del Tordo beach probably associated with the presence of some heavy minerals like magnetite (Kasper-Zubillaga *et al*. 2008a).

Rare earth elements patterns show differences in Eu anomalies for the samples studied from Boca del Tordo (Fig. 5) that can be attributed to the mix of felsic and mafic sources. This variation can also be explained due to the impoverishment of feldspars due to weathering (Kasper-Zubillaga *et al*. 2008b). Also Boca del Tordo concentrates more rare earth elements especially in samples 16 and 18,

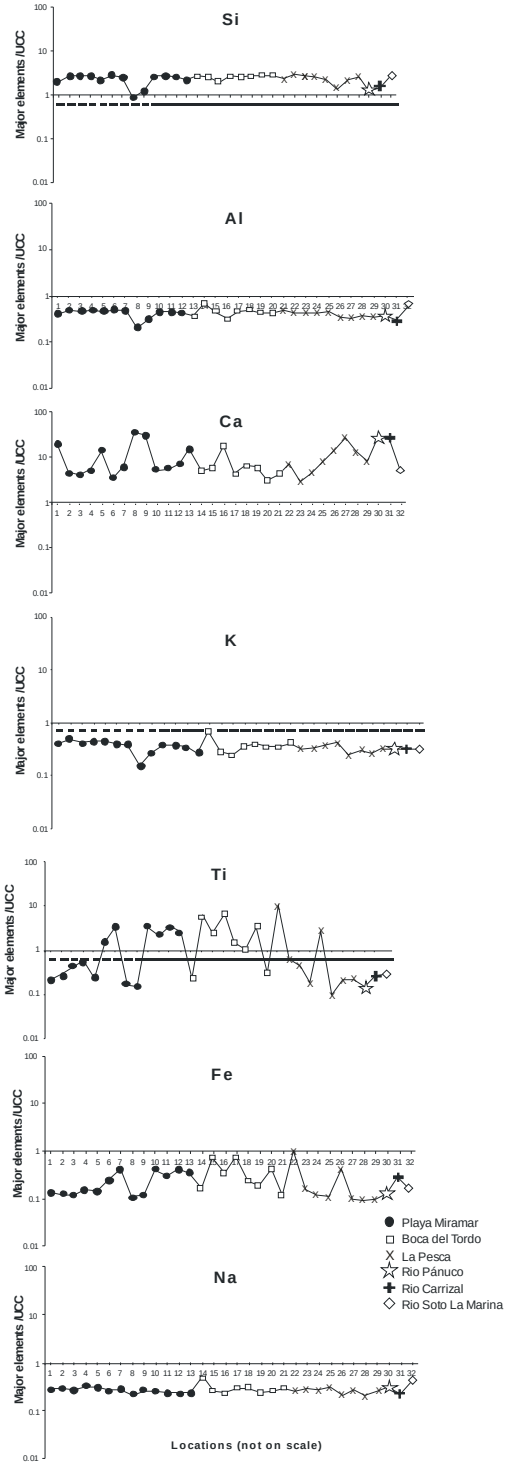

Fig.3. Spatial trends of major elements at beach and dune sands from the northeastern coast of Mexico.

which is probably due to the presence of some heavy minerals that are potential carriers of rare earth elements (Kasper-Zubillaga *et al*. 2008b). The possible source of volcanic is mainly through the Panuco River that intersects volcanic from the Trans-Mexican Volcanic Belt.

CONCLUSIONS

(1) Major element trends show that Northeastern Mexican beaches are influenced by heavy minerals and plutonic and sedimentary outcrops.

(2) Trace element tendencies suggest that the Boca del Tordo beach is more influenced by the presence of magnetite than other beaches.

(3) Rare earth element trends show negative and positive Eu anomalies in some samples studied from the North-eastern beaches suggesting a mix of felsic and mafic source rocks and feldspar weathering.

ACKNOWLEDGMENTS

We are indebted to Rufino Lozano and Ofelia Morton for the geochemical analyses carried out at the Instituto de Geologìa and Instituto de Geofisica, respectively, from the Universidad Nacional Autònoma de Mexico, Mexico.

REFERENCES

ARMSTRONG-ALTRIN, J.S., VERMA, S.P., MADHAVARAJU, J., LEE, Y.I., & RAMASAMY, S. 2003. Geochemistry of upper Miocene Kudankulam limestones, southern India. *International Geological Review,* **45**, 16-26.

ARMSTRONG-ALTRIN, J.S., LEE, Y.I., VERMA, S.P., & RAMASAMY, S. 2004. Geochemistry of sandstones from the Upper Miocene Kudankulam Formation, Southern India: implications for provenence, weathering and tectonic setting. *Journal of Sedimentary Research*, **74**, 285-297.

CARRANZA-EDWARDS, A., ROSALES-HOZ, L., & SANTIAGO-PÉREZ, S. 1994. Provenance memories and maturity of holocene sands in Northwest Mexico. *Canadian Journal of Earth Sciences*, **31**, 1550-1556.

CARRANZA-EDWARDS, A., BOCANEGRA-GARCIA, G., ROSALES-HOZ, L. & DE PABLO GALÁN, L. 1998. Beach sands from Baja California Peninsula, México. *Sedimentary Geology*, **119**, 263-274.

CRITELLI, S., LE PERA,, E., & INGERSOLL, R.V. 1997. The effects of source lithology,

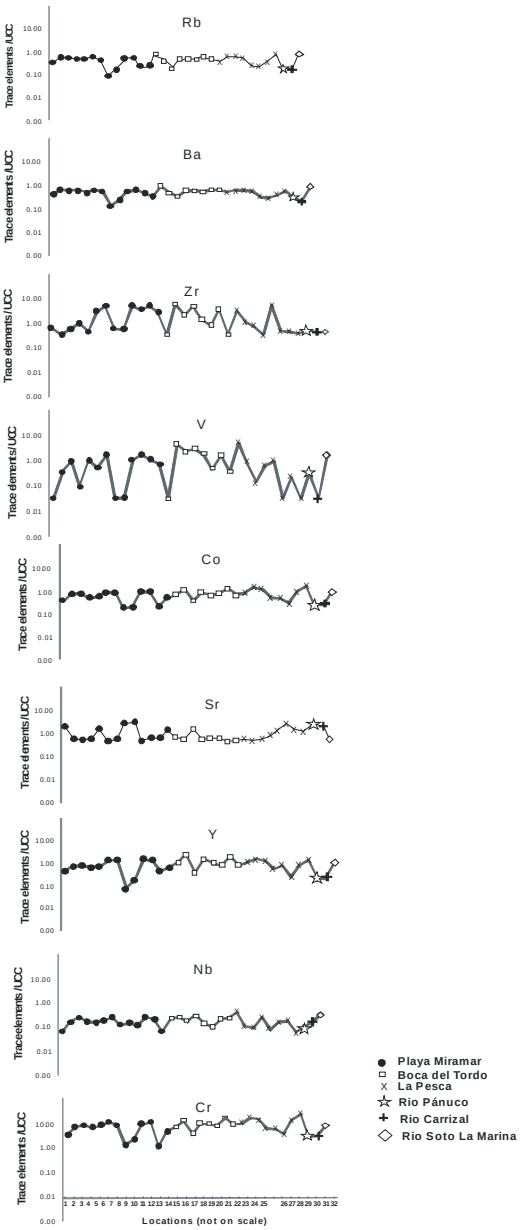

Fig.4. Trace elements tendencies along the northeastern coast of Mexico.

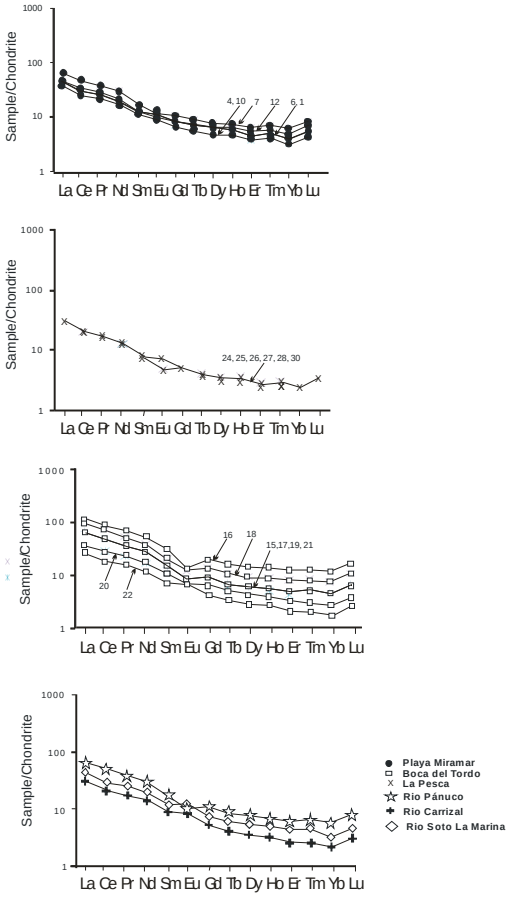

Fig.5. Rare earth elements in the northeastern coast of Mexico.

KASPER-ZUBILLAGA, J.J. & CARRANZA-EDWARDS, A., 2005. Grain size discrimination between sands of desert and coastal dunes from northwestern Mexico. *Revista Mexicana de Ciencias Geológicas,* **22**, 383-390.

KASPER-ZUBILLAGA, J.J., ACEVEDO-VARGAS, B., MORTON-BERMEA, O., & ORTIZ-ZAMORA, G., 2008a. Rare earth elements of the Altar Desert dune and coastal sands, North-western Mexico. *Chemie Der Erde Geochemistry*, **68**, 45-69.

KASPER-ZUBILLAGA, J.J., CARRANZA-EDWARDS, A., & MORTON-BERMEA, O. 2008b. Heavy minerals and rare earth elements in coastal and inland dunes of El Vizcaino Desert Baja Califonia Peninsula, Mexico. *Marine Geo-resources and Geotechnology*, **26**, 172-188.

SUTARNO, R. & STEGER, H.F., 1985. The use of certified reference materials in the ver-ification of analytical data and methods. *Talanta*, **32**, 439-445.

transport, deposition and sampling scale on the composition of southern California sand. *Sedimentology*, **44**, 653-671.

EVENSEN, M.N., HAMILTON, P.J., & ONIONS. P.K., 1978. Rare earth abundance in chondrite meteorites. *GeochimIca et. Cosmochimica Acta*, **42**, 1199-1212.

FOLK, R. L., 1974. *Petrology of Sedimentary Rocks.* Hemphill Publishing Co., Austin, TX.

IBBEKEN, H. & SCHLEYER, R., 1991.*Source and Sediment.* Springer Verlag. Berlin.

The Chemistry of black shale and exploration for VHMS, Mount Read Volcanics, Western Tasmania

Andrew W. McNeill[1]
1CODES, University of Tasmania, Private Bag 79, Hobart, TAS 7001 AUSTRALIA
(e-mail: andrew.mcneill@utas.edu.au)

ABSTRACT: Black shales in the hanging wall to the Pb-Zn VHMS deposits of the Mount Read Volcanics may have been altered by the underlying hydrothermal systems and the signature of such alteration may provide vectors to mineralisation. The major and trace element chemistry of the Rosebery Hanging wall Shale and the trace element chemistry of the pyrite and pyrrhotite that it contains have been investigated. Preliminary results indicate that a whole-rock Sb and Tl 'halo' at the base of the shale unit is not as extensive as has previously been suggested. The elevated Co, Zn, As and Mo contents and Co/Ni of 'early' pyrite, proximal to the orebody may provide vectors to underlying mineralisation.

KEYWORDS: *Exploration, Shale, VHMS, pyrite, geochemistry*

INTRODUCTION

The geochemical signature of footwall alteration of the major Pb-Zn VHMS deposits of the Mt Read Volcanics (MRV) is well constrained (Large *et al.* 2001b), and vectors such as elevated Tl have been used successfully (e.g., discovery of Y lens at the Rosebery Mine; McNeill, unpublished).

However, the characteristics of any hanging wall alteration, particularly in the black shales that overly Rosebery and Hellyer, the two major Pb-Zn VHMS deposits in the MRV, are not as well constrained. Previous studies of the well developed hanging wall alteration zone at Hellyer have defined its whole-rock geochemical signature (Sinclair 1994; Gemmell & Fulton, 2001) while studies of the sulfide trace element signature are ongoing (Layton-Matthews *et al.* 2008).

At Rosebery, studies of the hanging wall alteration by Large et al (2001a) indicated that, based on a limited dataset, whole-rock Tl, Sb, and Ba were all elevated in shale above the orebody, while characterisation of the trace element signature of sulfides is limited to two analyses of Co and Ni in pyrite by Loftus-Hills and Solomon (1967).

In this contribution I present the preliminary results of an investigation into the alteration signature of the Rosebery Hanging wall shale, using an expanded whole-rock chemical dataset and trace element analyses of pyrite and pyrrhotite, the major sulfide minerals in the shale.

METHODS

Rosebery Hanging-wall Shale samples were selected from drill core in proximal (<120m from ore), medial (~1000m) and distal (>4km) locations.

Whole-rock compositions were determined by XRF and solution ICP-MS using the methods outlined by Yu *et al.* (2001) and Robinson (2003).

LA-ICPMS analyses of pyrite and pyrrhotite in both spot and imaging mode (for 32 and 22 elements respectively) were completed on a New Wave 213nm solid-state laser microprobe coupled to an Agilent 4500 quadrupole ICPMS using the procedures of *Large et al.* (*submitted*).

WHOLE-ROCK GEOCHEMISTRY

Vertical sections through the Rosebery Hanging wall shale were sampled in drill holes from proximal and medial locations and results compared with those from

distal locations, including shale units stratigraphically higher and lower in the sequence.

Preliminary results indicate that base and precious metal, As, and Ba contents of shale in proximal and medial locations are within the range of shale samples from distal locations. Only Sb, up to 23 ppm, and Tl, up to 9 ppm, in the lower 10-15m of the hanging wall shale are significantly higher than in medial and distal samples, with <8 ppm Sb and <1.4 ppm Tl.

SULFIDE MINERAL CHEMISTRY

Pyrrhotite

Anhedral pyrrhotite, from <10-200 μm in diameter, occurs in the matrix and in veins in all but one of the analysed samples. Visually the pyrrhotite appears to be inclusion-free, but Rare Pb- and Zr+REE-rich inclusions were found during analysis and it was noted that pyrrhotite in contact with pyrite generally has lower Co contents than other grains (3 ppm vs 280ppm, respectively, in samples from one drill hole) and have not been used for interpretation.

Trace elements, in order of decreasing abundance are Ni, Co, Se, Pb, Sb, Ag and Bi. The only statistically significant difference in composition between pyrrhotite from proximal and distal samples is the lower Co contents of the latter.

Pyrite

Three textural types of pyrite occur in all samples examined; 1) early framboids or irregular masses, 2) isolated euhedra, and 3) pyrites with massive cores and 'spongy' or porous rims (Fig. 1). Types 2 and 3 occur in both shale and cross-cutting to bedding parallel veins, whereas type 1 occurs in shale only.

Compositional variations among all textural types are obvious (Fig. 1) and a comparison of type 1 pyrite in proximal and distal locations is shown in Fig. 2 (Note that data have not been included for elements where a large proportion [>40%] of results were below detection limit).

The elevated Zn, As, Co and Mo which appear to distinguish proximal from distal

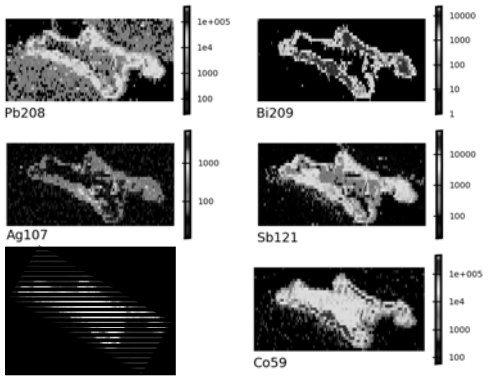

Fig. 1. LA-ICPMS maps of trace element variations in pyrite from a bedding parallel quartz-carbonate vein. The two textural types are a "spongy" discontinuous rim with higher Pb, Bi, Ag, Sb and Co contents than the 'massive' core.

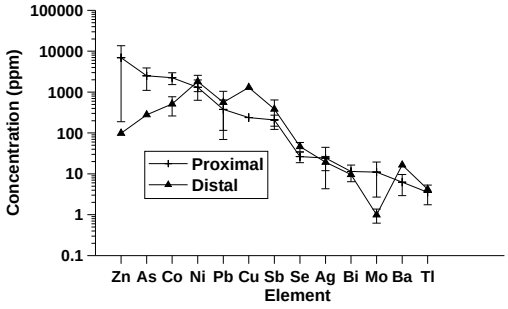

Fig. 2. Trace element variations in type 1 pyrite. Average values for pyrite in proximal (n=10) and distal (n=5); bars indicate 1σ. Note log scale.

type 1 pyrite result from the presence, interpreted from the time-integrated LA-ICPMS signal profile, of inclusions and micro-inclusions in the case of Zn and predominantly lattice substitution, as indicated by generally smooth profiles, in the case of Mo, Co and As.

The Co/Ni of type 1 pyrite from distal samples is 0.15-0.5 compared with 1.0-4.0 in proximal samples, consistent with the results of Loftus-Hill and Solomon (1967) who recorded ratios of 0.03-0.4 and 0.8 respectively (note that the 'distal samples in this earlier study are largely from shale units closer to the Hellyer orebody).

CONCLUSIONS

Preliminary results indicate that the alteration signature of shales in the Hanging wall of the Rosebery orebody is characterised by:
(1) Elevated Co in pyrrhotite.
(2) Elevated Zn, As, Co and Mo and Co/Ni in early (type 1) pyrite.
(3) Elevated Sb and Tl in whole-rock samples from the lower 10-15m of the shale unit proximal (<120m) to the orebody.

These represent potential vectors to mineralisation that may be applied in exploration drill programs.

ACKNOWLEDGEMENTS

I thank Zinifex Limited (now Oz Minerals) for financial support and for permission to present these results. D. Hicks, C. Archer and M. Skirka (Zinifex) and M. Jacobson (MRT) facilitated access to drill core and other data. P. Robinson, K. McGoldrick and S. Gilbert completed the XRF and solution ICPMS analyses and S. Gilbert provided assistance and advice on LA-ICPMS analyses.

REFERENCES

GEMMELL, J.B. & FULTON, R.L. 2001. Geology, genesis and exploration implications of the footwall and hanging-wall alteration associated with the Hellyer volcanic-hosted massive sulfide deposit, Tasmania, Australia. *Economic Geology*, **96**, 1003-1035.

LARGE, R.R. *et al. Submitted*. Gold and trace element zonation in pyrite using a laser imaging technique; implications for the timing of gold in orogenic and Carlin-style sediment-hosted deposits. *Economic Geology*.

LARGE, R.R., ALLEN, R.L., BLAKE, M.D., & HERRMANN, W. 2001a. Hydrothermal alteration and volatile element haloes for the Rosebery K Lens volcanic-hosted massive sulfide deposit, Western Tasmania. *Economic Geology*, **96**, 1055-1072.

LARGE, R.R., MCPHIE, J., GEMMELL, J.B., HERRMANN, W., & DAVIDSON, G.J. 2001B. The spectrum of ore deposit types, volcanic environments, alteration halos and related exploration vectors in submarine volcanic successions: some examples from Australia. *Economic Geology*, **96**, 913-938.

LAYTON-MATTHEWS, D., GEMMELL, J.B., LARGE R.R., & PETER J. 2008. Trace-element budget of the Que River shale: exploration implications of hanging-wall modification of sulfide minerals at the Hellyer deposit, Tasmania, *Abstract. 33rd International geological Congress, Oslo.*

LOFTUS-HILLS, G & SOLOMON, M. 1967. Cobalt, Nickel and Selenium in sulphides as indicators of ore genesis. *Mineralium Deposita*, **2**, 228-242.

ROBINSON, P. 2003. *XRF* analysis of flux-fused discs. Abstract. *Geoanalysis 2003, Finland.*

SINCLAIR, B.J. 1994. *Geology and geochemistry of the Que River Shale, western Tasmania.* BSc (Hons.) Thesis, University of Tasmania, Hobart.

YU, Z, ROBINSON, P., & MCGOLDRICK, P. 2001. An evaluation of methods for the chemical decomposition of geological materials for trace element determination using ICP-MS. *Geostandards Newsletter*, **25**, 199-217.

Weathering-related rare earth element patterns in the regolith of the Cobar region, western New South Wales

K.G. McQueen
Faculty of Applied Science, University of Canberra, ACT, 2601
AUSTRALIA (e-mail: Ken.McQueen@canberra.edu.au)

ABSTRACT: Analysis of REE distributions through weathered profiles on siliclastic metasedimentary rocks in the Cobar region indicates that older profiles (60-20 Ma), beneath Paleocene lake sediments and Early Miocene lava flows, commonly show depletion of light rare earths (LREE) in the upper saprolite. Cerium which is depleted in the upper saprolite can be markedly enriched near the base. Younger profiles formed after erosional stripping in the Miocene (<20 Ma) and under drier climatic conditions do not show LREE fractionation (flat pattern) and either have REE abundances similar to the unweathered parent rock or show some overall REE enrichment due to profile leaching, collapse and concentration of host resistate minerals. These various patterns reflect different climatic and weathering regimes in the long history of sub-aerial exposure of the Cobar terrain. The REE patterns could be used to identify weathering profiles of different ages and different degrees of chemical leaching.

KEYWORDS: *REE, fractionation, weathering, climate, geochemistry*

INTRODUCTION

The Rare Earth Elements (REE-Lanthanides and Y) are commonly used to unravel rock-forming processes because of their similar chemical properties, typically low solubilities and assumed resistance to fractionation in crustal and surface environments. However, under some weathering conditions REE are significantly mobilised and fractionated (e.g., Nesbitt 1979; Duddy 1980; Sharma & Rajamani 2000).

REE patterns have been investigated down a series of weathered profiles formed under different weathering regimes in the Cobar region of western New South Wales. The patterns vary and appear to reflect the weathering history of individual profiles, providing a means for recognising different weathering regimes and the associated processes of leaching and element dispersion. This knowledge could assist geochemical exploration in regolith dominated terrains.

GEOLOGICAL SETTING

The Cobar region is underlain by Palaeozoic rocks of the central Lachlan Orogen of eastern Australia. It contains mainly siliclastic metasedimentary rocks (originally turbiditic shales, siltstones and quartzites), some mafic to felsic volcanic rocks and granites. The region is a major metallogenic province for base metal and gold deposits, with more than 12 mined deposits and active exploration. The bedrocks and contained mineral deposits have had a long history (>65 Ma) of sub-aerial exposure and weathering under contrasting climatic regimes. Weathering, erosion and deposition have produced an extensive regolith with both *in situ* and transported components that renders mineral exploration difficult.

WEATHERING HISTORY

The climatic and weathering history of the Cobar region has been established using a combination of palynological records, palaeomagnetic dating of ferruginous weathering zones, $^{40}Ar/^{39}Ar$ dating of manganese oxides, $\delta^{18}O$ characteristics of weathering clays and relative dating techniques (Fig. 1). In broad terms, climatic conditions were warm and humid from the Late Cretaceous to the Early Miocene with some cooler periods. The climate then became predominately cooler, drier and more seasonal through

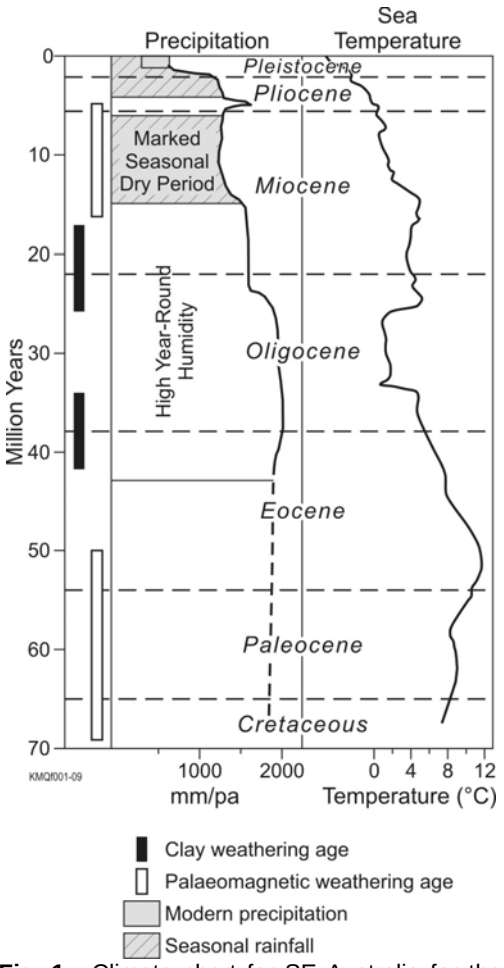

Fig. 1. Climate chart for SE Australia for the Cenozoic with dated weathering features from the Cobar region. Estimated precipitation from palynological records (Martin 1991), ocean water temperature (Zachos *et al*. 2001), hematite fixation and clay weathering ages (McQueen *et al.* 2002, 2007; Smith 2006).

the later Cenozoic, but with a significant short warmer and wetter period in the Late Miocene. Palaeomagnetic dating indicates periods of intense oxidation and possible drying of profiles after prolonged weathering in the Late Cretaceous to Paleocene (ca. 60±10 Ma) and the Early Miocene (15±5 Ma).

METHODS

Most of the samples for this study were collected by air-core drilling through the regolith. Samples were 1 kg splits taken with a sample spear from larger bulk samples representing 1 m intervals. One exposed weathered profile preserved beneath a Miocene leucitite lava flow was sampled in outcrop. Sub-samples from the homogenised and pulverised samples were analysed by fusion disc X-ray fluorescence (XRF) for major elements. REE and other trace elements were analysed by inductively coupled plasma mass spectrometry (ICP MS) following multi-acid digestion of the fusion discs.

RARE EARTH ELEMENT PATTERNS

Four weathered profiles in different landscape settings and of different ages were examined. All profiles were developed on siliclastic metasedimentary rocks (siltstone-sandstone).

The oldest profile (CBAC 215) was preserved beneath Paleocene lake sediments. The least weathered saprock in this profile (59 m beneath the unconformity) has a REE pattern very similar to North American shale composite (NASC). The light REE show marked relative depletion in the upper part of the profile and enrichment near the weathering front. Cerium shows marked enrichment at depth (Fig. 2).

The second profile is Early Miocene in age and preserved beneath a leucitite lava flow dated at 17.1±0.2 Ma. The ferruginised upper part of the profile has been palaeomagnetically dated at 15±5Ma (McQueen *et al*. 2007). This profile also shows light REE depletion in the upper part, but not as marked as in the older profile (Fig. 3). There is also slight, relative enrichment in the heavy REE in the upper part of the profile.

A third profile (BRAC 1) was examined beneath Late Miocene alluvial sands and ferruginous gravels. This profile is considered to be mid Cenozoic in age and has been partly eroded. The upper part of this profile below the unconformity has a similar REE pattern to NASC. Deeper in the profile there is relative enrichment in all the REE, but slightly more marked in the light REE (Fig. 4).

The fourth weathering profile is in an area of post Miocene erosion, which has exposed areas of saprock. This profile

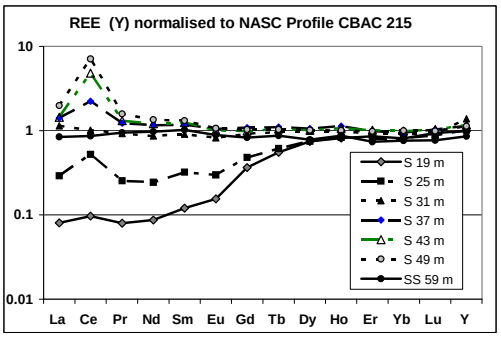

Fig. 2. REE pattern in a Late Cretaceous to Paleocene weathering profile preserved beneath Paleocene lake sediments. S is saprolite, SS is saprock.

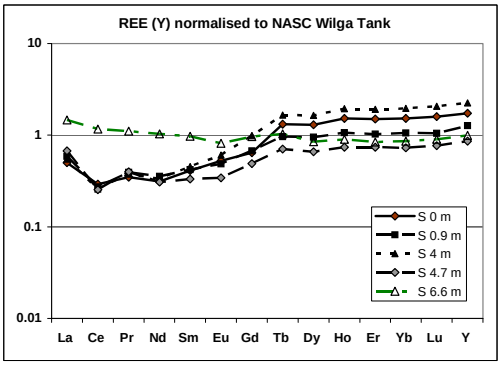

Fig. 3. REE pattern in Miocene profile preserved beneath leucitite lava flow at Wilga Tank. S is saprolite.

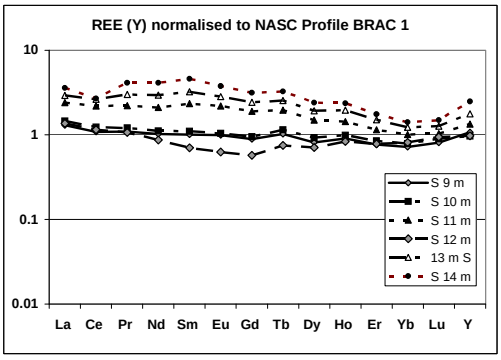

Fig. 4. REE pattern in a partly eroded mid Cenozoic weathering profile beneath Late Miocene alluvial sediments. S is saprolite.

was sampled above the current water table and weathering front. It shows a REE pattern for all samples very similar to NASC, with no significant depletion or enrichment (Fig. 5).

DISCUSSION

The various differences in the REE patterns reflect both the regolith-landform setting and the timing of profile formation within the long history of weathering that has occurred under contrasting climatic regimes. The main control on REE patterns is the varying stability of accessory REE host minerals (particularly apatite, monazite, titanate and zircon) under the different weathering regimes. Oxidation of Ce^{3+} to Ce^{4+} and precipitation of CeO_2 is a likely mechanism for Ce concentration deeper in profiles at redox boundaries. Interestingly, Ce has also been concentrated in carbonates within saprolite surrounding the New Cobar sulfide deposit. This deposit was exposed and weathered through the Cenozoic. Residual concentration and mechanical transfer of residual resistate minerals during profile compaction and collapse have probably also affected REE abundances, particularly the overall enrichment in profile BRAC 1.

The different REE patterns provide a technique for identifying weathered profiles formed under particular climatic and weathering regimes at different stages of the Cobar weathering history. This would be very useful at sites where there are no other age constraints. REE fractionation also provides a means of recognising *in situ* regolith that has been subjected to intense and prolonged chemical weathering and element leaching. Identifying strongly leached regolith has important implications for sampling and anomaly detection during geochemical exploration.

CONCLUSIONS

REE patterns in weathered siliclastic metasedimentary rocks in the Cobar region vary depending on the stage and conditions of weathering.

(1) Older profiles formed under warm and humid climates show depletion of LREE in the upper saprolite and enrichment (particularly for Ce) towards the base

(2) Post Miocene profiles show little fractionation, but in some cases have been residually enriched in all the REE.

(3) REE can be significantly mobilised

.

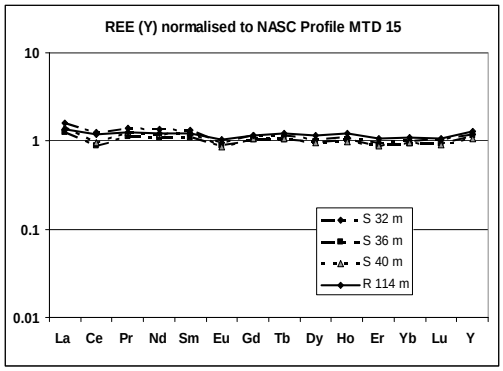

Fig. 5. REE pattern in a post Miocene weathering profile. S is saprock/saprock, R fresh rock.

during intense and prolonged weathering depending on the stability of their host minerals.

ACKNOWLEDGEMENTS

The work reported here was supported by the Australian Government Cooperative Research Centre Program within CRC LEME. The regolith drilling was carried out by the NSW Department of Primary Industries and by Cobar Management Pty Ltd. Sample analyses were performed at Geoscience Australia with the assistance of Bill Papas. I thank my many colleagues in CRC LEME for their help in sampling.

REFERENCES

DUDDY, I.R. 1980. Redistribution and fractionation of rare-earth and other elements in a weathering profile. *Chemical Geology,* **30**, 363-381.

MARTIN, H.A. 1991. Tertiary stratigraphic palynology and palaeoclimate of the inland river systems in New South Wales. In: WILLIAMS, M.A.I., DE DEKKER, P., & HERSHAW, A.P. (eds.), *The Cainozoic in Australlia: A re-appraisal of the evidence.* Geological Society of Australia Special Publication, **18**, 181-194.

MCQUEEN, K.G., GONZALEZ, O.R., ROACH, I.C.. PILLAND, B.J., DUNLAP, W.J., & SMITH M.L. 2007. Landscape and regolith features related to Miocene leucitite lava flows, El Capitan northeast of Cobar, NSW, Australia. *Australian Journal of Earth Sciences,* **54**, 1-17.

MCQUEEN, K.G., PILLANS, B.J., & SMITH, M.L. 2002. Constraining the weathering history of the Coare region, western NSW. In: PREISS, V.P. (ed.), *Geoscience 2002: Expanding Horizons, Abstracts of the 16th Australian Geological Convention, Adelaide, 1-5 July 2002*, **67**, 246.

NESBIT, H.W. 1979. Mobility and fractionation of rare earth elements during weathering of a granodiorite. *Nature,* **279**, 206-210.

SHARMA, A. & RAJAMANI, V. 2000. Major element, REE and other trace element behaviour in amphibolite weathering under semiarid conditions in southern India. *The Journal of Geology,* **108**, 487-496.

SMITH, M.L. 2006. *Towards a geochronology for long-term landscape evolution of northwestern New South Wales, Australia.* Ph`D thesis, Australian National University.

ZACHOS, J. PAGANI, M., SLOAN, L., THOMAS, E. & BILLUPS, K. 2001. Trends, rhythms, and aberrations in global climate 65 Ma to present. *Science*, **292**, 686-693.

Lithogeochemical vectors to ore: a study of the Elura Zn-Pb-Ag deposit, Cobar, NSW, Australia

K.G. McQueen[1] & M.A.I. Whitbread[2]
1Faculty of Applied Science, University of Canberra, ACT, 2601 AUSTRALIA
(e-mail: Ken.McQueen@canberra.edu.au)
2Io Geochemistry, PO Box 433, Sumner Park BC, QLD, 4074 AUSTRALIA

ABSTRACT: Hydrothermal alteration around the Elura Zn-Pb-Ag sulfide deposit has produced detectable and systematic chemical changes that are also reflected in subtle mineralogical features. Iron carbonate development accompanied by potassic alteration, the destruction of albite and absence of chlorite are the dominant mineral alteration effects in the surrounding host rocks. Key elements enriched in the primary dispersion zone are Zn, Pb, Ag, As, Rb, Tl, and particularly Sb. Sodium is strongly depleted. Cryptic alteration and primary dispersion can be detected up to 300 m from the ore body below the weathering front. Pearce Element Ratio (PER) and General Element Ratio (GER) techniques more clearly identify and quantify this alteration and could assist in vectoring towards high intensity alteration adjacent to ore during exploration drilling.

KEYWORDS: *lithogeochemistry, exploration, hydrothermal, alteration, drilling*

INTRODUCTION

Mineral exploration for blind ore systems is increasingly dependant on better methods of vectoring to mineralisation during drilling. Lithogeochemical features in and around ore deposits, particularly recognition of cryptic alteration and primary dispersion zoning, can indicate relative proximity to ore and provide tools to navigate within the ore system. This study of the Elura Zn-Pb-Ag deposit has defined the key lithogeochemical features developed around a sediment-hosted, structurally controlled, hydrothermal ore system. The approach used for detecting cryptic alteration could be applied in exploration for similar deposits.

NATURE OF THE ELURA DEPOSIT

The Elura deposit (45 Mt @ 8.5% Zn, 5.3% Pb, 69 ppm Ag) is located 43 km north-northwest of Cobar in western New South Wales (Lorrigan 2005). The deposit is hosted by weakly metamorphosed and deformed turbiditic sedimentary rocks of the Early Devonian Cobar Basin. It consists of a series of vertical, pipe-like sulfide concentrations composed of varying proportions of pyrrhotite, pyrite, sphalerite, galena and accessory sulfide minerals. The sulfide-rich pods are discreet entities aligned along a NNW trend. They are connected along strike, attaining a sheet-like morphology to the north. The outer part of the ore system consists of enveloping low-grade vein and stringer mineralisation (Lawrie & Hinman 1998; Schmidt 1990). The main sub-cropping pod was discovered by its magnetic signature and near surface geochemical expression in the regolith, and by drilling. The deeper northern pods were not detected until after mining of the main pod had commenced.

METHODS

The primary dispersion halo and wallrock alteration around the Elura deposit was established from integrated petrographic, mineralogical and geochemical (major-, minor- and trace-element) analysis of diamond drill core samples. Seventy eight samples of variably altered and unaltered host rocks, as well as 67 near-surface weathered equivalents, were analysed for major elements using fusion disc, X-ray fluorescence analysis (XRF). Trace elements were determined by pressed powder XRF analysis. Carbonate carbon

and absorbed and structural H_2O were determined by LECO analysis.

A key aspect of the study was the separate investigation of the silt-sand and clay dominant components of the turbiditic host rocks. The Pearce Element Ratio (PER) technique was used to avoid closure effects in the compositional data for variably altered rocks around the ore system, and to assess element changes (Pearce 1968; Stanley & Medeisky 1995). As a second step in the data analysis the General Element Ratio (GER) technique was applied to test the likely mineral assemblages in unaltered, altered and weathered rocks and to explore changes in these assemblages caused by alteration and subsequent weathering.

RESULTS

Preliminary analysis of the geochemical data indicated that Ti and Nb, significantly concentrated in fine-grained rutile-anatase, were the most conserved elements during hydrothermal alteration and weathering. Due to its greater abundance and lower relative analytical error, Ti was selected as the conserved denominator element in the PER analysis. Changes in PER values for major- and trace-elements with distance from ore are listed in Table 1.

Key indicators of alteration and proximity to ore are: increased K_2O (particularly in the shale component); near complete loss of Na_2O; increased FeO (particularly in the siltstone-sandstone component); and increased CO_2 in shale. These changes reflect the development of iron carbonate (siderite and ankerite) by carbonate introduction and some alteration of existing calcic carbonate in siltstone-sandstone samples. Destruction of albite, absence of chlorite and increased abundance of muscovite due to potassic alteration, are the other major mineral alteration effects in the altered host rocks. Trace elements enriched in the primary dispersion zone are Zn, Pb, Ag, Sb, As, Rb, and Tl. Antimony provides the most consistent and extensive trace element dispersion halo around the deposit and is also preserved in most of the weathered alteration zone rocks. Figures 1-3 illustrate key element variation patterns within the cryptic alteration zone around the Elura deposit.

Table 1. Summary of PER changes in altered host rocks with distance from the Elura orebody. Sst = siltstone-sandstone component.

Element/ oxide	*PER variations (El/TiO_2) with distance from orebody.*
Ag	Increased up to 80 m.
As	Increased but poor resolution.
Ba	Increased but poor resolution.
Pb	Spot highs, unreliable.
Rb	Increased up to120 m in shale 80 m in sst.
Sb	Increased up to 200 m.
Tl	Increased up to 40 m in shale.
Zn	Spot highs unreliable.
CaO	No systematic difference.
CO_2	Increased in shale.
FeO	Increased up to 100 m in sst.
K_2O	Increased up to 130 m in shale 70 m in sst.
MgO	Loss in shale, gain in sst
Na_2O	Near complete loss >250 m.

GER analysis incorporating element combinations designed to reflect the main minerals of the unaltered, altered and weathered rocks reveals clear separation of these different compositions and explains the mineralogical changes during alteration (Fig. 4). Unaltered shale compositions cluster toward the muscovite/ankerite node of the muscovite/ankerite-chlorite/albite/calcite assemblage, whereas unaltered siltstone-sandstone samples cluster towards the chlorite/albite/calcite node. The altered equivalents plot closer to the muscovite/ankerite node and most of the altered shale lies beyond this node, consistent with the presence of significant non-calcic carbonate (e.g., siderite). This provides a method for clearly defining the altered rocks around the Elura deposit. The compositions of weathered rocks from both unaltered and altered precursors define a clear trend towards the goethite/hematite/kaolinite node. This trend is explained by the initial weathering breakdown of calcite-albite and most

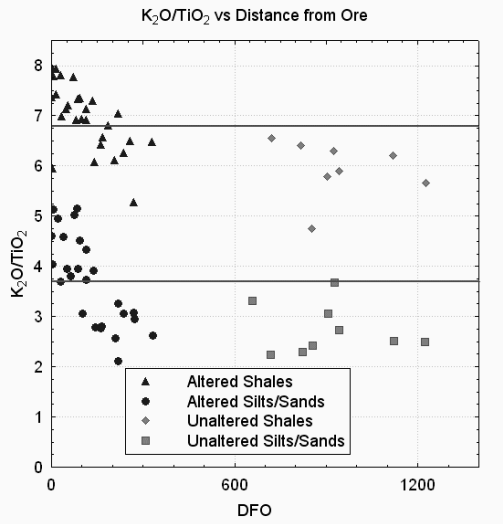

Fig. 1. Variation in K_2O/TiO_2 with distance (m) from the Elura ore deposit.

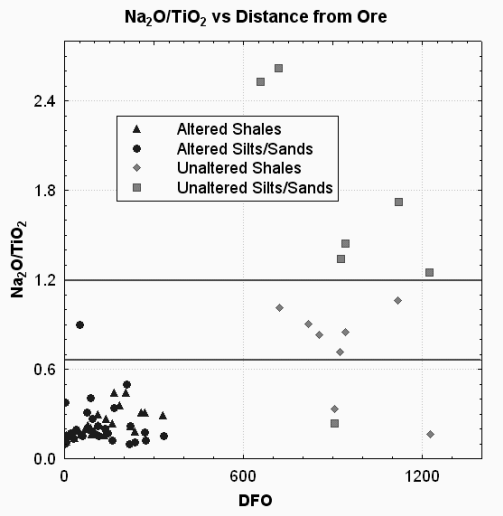

Fig. 2. Variation in Na_2O/TiO_2 with distance (m) from the Elura ore deposit.

chlorite to produce an assemblage dominated by relict muscovite and some kaolinite-goethite and then a progressive increase in goethite-hematite-kaolinite with further chemical weathering. Unfortunately any distinction between altered and unaltered precursor rocks is largely lost during the weathering.

DISCUSSION

Hydrothermal alteration associated with the formation of the Elura deposit has produced visible mineralogical changes in

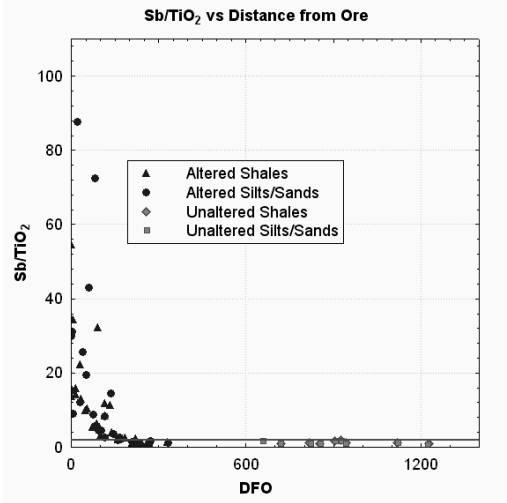

Fig. 3. Variation in Sb/TiO_2 with distance from ore (DFO) in metres at the Elura ore deposit.

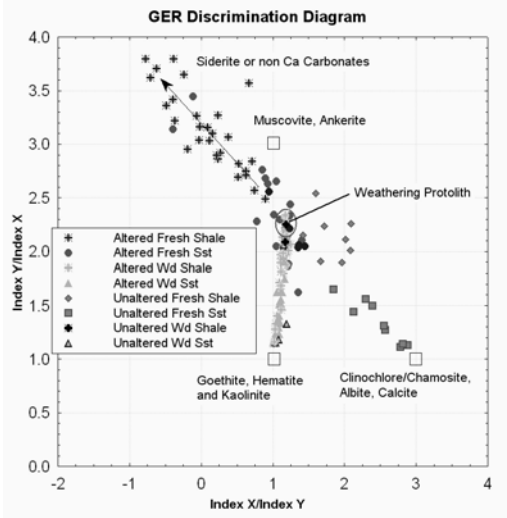

Fig. 4. GER discrimination diagram for unaltered, altered and weathered rocks around the Elura ore deposit. Also shown are the nodal positions of major minerals in the various rocks and their weathered equivalents.

a narrow zone around the deposit. These include an inner irregular zone of silicification with some sericitization and a surrounding zone 5-70 m wide of carbonate spotting.

Lithogeochemical analysis can detect the cryptic alteration that extends around the visible alteration zone out to 300 m from the orebody. The key major element features are: increased K_2O content; increased FeO in carbonates; increased

CO_2, most obvious in shale; and depletion of Na. Many ore-related elements show primary dispersion (up to 300 m in the case of Zn), but their distribution is patchy or inconsistent. Antimony provides the most consistent primary dispersion pattern for the trace elements.

Pearce Element Ratios provide a clearer indication of the chemical alteration effects and the true change in intensity with proximity to ore. The technique can be applied in both visibly and cryptically altered rocks with a very high degree of success in classifying alteration in unweathered rocks. General Element Ratios (GERs) are also useful in separating unaltered, altered and weathered rock compositions and in understanding the mineralogical controls involved.

This study has shown that there are important differences in the alteration effects observed in the fine and coarse fractions of the host turbidite units. It is critical to examine and analyse these end members separately as many of the key lithogeochemical features of the alteration would be obscured in bulk samples.

The very prolonged weathering of the Cobar terrain under a wide range of climatic conditions has destroyed most of the key lithogeochemical features in the resulting regolith. However, indications are variably provided by molar K/Al ratios and preserved relative enrichment in some trace elements (Sb, Tl, Ag, and patchy Pb).

CONCLUSIONS

Hydrothermal alteration related to formation of the Elura deposit can be detected in the host rocks up to 300 m from ore using lithogeochemical techniques. The effects can be reliably quantified within 250 m of the ore.

Proximity to ore is best indicated by PER values of:
(1) Molar K vs Al in shale;
(2) Molar K vs (Al-Na) in sandstone-siltstone;
(3) Molar Ca vs carbonate C in shale; and
(4) Sb in both rock types.

ACKNOWLEDGEMENTS

We thank the management and staff of Pasminco Exploration for initiating and assisting with research on the Elura deposit. The work was conducted as part of a CRC LEME PhD project. MW acknowledges the support of a CRC LEME scholarship. Sample analyses were performed by INAX Services, Australian National University.

REFERENCES

LAWRIE, K.C. & HINMAN, M.C. 1998. Cobar-style polymetallic Au-Cu-Ag-Pb-Zn deposits. *AGSO Journal of Australian Geology and Geophysics,* **17**,169-187.

LORRIGAN, A.N. 2005. Elura Zn-Pb-Ag deposit, Cobar district, NSW. In: BUTT, C.R.M., ROBERTSON, I.D.M., SCOTT, K.M., & CORNELIUS, M. (eds), *Regolith Expression of Australian Ore Systems*. CRC LEME, Perth, 143-145.

PEARCE, T.H. 1968. A contribution to the theory of variation diagrams. *Contributions to Mineralogy and Petrology*, **19**, 142-157.

SCHMIDT, B.L. 1990. Elura zinc-lead-silver deposit, Cobar. In: HUGHES, F.E. (ed.), *Geology of the Mineral Deposits of Australia and Papua New Guinea.* The Australasian Institute of Mining and Metallurgy, Melbourne, **2**, 1329-1326.

STANLEY, C.R. & MADEISKY, H.E. 1995. Pearce element ratio analysis in lithogeochemical exploration. *17th International Geochemical Exploration Symposium, Association of Exploration Geochemists, Annual Meeting, Short Course,* Townsville, Queensland, Australia, May, 96 p.

Lithogeochemistry of the Quebrada Blanca Porphyry Cu Deposit, Atacama Desert, Northern Chile

Tamara Moss & Cliff Stanley
Dept. of Earth & Environmental Science, Acadia University, Wolfville, Nova Scotia, CANADA B4P 2R6
(e-mail: 091163m@acadiau.ca)

ABSTRACT: Despite intense weathering, the geology of the supergene and leached cap zones at the Quebrada Blanca (QB) porphyry Cu deposit, northern Chile, can be understood using major oxide lithogeochemical data. Five supergene and four hypogene drill cores from a NS cross-section across the QB open pit were logged, and samples from the hypogene zone were examined mineralogically and petrographically. Pre-existing major oxide lithogeochemical data, mostly from drill cores through the supergene zone (n = 7540), and new petrological and lithogeochemical data (n = 178) from deep drill cores through the hypogene zone, were evaluated. Lithologies at QB include Carboniferous diorite intruded by Late Eocene equigranular granodiorite, and then by quartz-feldspar porphyry dykes associated with mineralization. In general, weak to moderate potassic alteration in these three lithologic units is locally overprinted by strong phyllic alteration. Weathering processes significantly affect the supergene rocks, but do not impede recognition of lithology or hydrothermal alteration style and intensity in the supergene and leached cap zones.

KEYWORDS: *Quebrada Blanca, Collahuasi district, porphyry Cu deposit, lithogeochemistry, molar element ratio, supergene weathering, Chile.*

INTRODUCTION

The Quebrada Blanca (QB) porphyry Cu deposit (21°24' S, 68°55' W) is located 1,500 km north of Santiago in the Tocopilla Province, Chile (Region 1). Located at 4,300 m elevation in the Atacama Desert, QB is less than 10 km west of the Rosario and Ujina porphyry Cu deposits, which together with QB make up the Collahuasi porphyry Cu district. QB is also located east of the West Fissure within the Domeyko fault system, a major crustal structure controlling the location of large economic porphyry Cu deposits, including the Chuquicamata porphyry Cu deposit located ~150 km south of QB.

To date, only the supergene enrichment zone at QB has been mined. Unfortunately, intense weathering has impeded a thorough understanding of the geology of this zone. This research attempts to advance knowledge of the geology at QB by investigating: (*a*) the igneous rocks that host mineralization, (*b*) the nature of hydrothermal alteration that has affected these rocks, (*c*) how host rock compositions control the resulting alteration mineral assemblages, and (*d*) how weathering processes have affected hypogene rocks.

METHODS

Two lithogeochemical datasets were investigated to advance understanding of the lithologies, mineralization, and hydrothermal alteration at QB. The first dataset consists of 7540 samples from historic NQ core and RC chips mostly from the supergene enrichment and leached cap zones (the 'supergene dataset'). These were analyzed for major oxides and some trace elements by XRF at several laboratories in Chile. The second dataset was smaller (n = 178), but consists only of recent NQ drill core samples from the hypogene zone (the 'hypogene dataset'). These were analyzed for major oxide and a more extensive suite of trace elements by fusion or aqua regia/ICP-OES or ICP-MS at Acme Analytical Laboratories, Canada.

Geological control for data interpretation was provided by detailed logging of nine drill cores through the QB supergene

(DDH098, 023, 112, 115, 125) and hypogene (DDH313, 275, 259, 270) zones. The drill cores are from the 19,600 m E cross-section through the open pit. Samples from the hypogene cores were collected and examined via thin section petrography, Na-cobaltinitrate staining, electron microprobe analysis, scanning electron microscopy, and x-ray diffraction analysis. Results provide constraints to interpret the characteristics of both supergene and hypogene lithogeochemical datasets.

Molar element ratio (MER) analysis was carried out on both lithogeochemical datasets because of its ability to avoid closure and isolate the impacts of different geochemical processed using projective geometry Because weathering did not affect the hypogene dataset, the un-weathered samples provided the geological control necessary to interpret results from the supergene dataset.

PETROLOGY

Three intrusions occur in the QB open pit and drill core. These consist of: (*i*) Carboniferous diorite that was intruded by (*ii*) Late Eocene granodiorite, and (*iii*) later quartz-feldspar porphyry dykes of granodiorite composition.

Diorite is medium grey, equigranular and composed of plagioclase (cgr, anh, 50 - 80 %) and biotite (fgr, anh, 20 - 50 %), probably after clinopyroxene. Equigranular granodiorite (formerly known as quartz monzonite) is light to medium grey and composed of quartz (fgr to cgr, anh, 20 - 75 %), plagioclase (fgr to mgr, anh, 10 - 60 %), biotite (fgr to cgr, in clusters, 5 - 25 %), and chlorite after biotite (vfgr to cgr, in clusters, 2 – 10). Quartz-feldspar porphyry (QFP; formerly known as feldspar porphyry or plagioclase porphyry) is white to dark grey and composed of plagioclase (mgr to cgr, euh, porphyritic, 30 - 60 %), quartz (fgr to mgr, porphyritic, partially resorbed 'eyes' & some square section cristobalite, 2 - 40 %), biotite (vfgr to cgr, porphyritic, subh, 3 - 15%), chlorite (cgr, partially replacing biotite, 5 %) in a very fine grained groundmass of biotite and subordinate quartz (Fig. 1).

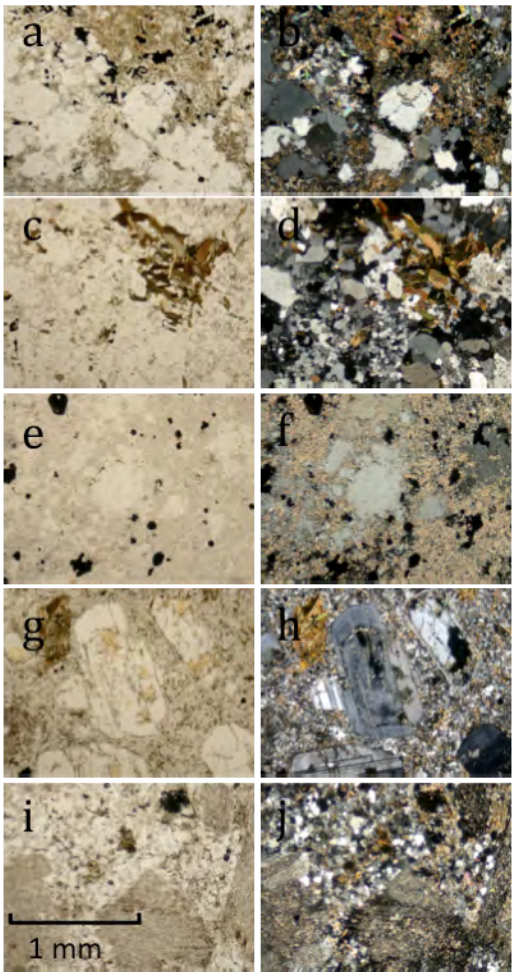

Fig. 1. Phyllically altered diorite in (a) PPL and (b) XPL; fresh granodiorite in (c) PPL and (d) XPL; phyllically altered granodiorite in (e) PPL and (f) XPL; fresh QFP in (g) PPL and (h) XPL; phyllically altered QFP in (i) PPL and (j) XPL. All samples are from hypogene drill cores and are un-weathered.

LITHOGEOCHEMICAL ANALYSIS

Hypogene Dataset

A conserved element scatterplot of the hypogene lithogeochemical dataset (Fig. 2) illustrates that Zr/TiO_2 ratios can be used to identify QB intrusive rocks.

Furthermore, a Pearce element ratio (PER) scatterplot testing feldspar compositional control (Fig. 3) illustrates that some hypogene rocks have compositions controlled by feldspar (primary igneous or potassic alteration),

whereas others are controlled by muscovite (phyllic alteration). Lastly, diorite samples have lower Al/Ti ratios than granodiorite samples, which in turn have lower Al/Ti ratios than QFP samples.

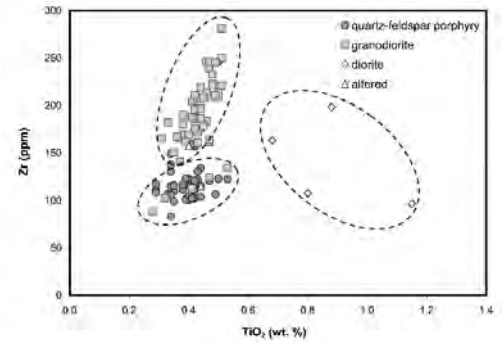

Fig. 2. A conserved element scatterplot of TiO_2 vs. Zr can be used to classify the hypogene data.

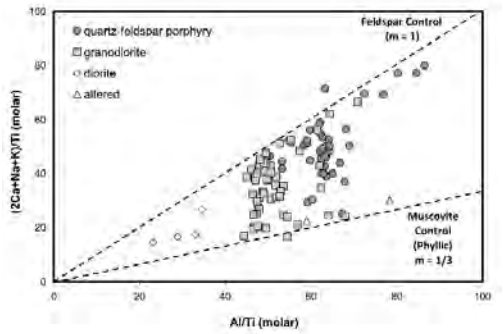

Fig. 3. PER scatterplot of hypogene data testing feldspar (fresh igneous or potassic alteration) and muscovite (phyllic alteration) compositional controls.

A MER scatterplot (Fig. 4) illustrates that most of the intensely phyllically altered samples within the hypogene dataset are granodiorite. Additionally, Figure 5 illustrates that hypogene samples can be compositionally described as mixtures of muscovite (phyllic alteration) and albite, andesine, or oligoclase (fresh igneous plagioclase). Many QFP samples are fresh or have only minor propylitic alteration. Less altered samples contain An_{10} (in the granodiorite) or An_{10} to An_{35} (in the QFP). Figure 6 illustrates that the hypogene dataset does not contain strongly potassically-altered samples.

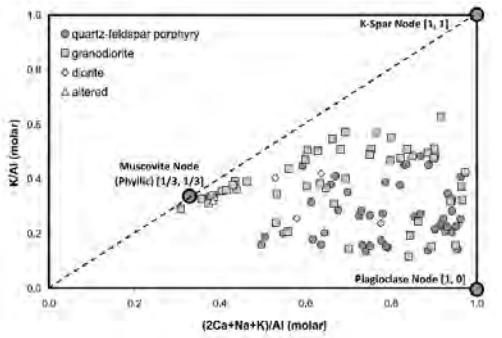

Fig. 4. MER scatterplot of hypogene data identifying which samples have muscovite (phyllic alteration) compositional control.

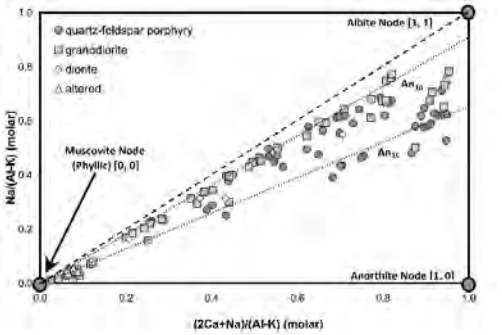

Fig. 5. MER scatterplot of hypogene data capable of determining plagioclase compositions in un-altered rocks using the trends away from muscovite.

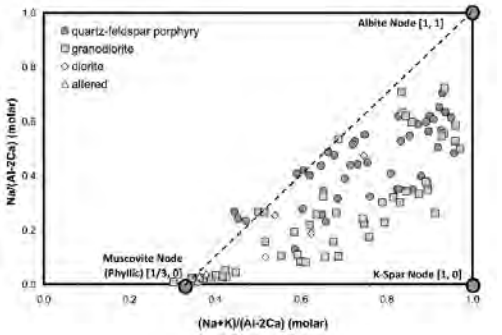

Fig. 6. MER scatterplot of hypogene data capable of detecting and quantifying the intensity of potassic alteration.

Supergene Dataset

The above investigation of QB hypogene lithogeochemistry provides insight into the overlying supergene enrichment zone. In the following plots, supergene data has been expressed using shaded point densities because the large number of samples causes significant overlap. Most

of the same MER diagrams used to investigate the hypogene dataset have been plotted below using the supergene dataset.

A scatterplot of TiO_2 *vs.* Zr (Fig. 7) illustrates that three distinct modes are present in the supergene dataset (granodiorite, QFP, and diorite).

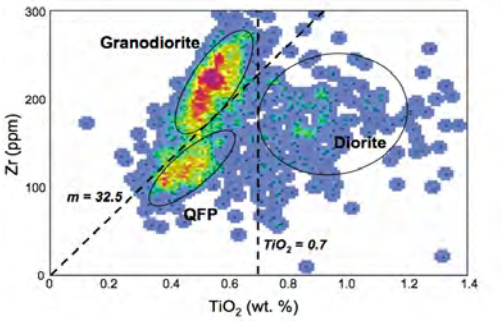

Fig. 7. Conserved element scatterplot of supergene data identical to Figure 2.

The PER diagram of Figure 8 illustrates that intense phyllic alteration affected most supergene rocks. The Al/Ti ratios in this supergene dataset also discriminate between diorite, granodiorite and QFP, just like the hypogene dataset.

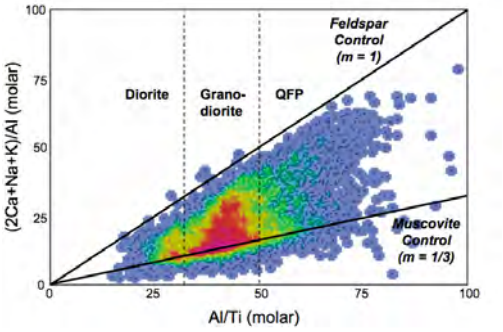

Fig. 8. PER scatterplot of supergene data identical to Figure 3.

MER scatterplot diagrams of the supergene dataset (Figs. 9 & 10) illustrate that most samples are phyllically altered. Similar to the hypogene dataset, supergene samples contain An_{10} to An_{35} plagioclase compositions, and do not contain samples that are strongly potassically altered.

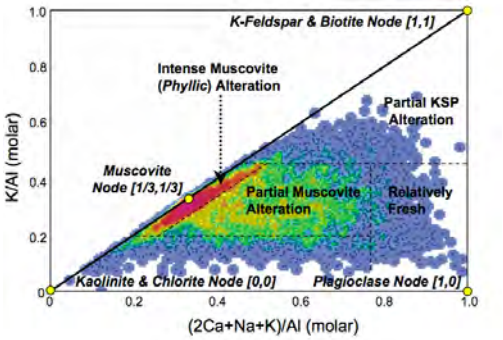

Fig. 9. MER of supergene data identical to Figure 4.

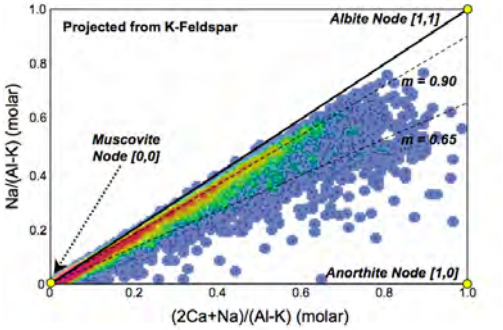

Fig. 10. MER scatterplot of supergene data identical to Figure 5.

CONCLUSIONS

Diorite, granodiorite, and QFP can be discriminated using TiO_2 concentrations and Zr/TiO_2 mass and Al/Ti molar ratios. Granodiorite with An_{10} plagioclase was intruded by QFP with up to An_{35} plagioclase. Granodiorite is intensely phyllically altered whereas QFP is commonly less altered. Potassic alteration is not well expressed in this lithogeochemical dataset.

Supergene lithogeochemical results are similar to hypogene results. Thus, supergene lithogeochemistry can be used to understand the lithologies and hydrothermal alteration of intensely weathered rocks.

ACKNOWLEDGEMENTS

This research was supported by Compañia Minera Quebrada Blanca S.A. and a National Science & Engineering Research Council Discovery Grant # 220302-217290 to C.R. Stanley.

Classification of Igneous Rocks Using Lithogeochemistry Data, Essential Rock Mineralogy, and Projective Geometry in a Streckeisen Ternary Diagram Approach

Cliff Stanley
Dept. of Earth & Environmental Science, Acadia University, Wolfville, Nova Scotia, B4P 2R6
(e-mail: cliff.stanley@acadiau.ca)

ABSTRACT: A rigorous yet adaptable method for the classification of igneous rocks uses numerical manipulation of major oxide lithogeochemical data instead of modal petrographic estimates. Essential mineralogy constraints and projective geometry are employed in a classification procedure that involves: (*i*) conversion of weight percent oxide concentrations to molar element quantities through division by gram formula weights, (*ii*) calculation of independent geochemical parameters describing the amount of each mineral used in classification, (*iii*) conversion of these quantities to volume modes through multiplication by the appropriate molar volumes, and finally (*iv*) standardization to a sum of unity to allow plotting on Streckeisen ternary diagrams and subsequent classification. These procedures can be employed to classify igneous rocks using any ternary diagram and the presence of minerals not used in classification does not impact the results. Such lithogeochemical classifications exhibit excellent correspondence with petrologically defined classifications, but are more representative, accurate and precise than conventional results, because, provided that adequate sample preparation methods and modern analytical procedures are used, they avoid human visual estimation errors and sample mass representativity problems introduced by thin section or slab point count or image analysis procedures.

KEYWORDS: *igneous rocks, petrographic classification, lithogeochemistry, projective geometry, Streckeisen ternary diagrams.*

INTRODUCTION

Plutonic rock classification by petrologic means is a simple procedure involving the use of Streckeisen ternary diagrams. Unfortunately, classification suffers from modal estimation errors involving visual estimates, or representativity issues from point counts or image analysis procedures applied to thin sections or slabs of insufficient size.

In contrast, volcanic rock classification by petrologic means is generally difficult because complete crystallization is not achieved, making it impossible to use the modal rock petrography as a classification criterion. As a result, classification of volcanic rocks has historically relied on lithogeochemistry, and the most successful approaches have employed conserved, trace element concentration ratios. These have been used as proxies for petrology to empirically classify volcanic rocks. Unfortunately, these trace elements are imperfect proxies for rock petrology, and represent only a small proportion of the rock mass, allowing their concentrations to be modified by even subtle geological processes. Thus, igneous rock classification can pose substantial challenges to the geoscientist.

Below, a numerical method for igneous rock classification is described that uses representative, accurate and precise lithogeochemical major oxide data to obtain independent geochemical parameters that describe the volume proportions of the three minerals defining any Streckeisen ternary diagram. This approach is analogous to classical Streckeisen petrological classification procedures, and thus can be compared with petrologic-based classification results to determine how similar the two methods are. Furthermore, because this approach uses major oxide concentrations and is constrained by the essential petrology of the rocks, it can be used to classify

volcanic rocks, and may provide better results than conserved trace elements.

METHOD

Lithogeochemical concentrations can be used to classify igneous rocks by first converting the wt. % concentration data into un-standardized molar element quantities through division of the gram formula weight of the oxide or element. For di-cationic oxides (*e.g.*, Al_2O_3, K_2O), dividing by one half the gram formula weight converts the oxide mass concentration into the appropriate molar (cation) element quantity.

Then, the compositions of the essential (> 5 volume %) minerals in the rocks to be classified are defined in a 'composition matrix' (*C*) and used, in conjunction with a second matrix (*T*) defining what minerals are employed in classification (the 'classifying minerals'; *e.g.*, quartz, plagioclase, alkali feldspar), to obtain a third matrix (*W*) containing a set of independent vectors containing major element coefficients. When multiplied by the un-standardized molar element quantities, they produce un-standardized molar classifying mineral quantities that are un-affected by the presence of non-classifying minerals in the rocks.

These quantities are then multiplied by their associated molar volumes to convert them into volume classifying mineral quantities. After standardization to a unit sum, these become volume proportions than can be plotted on Streckeisen ternary diagrams for classification.

EXAMPLE CALCULATION

If one considers a granitoid rock containing essential amounts of quartz (*QZ*), plagioclase (*AN*, *AB*), alkali feldspar (*KS*) and biotite (*BT*) that requires classification, an appropriate composition matrix (*C*), where *FM* = Fe+Mg, is:

$$C = \begin{array}{c|ccccccc} & Si & Al & FM & Ca & Na & K & OH \\ \hline QZ & 1 & 0 & 0 & 0 & 0 & 0 & 0 \\ AN & 2 & 2 & 0 & 1 & 0 & 0 & 0 \\ AB & 3 & 1 & 0 & 0 & 1 & 0 & 0 \\ KS & 3 & 1 & 0 & 0 & 0 & 1 & 0 \\ BT & 3 & 1 & 3 & 0 & 0 & 1 & 2 \end{array} .$$

Classification of such a rock would employ the quartz (*QZ*)-plagioclase (*PL*)-alkali feldspar (*AF*) Streckeisen ternary diagram, and so geochemical parameters describing the proportions of quartz, plagioclase and alkali feldspar can be obtained using the *T* matrix:

$$T = \begin{array}{c|cccc} & V_{QZ} & V_{PL} & V_{AF} & V_{BT} \\ \hline QZ & 1 & 0 & 0 & 0 \\ AN & 0 & 1 & 0 & 0 \\ AB & 0 & 1 & 0 & 0 \\ KS & 0 & 0 & 1 & 0 \\ BT & 0 & 0 & 0 & 1 \end{array} .$$

Attaching these matrices side by side ($D = [C\ T]$) and then employing a Gauss-Jordan elimination procedure converts this (5×11) matrix into a new matrix consisting of a (5×5) identity sub-matrix on the left and a (5×6) sub-matrix of coefficients on the right. After discarding the identity matrix, the coefficient sub-matrix is further sub-divided into two sub-matrices. A (2×2) negative identity matrix is then appended to the bottom of the (5×2) left coefficient sub-sub-matrix and a (2×4) zero matrix is appended to the (5×4) right coefficient sub-sub-matrix, yielding a (7×6) solution matrix (*W*):

$$W = [O\ V] = \begin{array}{c|cc|cccc} & O_N & O_M & V_{QZ} & V_{PL} & V_{AF} & V_{BT} \\ \hline Si & 0 & 0 & 1 & 0 & 0 & 0 \\ Al & 1 & 0 & -3 & 0 & 1 & 0 \\ FM & 0 & 2/3 & 0 & 0 & -1/3 & 1/3 \\ Ca & -2 & 0 & 4 & 1 & -2 & 0 \\ Na & -1 & 0 & 0 & 1 & -1 & 0 \\ \hline K & -1 & 0 & 0 & 0 & 0 & 0 \\ OH & 0 & -1 & 0 & 0 & 0 & 0 \end{array} .$$

The last four columns of this matrix contain coefficients that can be used to determine the volume proportions of quartz, plagioclase, alkali feldspar and biotite in the rock to be classified using its major element composition, as described above. The first two columns of this matrix can be added in any linear combination to any of the last four vectors to produce alternative coefficients that yield the same independent measures of the classifying mineral proportions.

For example, a granitoid rock from the Sloggett pluton, Oberon batholith, New South Wales, Australia (Glen *et al*. 2006)

plots as a grey circle on Fig. 1 using the V_{QZ}, V_{PL}, and V_{AF} vectors from the above W matrix. Because the biotite volume proportion determined from V_{BT} in W is 2 %, this granitoid rock would be classified as a leucomonzogranite.

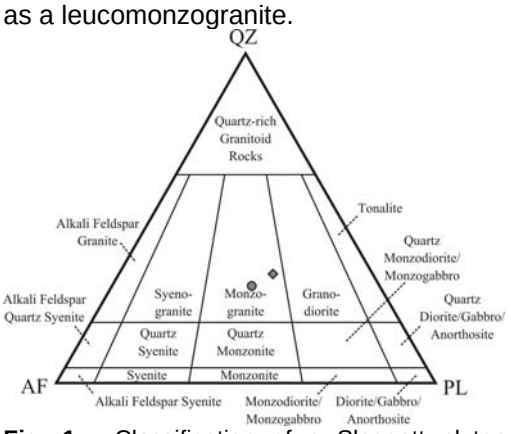

Fig. 1. Classification of a Sloggett pluton sample by two different means on a Streckeisen 'QAP' ternary diagram using major oxide lithogeochemical concentrations (data from Glen et al. 2006).

Note that in W, zero coefficients exist for OH in vectors V_{QZ}, V_{PL}, V_{AF}, and V_{BT}, making this classification appropriate when structural water (H_2O^+) is not analyzed. However, if this rock was affected by a material transfer process that modified its composition, say cut by calcite veins too small to be physically removed during sampling, classification could be negatively impacted. Fortunately, alternative classifications (*e.g.*, matrix W') can be obtained by adding linear combinations of the V_N and V_M vectors to V_{QZ}, V_{PL}, and V_{AF}, in this case to produce new vectors with zero Ca coefficients. These vectors are unaffected by the presence of the calcite veins, and thus will provide an accurate classification. The alternative classification using these vectors plots as a grey diamond on Fig. 1. This plots very close to the first classification, and also indicates that this rock is a leucomonzogranite.

PETROLOGIC VALIDATION

Plutonic rocks from the Emerald Lake pluton, Yukon, comprise four phases: (*i*) augite syenite, (*ii*) hornblende quartz

$$W' = \begin{array}{c|cccc} & V_{QZ}+2V_N & V_{PL}+1/2V_N & V_{AF}-V_N & V_{BT} \\ \hline Si & 1 & 0 & 0 & 0 \\ Al & -1 & 1/2 & 0 & 0 \\ FM & 0 & 0 & -1/3 & 1/3 \cdot \\ Ca & 0 & 0 & 0 & 0 \\ Na & -2 & 1/2 & 0 & 0 \\ K & -2 & 0 & 1 & 0 \\ OH & 0 & 0 & 0 & 0 \end{array}$$

syenite, (*iii*) hornblende quartz monzonite, and (*iv*) biotite granite (classified based on field observations; Smit 1984). Contacts between these units are generally intrusive, except for the contact between phases (*ii*) and (*iii*), which is transitional because they are likely related via fractional crystallization.

Image analysis of stained slabs (Duncan 1999) indicates these rocks should probably be referred to as: (*i*) augite syenite, (*ii* & *iii*) hornblende quartz syenite, and (*iv*) biotite syenogranite (from mean petrographic classification; Fig. 2).

Fig. 2. Classification Emerald Lake pluton samples on a Streckeisen 'QAP' ternary diagram using stained slab image analysis results (data from Duncan 1999).

Unfortunately, these rock textures are relatively coarse compared to the size of the slabs used in classification (Duncan 1999). Thus, representativity is low, likely explaining why these image analysis results exhibit high scatter in Fig. 2.

Lithogeochemical classification of these same rocks was undertaken to provide an alternative classification. This was done using three different essential mineral suites (with different C and T matrices) because: (*a*) the augite syenite contains

alkali feldspar, plagioclase, and augite, (*b*) the hornblende quartz syenite and hornblende quartz monzonite contain alkali feldspar, plagioclase, quartz and hornblende, and (*c*) the biotite granite contains quartz, plagioclase, alkali feldspar, and biotite (note that the classification calculations undertaken for this last phase are identical to the Sloggett pluton example, above). Results are plotted on a Streckeisen diagram (Fig. 3).

Fig. 3. Classification of Emerald Lake pluton samples on a Streckeisen 'QAP' ternary diagram using major oxide lithogeochemical concentrations (data from Duncan 1999).

These lithogeochemical classification results are similar to the petrographic classifications of Fig. 2. Nevertheless, they do suggest that the four units should actually be referred to as: (*i*) augite quartz syenite, (*ii* & *iii*) hornblende syenogranite, and (iv) biotite monzogranite. Furthermore, these lithogeochemical classification results exhibit much less scatter than the petrographic data, principally because the samples used to obtain the lithogeochemical concentrations used in the calculations have a much larger volume than the stained slabs used in image analysis.

CONCLUSIONS

Classification of igneous rocks can be undertaken using: (*i*) major oxide lithogeochemical concentrations, (*ii*) knowledge of the essential mineralogy of the rock, (*iii*) matrix algebra procedures and (*iv*) Streckeisen ternary classification diagrams. Results are generally consistent with petrographic classifications, but are likely more accurate, precise and representative. This is because lithogeochemical classification is based on quantitative data with high accuracy and precision derived from samples that typically have larger mass than the stained slabs or thin sections used in point counting or image analysis. The flexibility of the approach allows accurate classification of igneous rocks that are not entirely fresh, and can be used for volcanic rocks if the essential mineral assemblage can be identified/postulated.

ACKNOWLEDGEMENTS

This research was supported by NSERC Discovery Grant # 220302-217290 to the author.

REFERENCES

DUNCAN, R.A. 1999. *Physical and Chemical Zonation in the Emerald Lake Pluton, Yukon Territory.* M.Sc. thesis, Inv. of B.C., Vancouver.

GLEN, R.A., DAWSON, M.W., COLQUHOUN, G.P. 2006. Eastern Lachlan Orogen Geoscience Database (on DVD-ROM) Version 2, NSW Department of Primary Industries – Minerals, Geol. Surv. of NSW, Maitland, NSW, Australia.

SMIT, H. 1984. *Petrology, chemistry, age, and isotope study of the high potassium Emerald Lake pluton, eastern Yukon Territory.* B.Sc. thesis, Univ. of B.C., Vancouver.

STRECKEISEN, A., ZANETTIN, B.A., LE BAS, M.J., BONIN, B., BATEMAN, P., BELLIENI, G., DUDEK, A., EFREMOVA, S., KELLER, J., LAMEYRE, J., SABINE, P.A., SCHMID, R., SORENSEN, H., WOOLLEY, A.R. 2002. *Igneous rocks; a classification and glossary of terms; recommendations of the International union of Geological Science Subcommission on the Systematics of Igneous Rocks*. Cambridge University Press, Cambridge, U.K., 800 p.

Distal exhalative manganese enriched stratigraphy to carbonate-hosted zinc deposits, Adirondack Lowlands, New York State, U.S.A.

Alex Tolson[1]& Norm Duke[2]

1Exploration Geologist Consultant, 56-C Medhust Dr., Ottawa, ON, K2G 4V2 CANADA
(e-mail: alextolson@hotmail.com)
2Economic Geology Professor, University of Western Ontario, Rm 118-A Biology & Geology Bldg. University of Western Ontario, London, ON, N6A 5B7 CANADA

ABSTRACT: The Arnold Pit is an industrial talc/tremolite deposit near Gouverneur, New York. The mine is located in the Balmat-Edwards Mining District in the Adirondack Lowlands of the Grenville Province. The Balmat-Edwards SEDEX-type zinc deposits, hosted within a metamorphosed evaporitic carbonate sequence, are located within a few kilometres of the Arnold Pit. This pit exposes a manganese-rich unit overlying stromatolitic marble and calc-silicate gneisses and is capped by talc-dominated schists. Electron microprobe analysis together with bulk rock major- and trace-element geochemistry confirms manganese enrichment in oxide, carbonate, and silicate phases; up to 13% Mn, 5.9% Fe, 192 ppm Zn, and 13700 ppm Ba are preserved in the metamorphic assemblage. Spessartine garnets, tirodite, tephroite, and kutnohorite are intergrown with Mg-rich staurolites, trace pyrolusite is intergrown with sphalerite. The depositional setting is a distal exhalative environment to the zinc ore and such Mn-enrichments may be utilized for targeting stratiform base-metal mineralization even in high-grade metamorphic terranes.

KEYWORDS: *Manganese, SEDEX, Balmat-Edwards, Distal exhalative, Adirondack Lowlands*

INTRODUCTION

The Arnold Talc Mine, near the town of Gouverneur, New York, is located in the Balmat-Edwards Mining District within the Frontenac-Adirondack Terrane of the Grenville Province. The district hosts SEDEX-type zinc deposits, and these occur within a few km of the Arnold pit. A significant manganese-rich unit is exposed in the pit and its relationship to the ore has not been determined. Twenty-five samples were collected from the Arnold Pit in September of 2005 to study the stratigraphic position and geochemistry of the Mn-subunit in detail. Qualitative microprobe analyses determined manganese in several silicate, carbonate and oxide phases. Bulk rock major- and trace-element geochemistry of six samples provide quantitative evidence for the enrichment of an elemental suite consistent with being distal products of an exhalative hydrothermal system.

REGIONAL GEOLOGICAL SETTING

The Mesoproterozic Grenville Province extends from Labrador to Texas (Rivers 2005). The province has been subdivided into terranes, based on lithology, structure, and metamorphic ages (Easton 2005). The main divisions within the Ontario/New York segment are: the Central Gneiss Belt to the northwest, the Central Metasedimentary Belt, and the Central Granulite Terrane to the southeast. The Balmat-Edwards district is located within the Frontenac-Adirondack Terrane, specifically within the Adirondack Lowlands of the Central Metasedimentary Belt (DeLorraine & Carl 1993). The Adirondack Lowlands is a supracrustal gneissic terrane noted for its extensive marble that hosts the stratiform zinc deposits (Chiarenzelli *et al*. 1993). The Lowlands stratigraphy includes pelitic schists, metavolcanic gneisses and two major marble units (Whelan *et al*. 1990). It underwent upper amphibolite to granulite facies metamorphism during the 1190-1140 Ma Shawinigan Orogeny (Rivers 2005). Metamorphic conditions in the Lowlands reached peak pressure and

temperatures of >6 Kbars and 625°C (Charenzelli *et al*. 1993).

The Balmat-Edwards District is underlain by four main stratigraphic divisions (DeLorraine & Carl 1993). The basal Hyde School Gneiss is composed of leucogneisses with thin concordant amphibolite layers. This is overlain by the Lower Marble Formation which is dominated by graphite-phlogopite-calcite marble containing disseminated tourmaline. The Popple Hill Gneiss, in tectonic contact above the Lower Marble, is a variably migmatitic gneiss of dacitic composition. The Upper Marble capping the regional stratigraphy hosts the zinc mineralization and has an inferred age between 1150 to 1300 Ma (Whelan *et al*. 1990). The Upper Marble is further subdivided into 16 distinct stratigraphic units of relatively pure and variably dolomitic limestone interbedded with calc-silicate units after impure marlstone (DeLorraine & Carl 1993). The interbedded dolomitic and calc-silicate marble members indicate shallow basin margin environments. Original evaporative conditions are clearly indicated by the presence of thick (up to 15 m) gypsum/anhydrite in Unit 13. Extensive dolomitization is common in evaporative basins (Warren 1990). Sulfur and oxygen isotope studies on the gypsum support evaporative deposition from seawater and protracted hydrothermal activity related to the nearby base-metal mineralization may be involved in sulfate reduction (Whelan *et al*. 1990).

LOCAL STRATIGRAPHY EXPOSED IN THE ARNOLD PIT

The Arnold Pit is on the steeply dipping, overturned limb of the Sylvia Lake Syncline, the structural hanging wall is the stratigraphic footwall. Commercial talc occurs in Unit 13 near the contact with Unit 14 of the Upper Marble from the metamorphism or impure evaporative dolomite. The upper section of Unit 13 grades from tremolite-rich talc ore into a pure talc schist up section. Unit 12 is a white massive dolomitic marble with convolute bands of grey and orange to purple calc-silicate marble. A metre thick lens of stromatolitic marble, occurring just below the base of Unit 13, suggests a shallow subtidal to supratidal sabkha environment (Whelan *et al*. 1990).This is stratgraphically overlain by banded quartz diopside gneiss. The manganiferous subunit of this study directly overlies the pyritic quartz diopside gneiss and has a calc-silicate hanging wall rich in talc and tremolite, i.e., the Mn-rich member underlies Unit 14, the host of the Balmat-Edwards zinc deposits. It has an apparent thickness of about 2 to 3 m in width and is concordant with the local stratigraphy. Both upper and lower contacts are sharp and distinct. It is very dense and black to dark brown in colour. Internal compositional banding is visible in outcrop. The subunit contains carbonate, as well as brownish to yellowish bands of coarse grained manganese-bearing silicates. Petrographic study of samples from the Mn unit identified several Mn-bearing phases including spessartine garnets, tirodite, tephroite, and kutnohorite. Pyrolusite was found intergrown with sphalerite. The mineralogy is a direct reflection of the amphibolite facies overprint of an original Mn-rich sediment.

GEOCHEMICAL RESULTS

Six samples were analyzed by C. Wu at the University of Western Ontario for major and trace-element bulk rock lithogeochemistry using X-Ray Fluorescence (XRF) and Induced Coupled Plasma Atomic Emission Spectrometry (ICP-AES). The results of the analyses are shown in Tables 1 and 2, respectively.

Significant Zn, Pb, Ba, and Sr is detected in sample 07A from the base of the manganese subunit. Sample 07B, collected higher in stratigraphy than 07A, is dominantly comprised of kutnohorite and Mn-bearing amphiboles, and this has the highest amount of manganese (13.03 %) determined. Sample 07B also has anomalous base metals as well as the greatest Ba enrichment of all the analyzed samples at 13700 ppm. The 1140 ppm value for sulfur reflects barite content.

Table 1. Major Element Oxides (in wt %) (recalculated to 100%).

Sample	SiO_2	TiO_2	Al_2O_3	Fe_2O_3	MnO	MgO	CaO	K_2O	Na_2O	P_2O_5	L.O.I.	Total
04	76.77	0.10	1.64	0.85	0.66	10.61	5.46	0.10	0.88	0.03	2.32	99.43
07A	54.39	0.05	0.73	1.97	9.10	21.56	6.67	0.02	0.49	0.05	4.31	99.33
07B	43.73	0.02	0.84	1.33	13.03	20.46	5.79	0.04	0.16	0.09	12.47	97.97
08A	42.81	1.28	10.50	5.90	0.42	22.42	5.91	0.93	0.63	0.89	7.56	99.24
10A-S	52.03	0.60	6.59	4.28	11.78	16.88	2.79	0.06	0.68	0.06	3.49	99.26
10A-G	46.33	0.22	2.24	2.73	12.66	19.96	5.06	0.01	0.33	0.06	9.56	99.16

Table 2. Trace Element Analyses (in ppm).

Sample	Nb	Zr	Y	Sr	Rb	Ba	Mo	Pb	Zn	Cu	Ni	Co	Cr	V
04	98	181	28	590	< 50	728	128	357	< 25	< 30	< 25	< 25	< 25	82
07A	62	120	22	135	< 50	200	102	247	153	< 30	< 25	< 25	< 25	141
07B	55	152	21	119	< 50	13700	900	243	72	< 30	< 25	< 25	< 25	57
08A	91	199	128	835	110	207	975	258	192	36	309	105	146	467
10A-S	68	169	22	131	< 50	936	104	283	29	< 30	25	63	< 25	575
10A-G	60	158	42	436	< 50	175	884	221	131	38	26	53	< 25	78

.

Sample 10A was divided into Mg-staurolite dominated "S" and a garnet dominated "G". Sample 10A-S has ~6 % Al2O3 and significant SiO2 (~52%), Fe (~4.3%), MgO (16.88%), MnO (11.78%), and lesser CaO (2.79%), consistent with the staurolite-amphibole-dominated assemblage. This sample contains low Zn (29 ppm), although trace disseminated sphalerite was identified. It has 283 ppm lead and significant (970 ppm) Ba enrichment. Sample 10A-G has significant SiO_2, MgO, MnO (~12 %), and CaO. The garnet-rich nature of the sample 10A-G accounts for its Y enrichment, containing double the amount detected in the other samples. The trace-element analysis shows minor enrichments in Zn (131 ppm) consistent with observed sphalerite, as well as elevated Pb (221 ppm), Ba (175 ppm), and Cu (38 ppm) values. Sample 04 is from the quartz diopside gneiss adjacent to the Mn unit and sample 08A from an ultramafic boudin from the pit.

DISCUSSION

Irish-type SEDEX deposits are carbonate-hosted stratiform to stratabound sulfide deposits that occur as syngenetic exhalative to early diagenetic replacement bodies (Coleman *et al*. 1989). Many SEDEX deposits have formed in Proterozoic intracontinental rifts and Phanerozoic deposits occur in similar environments (Lydon 1996). Evaporite dissolution provides Cl^- ions to complex with base metals to promote hydrothermal solubility (Warren 1990). The presence of evaporite minerals or their pseudomorphs, as well as stromatolites, indicate the stratiform zinc deposits of the Balmat-Edwards District occur in a hydrothermally active evaporite setting (Warren 1990; Goodfellow 2004). Manganese is not associated with typical evaporite mineral assemblages especially in the significant concentration observed. However, in hydrothermal systems there is well documented geochemical zonation from proximal to distal facies relative to the original hydrothermal feeder zone (Lydon 1996). There is a shift from reduced Cu-, Pb- and Zn-rich sulfide facies to Ba-, Fe- and Mn-rich oxide facies away from the zone of hydrothermal discharge (Lydon 1996). Ba and Mn are typically distal elements. Distal hydrothermal products are characterized by deposition of chert, barite with minor sphalerite and pyrite and notable manganese enrichment (Lydon 1996).

Most SEDEX deposits are not precipitated directly adjacent to their feeder zone (Sangster 2002) therefore the geochemical zonation of distal products provides a valuable exploration tool. Manganese halos have been well documented for the Tynagh mine in

Ireland (Russell 1983), as well as the HYC and Lady Loretta deposits in Australia (Large & McGoldrick 1998; Large *et al*. 2000). Manganese associated with these hydrothermal systems is found in carbonates and oxides, as well as in spessartine garnets in metamorphosed terranes (Lydon 1996). Manganese halos have survived the effects of amphibolite to granulite facies metamorphism in the Proterozoic Zn-Pb deposits of South Africa such as the Gamsberg mine (Stalder & Rozendaal 2005). The manganese enrichment has been found several kilometres from known deposits (Lydon 1996).

The Mn-subunit exposed in the Arnold pit contains up to 13% Mn and 13700 ppm Ba with associated elements consistent with distal hydrothermal products. Microprobe analysis determined barite to be present as inclusions within and on the margins of pyrolusite, demostrating Mn and Ba deposition from the same fluid. Such anomalous enrichments are atypical of basinal settings other than those receiving input from hydrothermal discharge.

CONCLUSIONS

The Balmat-Edwards District in the Adirondack Lowlands contains several carbonate-hosted stratiform base-metals deposits hosted within a metamorphosed evaporite sequence. The nearby Gouvenour Talc Mine's Arnold Pit exposes stratigraphy distal to the zinc mines. Manganese is concentrated in a well defined stratigraphic subunit of calc-silicate gneiss in Unit 13 underlying Units 14, host to the zinc ores. The upper amphibolite facies metamorphic overprint caused the units to undergo prograde recrystallization, while retaining primary chemical composition at the micro-scale. The manganese partitioned into various carbonate, silicate, and oxide phases. Enrichment in Ba, Fe, and Zn is typical of distal facies of well documented SEDEX hydrothermal systems. There is therefore a direct genetic relationship between the chemical anomaly in the Arnold Pit and the base-metals deposits. The manganese is related to hydrothermal mineralizing brine that carried the mobile elements to a distal redox boundary where they were precipitated as exhalative sediments. When targeting SEDEX mineralization, one must consider such distal geochemical signatures. This is especially true in high-grade metamorphosed terranes where original stratigraphy has become obscure. Enrichment of manganese is of particular interest for regional target generation and as a vector for more detailed follow-up exploration. The stratigraphy, petrography, and geochemistry of the manganiferous unit at the Arnold Pit strongly support a link to direct hydrothermal input. The geochemical anomaly of Mn, Zn, Pb, and Ba is a clear demonstration that such distal exhalative products are preserved even under high-grade metamorphic conditions.

ACKNOWLEDGEMENTS

We thank Mr. John Kreider of the Gouverneur Talc Company for graciously granting access to the mine to collect samples during production.

REFERENCES

CHIARENZELLI, J.R. *et al.* 1993. Proterozoic rocks east and southeast of the Grenville front. In: RANKIN, D.W (ed.), *Precambrian: Conterminous U.S.* The Geological Society of America.

COLEMAN, T.B., JONES, D.G., PLANT, J.A., & SMITH, K. 1993. In: PLANT, J.A. & JONES, D.G. (eds.), *Metallogenic models and exploration criteria for buried carbonate-hosted ore deposits – a multidisciplinary study in eastern England.* The Institution of Mining and Metallurgy, British Geological Survey.

DELORRAINE, W.F. & CARL, J.D. 1993. Precambrian Geology of the northwest Adirondack Lowlands: a Stratigraphic Viewpoint. In: BURSNALL, J.T (ed.), *New York Geological Association Field Trip Guidebook,* 1-51.

EASTON, M. 2005. The Grenville Province in Ontario, what you need to know for effective mapping and exploration. In: *Geology and Mineral Deposits of the Grenville Province*. University of Western Ontario, Society of Economic Geologists Student Chapter, Short Course Manual.

GOODFELLOW, W.D. 2004. *Sediment-hosted Lead-Zinc Sulphide Deposits*. Narosa Publishing, 367p.

LARGE, R.R. & MCGOLDRICK, P.J. 1998. Lithogeochemical halos and geochemical vectors to stratiform sediment hosted Zn-Pb-Ag deposits; Part 1. Lady Loretta Deposit, Queensland. *Journal of Geochemical Exploration*, **63**, 37-56.

LARGE, R.R., BULL, S.W., & MCGOLDRICK, P.J. 2000. Lithogeochemical halos and geochemical vectors to stratiform sediment hosted Zn-Pb-Ag deposits; Part 2. HYC deposit, McArthur River, Northern Territory. *Journal of Geochemical Exploration*, **68**, 105-126.

LYDON, J.W. 1996. Sedimentary exhalative sulphides (Sedex). In: ECKSTRAND, O.R., SINCLAIR, W.D., & THORPE, R.I. (eds.), *Geology of Canadian Mineral Deposit Types.* Geological Survey of Canada, Geology of Canada, **8**, 130-152.

RIVERS, T. 2005. Architecture and tectonic evolution of the Grenville Province: Part of a long-lived hot wide orogen on the southeastern margin of Laurentia. In: *Geology and Mineral Deposits of the Grenville Province.* University of Western Ontario, Society of Economic Geologists Student Chapter, Short Course Manual.

RUSSELL, M.J. 1983. Major Sediment-Hosted Exhalative Zinc + Lead Deposits: Formation From Hydrothermal Convection Cells That Deepen During Crustal Extension. In: SANGSTER, D.F (ed.), *MAC Short Course in Sediment-hosted stratiform lead-inc deposits*.

SANGSTER, D.F. 2002. The role of dense brines in the formation of vent-distal sedimentary-exhalative (SEDEX) lead-zinc deposits: field and laboratory evidence. *Mineralium Deposita*, **37**, 149-157.

STALDER, M. & ROZENDAAL, A. 2005. Distribution and geochemical characteristics of barite and barium-rich rocks associated with the Broken Hill-type Gamsberg Zn-Pb deposit, Namaqua Province, South Africa. *South African Journal of Geology*, **108**, 35-50.

WARREN, J.K. 1989. *Evaporite Sedimentology.* Prentice Hall.

WHELAN, J.F., RYE, R.O., DELORRAINE W., & OHMOTO, H. 1990 Isotopic Geochemistry of a Mid-Proterozoic Evaporite Basin: Balmat, New York. *American Journal of Science*, **290**, 396-424

Lithogeochemical analysis through the deformed volcanosedimentary sequence hosting the Boomerang massive sulfide deposits, Tulks Belt, Central Newfoundland

Ryan M. S. Toole[1] & David R. Lentz[1]

1University of New Brunswick, Department of Geology, P.O. Box 4400, Fredericton, NB, E3B 5A3 CANADA
(e-mail: ryan.toole@unb.ca)

ABSTRACT: A detailed study of 8 drill cores through the Cambrian to middle Ordovician rocks hosting the 1.3 Mt Boomerang massive sulfide deposit in the Tulks Volcanic Belt, Central Newfoundland, attempts to unravel the complicated stratigraphy and enhance belt-scale correlations. Rock types include Greenschist facies felsic, intermediate, and mafic volcaniclastic rocks (ash, lapilli-tuff, agglomerate), mafic to intermediate dykes and sills, and sedimentary rocks (greywacke, siltstone, graphitic shale, and carbonaceous phyllite). Using immobile elements, the hanging wall (HW) volcaniclastic rocks are divided into four units (HW1, HW2, HW3, HW4), whereas footwwall (FW) volcaniclastic rocks are divided into five units (FW1, FW2, FW3, FW4, FW5). Compositionally these units span a range from basalt (HW2, HW3, FW3, FW4, FW5), to basaltic andesite (HW4, FW2), to andesite (FW1), to rhyodacite (HW1), shown by immobile element ratios (TiO_2/Zr and Al_2O_3/TiO_2). Four populations of fine grained dykes (D1, D2, D3, D4) have been compositionally identified (two basalts (D1, D2), andesite (D3), and rhyolitic dacite (D4)), based on discrimination diagrams, TiO_2 and $Na_2O + K_2O$.

KEYWORDS: *Chemostratigraphy, Volcaniclastics, VMS, Newfoundland, Discrimination plots*

INTRODUCTION

The Boomerang Zn-Pb-Cu-Ag-Au massive sulfide deposit, which was discovered by Messina Minerals in 2004, is located in the Tulks Volcanic Belt (TVB) of the Victoria Lake Supergroup approximately 20km southwest of Red Indian Lake (Fig. 1). Grading 7.09% Zn, 3.00% Pb, 0.51% Cu, with 110.43 g/t Ag and 1.66 g/t Au, Boomerang has an estimated reserve tonnage of 1.36 Mt with another 278 100 tonnes inferred grading 6.72% Zn, 2.88% Pb, 0.44% Cu, with 96.53 g/t Ag, &.29 g/t Au (Messina Minerals press release, June 21st, 2007).

During the summer of 2006, 200 petrographic and lithogeochemical samples were collected from the rocks that host the Boomerang massive sulfide deposit. In order to characterize the different rock types sampled ICP-AES and XRF analysis of these samples was completed by ALS Chemex (Sudbury Ontario), and Memorial University of Newfoundland, respectively.

GEOLOGICAL SETTING

Regional Geology

The Victoria Lake Supergroup (Evans & Kean 2002) is divided into northern and southern terranes, separated by the Rogerson Lake Conglomerate. The northern terrane consists of the Tally Pond Belt, the Diversion Lake Group, the Long Lake Belt, the Harbour Round Belt, the Harpoon Brook Belt and the TVB whereas the southern terrane contains the Point of the Woods Belt (Fig. 1; Evans & Kean 2002). The northern terrane is bounded by the Red Indian Line to the north and the Rogerson Lake Conglomerate to the south and consists predominantly of a volcano-sedimentary srocks. The southern terrane is bounded by the Rogerson Lake Conglomerate to the north and the Noel Paul's Line to the south and consists of a volcano-sedimentary sequence intruded by Siluro-Devonian biotite granite (Evans & Kean 2002).

Geology of the Tulks Volcanic Belt

The TVB extends for 65 km from Victoria

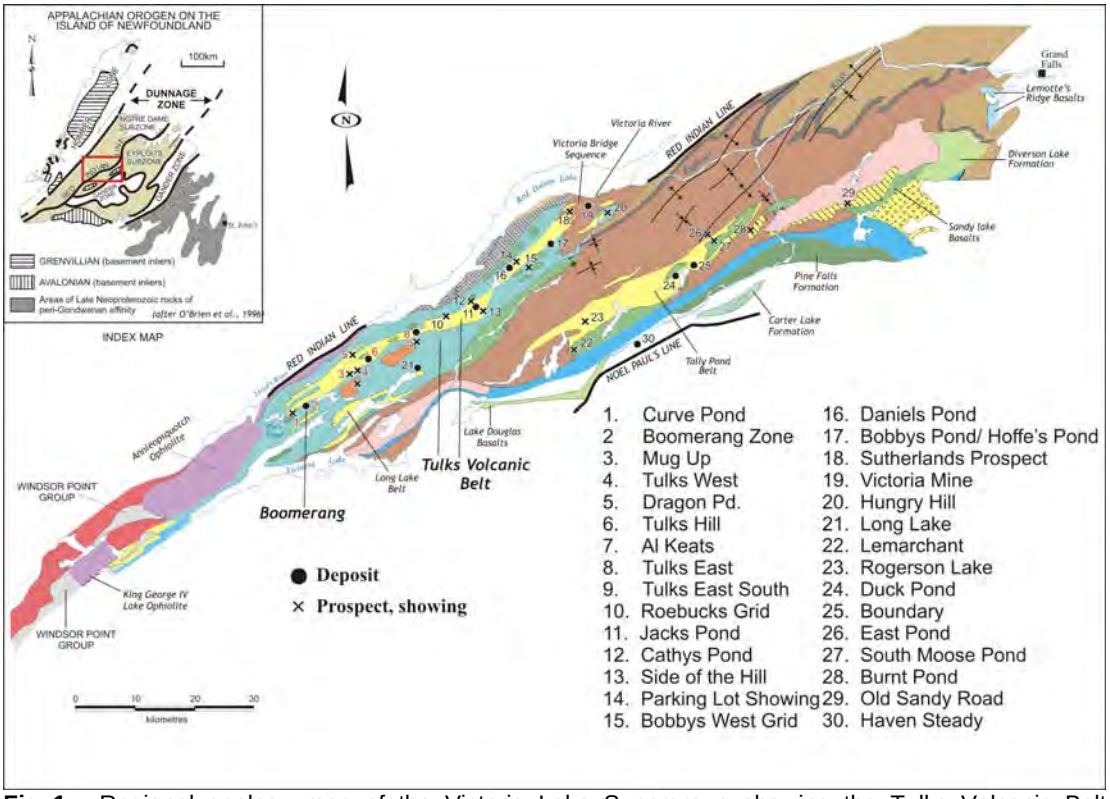

Fig 1. Regional geology map of the Victoria Lake Supergroup showing the Tulks Volcanic Belt occurring from the south west to the north central part of the map area. Also shown are the other volcanogenic massive sulfide deposits (modified from Hinchey 2007).

Lake to just south of where the Victoria River empties into Red Indian Lake (Fig. 1). Light grey-green to white, dacitic to rhyolitic quartz-feldspar-porphyritic pyroclastic flow deposits with 1 to 6 mm crystals, crystal-tuff breccia, ash tuff, flow banded rhyolite, and small subvolcanic quartz-feldspar porphyritic intrusions are included in the TVB (Evans & Kean 2002; Rogers & van Staal 2002). Mafic volcanic rocks of the TVB include tuff, lapilli tuff, volcanic breccia, and minor amygdaloidal pillow lava and breccia. Sedimentary rocks within the TVB include volcanogenic wacke, siltstone, and limestone (Evans & Kean 2002; Rogers & van Staal 2002).

There are twenty-one significant VMS deposits in the TVB with recent discoveries by Messina Minerals adding to this total (Evans & Kean 2002). These deposits include Daniels Pond, Jacks Pond, Bobbys Pond, Long Lake, Tulks East, Tulks Hill, Victoria Mine, Long Lake, Curve Pond Zone, and Boomerang all hosted within felsic volcanic rocks and spatially associated with black, locally graphitic shale and chert. (McKenzie *et al.* 1993; Evans & Kean 2002; Rogers & van Staal 2002, Squires & Moore 2004); however, the Boomerang deposit is spatially associated with significant volumes of volcaniclastic rocks of intermediate composition.

DISCUSSION

The volcaniclastic rocks hosting the Boomerang massive sulfide show a wide range of petrographic and chemical compositions. Petrographically the HW volcaniclastic rocks show increasing fine-grained white mica (muscovite/sericite) development with proximity to the mineralized horizon. The abundance of these phyllosilicates enhances the development of more intense foliation in

the vicinity of the deposit. Relative to the HW, the FW volcaniclastic rocks are typically more fine-grained and show increased chlorite, fine white micas, and a stronger foliation.

The HW volcaniclastic rocks have been divided into four units (HW1, n=35; HW2, n=4; HW3, n=7; HW4, n=36), based on immobile elements and immobile element ratios. All hanging wall rocks have dominantly volcanic arc signatures. Based on the Nb/Y vs Zr/TiO_2 discrimination diagram by Winchester & Floyd (1977), later revised by Pearce (1996), HW 1 has a rhyodacitic composition, HW2 has a basaltic andesite composition, whereas HW3 and HW4 have basaltic compositions (Fig 2). To further distinguish between the hanging wall rocks, TiO_2/Zr was plotted against TiO_2/Y and Al_2O_3/TiO_2. A positive correlation between TiO_2/Zr and TiO_2/Y is consistent with more mafic rocks. A negative correlation between TiO_2/Zr and Al_2O_3/TiO_2 is consistent with more mafic rocks having increased TiO_2/Zr affinities and decreased Al_2O_3/TiO_2 affinities.

The footwall volcaniclastic rocks are divided into five units (FW1, n=34; FW2, n=15; FW3, n=2; FW4, n=3; FW5, n=4), based on the same parameters used for the hanging wall rocks. All of the footwall rocks have volcanic arc signatures based on the fields of Pearce *et al*. (1984). Based on the Nb/Y vs Zr/TiO_2 discrimination diagram (Winchester and Floyd 1977 and revised by Pearce 1996), FW1 shows an andesitic composition, FW2 shows a basaltic andesite composition, and FW3, FW4, and FW5 show basaltic compositions (Fig. 3). To further distinguish between the HW populations, TiO_2/Zr was plotted against TiO_2/Y and Al_2O_3/TiO_2 resulting in the same correlation trends as found in the HW volcaniclastic rocks.

The intermediate and felsic dykes associated with the host volcaniclastic rocks are believed to postdate the youngest metamorphic event in the TVB, In contrast the mafic dykes post date all but the latest folding event. The dykes have been divided into 4 populations (D1, n=27; D2, n=4; D3, n=8; D4, n=17), based on mobile and immobile elements and their element ratios, as they are believed to have minimal alteration effects. Much like

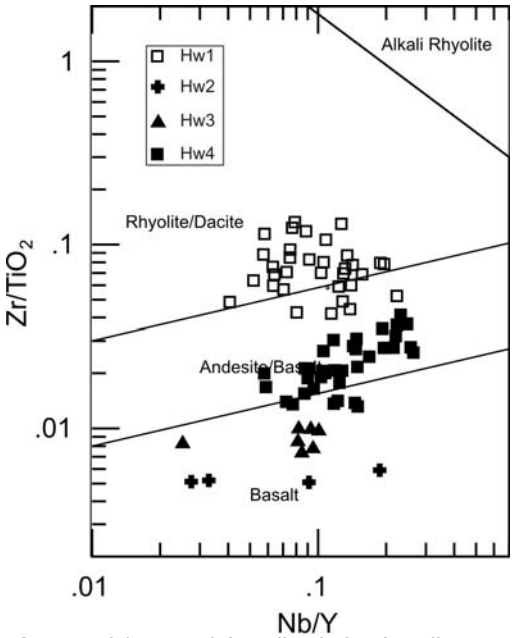

Fig. 2. Nb/Y vs Zr/TiO_2 discrimination diagram showing distribution of hanging wall tuff samples. Field boundaries are from Pearce (1996).

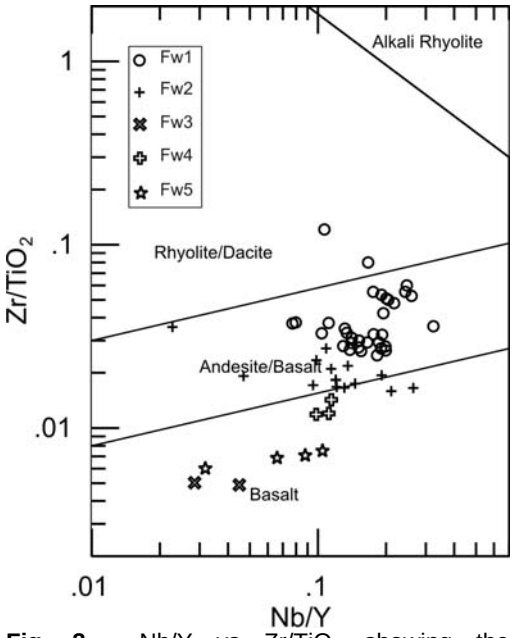

Fig. 3. Nb/Y vs Zr/TiO_2 showing the distribution of footwall tuff samples. Field boundaries are from Pearce (1996).

the HW and FW volcaniclastic rocks, the dykes and sills have volcanic arc signatures. Based on the Zr/TiO_2 vs SiO_2 discrimination diagram (Winchester and Floyd's 1977), D1 and D2 have basaltic compositions, D3 is andesitic and D4 is rholitic dacite composition. On the SiO_2 vs $Na_2O + K_2O$ discrimination diagram both D3 and D4 have a dominantly alkaline affinitiy, whereas D1 and D2 are subalkaline.

Although faulting and thrusting has complicated the distribution of rocks types one key aspect within 5 of 8 drill holes remains consistent. All HW volcaniclastic samples in direct contact with the ore horizon belong to HW4 and all FW volcaniclastic samples in direct contact with the ore horizon belong to FW1.

ACKNOWLEDGEMENTS

Thank you to Messina Minerals for allowing us to work such an interesting project and to all of their staff, specifically Gerry Squires for all his advice and input.

REFERENCES

EVANS, D.T.W. & KEAN, B.F. 2002. The Victoria Lake Supergroup, central Newfoundland – Its definition, setting, and volcanogenic massive sulfide mineralization. Government of Newfoundland and Labrador, Depart of Mines and Energy, Geological Survey Branch, *Open File* **NFLD/2790**, 68 p.

HINCHEY, J.G. 2007. Volcanogenic Massive Sulfides of the Southern Tulks Volcanic Belt, Central Newfoundland: Preliminary Findings and Overview of Styles and Environments of Mineralization. In: Current Research, Newfoundland and Labrador Department of Natural Resources, Geological Survey Branch, *Report* **07-1**, 117-143.

MCKENZIE, C.B., DESNOYERS, D.W., BARBOUR, D., & GRAVES, R.M. 1993. Contrasting volcanic-hosted massive sulfide styles in the Tulks Belt, Central Newfoundland. *Exploration and Mining Geology*, **2**, 73-84.

PEARCE, J.A. 1996. Sources and Settings of Granitic Rocks. *Episodes*, **19**, 120-125.

PEARCE, J.A., HARRIS, NIGEL, B.W., & TINDLE, A.G. 1984. Trace element Discrimination Diagrams for the Tectonic Interpretation of Granitic Rocks. *Journal of Petrology*, **25**, 956-983.

ROGERS, N. & VAN STAAL, C. 2002. Toward a Victoria Lake Supergroup: A provisional stratigraphic revision of the Red Indian to Victoria Lakes Area, Central Newfoundland. In: Current Research, Newfoundland Department of Mines and Energy, Geological Survey Branch, *Report* **02-1**, 185-195.

SQUIRES, G.C. & MOORE, P.J. 2004. Volcanogenic massive sulfide environments of the Tally Pond volcanics and adjacent area: geological, lithogeochemical and geochronological results. In: Current Research, Newfoundland Department of Mines and Energy, Geological Survey Branch, *Report* **04-1**, 63-91.

WINCHESTER, J.A. & FLOYD, P.A. 1977. Geochemical Discrimination of Different Magma Series and their Differentiation Products using Immobile Elements. *Chemical Geology*, **20**, 325-343.

Stratigraphic and geochemical interpretation of the Early Silurian Woodstock ferromanganese deposits, New Brunswick, Canada

Bryan C. Way[1], David R. Lentz, & David G. Keighley
1University of New Brunswick, 2 Bailey Dr., Box 4400, Fredericton, NB, E3B 5A3 CANADA (e-mail: bryan.way@unb.ca)

ABSTRACT: The Woodstock Fe-Mn deposits are a series of Early Silurian manganiferous banded iron formations (BIFs) that are hosted in the Late Ordovician to Early Silurian White Head Formation and the conformably overlying Silurian Smyrna Mills Formation. Six major lenticular-shaped Fe-Mn bodies were initially identified by gravimetric surveys (circa 1954) that followed southwest along the strike of the bedrock from Jacksontown to Green Road in western New Brunswick. These assemblages were identified within the Plymouth deposit as a series of manganese oxide and manganese carbonate-silicate-oxide units commonly in sharp contact with layers of red shale, green shale and (or) alternations of the two. Regional and local sedimentologic studies indicate these units as a transgression-regression wedge in a shallow marine basin under rapidly changing redox conditions. Lithogeochemical data from drill cores within the Plymouth deposit display strong inverse correlations between Al_2O_3 in relation to Fe_2O_3 and MnO, depletions of Eu, and high ratios of Ce/La (2.5 ± 0.2) suggesting that the source of Fe and Mn was from multiple sources (i.e., oceanic and terrestrial Fe-Mn) without direct volcanic or hydrothermal input as a source of Fe^{+2} and Mn^{+2}.

KEYWORDS: *Woodstock, Manganese, Banded Iron Formations, Plymouth Deposit.*

INTRODUCTION

The Woodstock area of western New Brunswick hosts a series of manganiferous banded iron formations (BIFs) that collectively constitute one of the largest manganese resources in North America (approximately 194 000 000 tonnes). This Woodstock deposits were exploited for iron from 1848 to 1884. It was during these Fe mining operations that high concentrations of Mn were first recognized. The Mn potential of the Woodstock deposits was reevaluated in the early 1900's (Sidwell 1957).

The Mn deposits are large lenticular bodies readily identified by gravimetric surveys (circa 1954). Six major ferromanganese zones were initially identified southwest along the strike from Jacksontown to Green Road, New Brunswick, with other occurrences found within similar strata in parts of eastern Maine (Sidwell 1957; Roberts & Prince 1990). Expansion of highway Route 95 from Houlton, ME to Woodstock, New Brunswick (Fig. 1) has exposed several new outcrops of the White Head and the Smyrna Mills formations that were unmappable until recently.

The purpose of this study is to examine and document the sedimentology and stratigraphy of the newly exposed section on highway Route 95. This work together with a compilation and reinterpretation of archived mineralogical data from the Plymouth Fe-Mn deposit will be used to aid in formulating a genetic model explaining the origin of the Woodstock Fe-Mn deposits.

REGIONAL GEOLOGY

The ferromanganese-rich units associated with the Woodstock deposits are hosted within the Late Ordovician to Early Silurian White Head Formation and the conformably overlying Silurian Smyrna Mills Formation (Fig. 1).The Fe-Mn mineralization was deposited during the Taconic Orogeny by precipitation of Fe, Mn, and Si within a shallow marine transgression-regression wedge (Roberts & Prince 1990; Force & Maynard 1991). Laminations in the BIFs are attributed to seasonal fluctuations of Fe, Mn, and Si

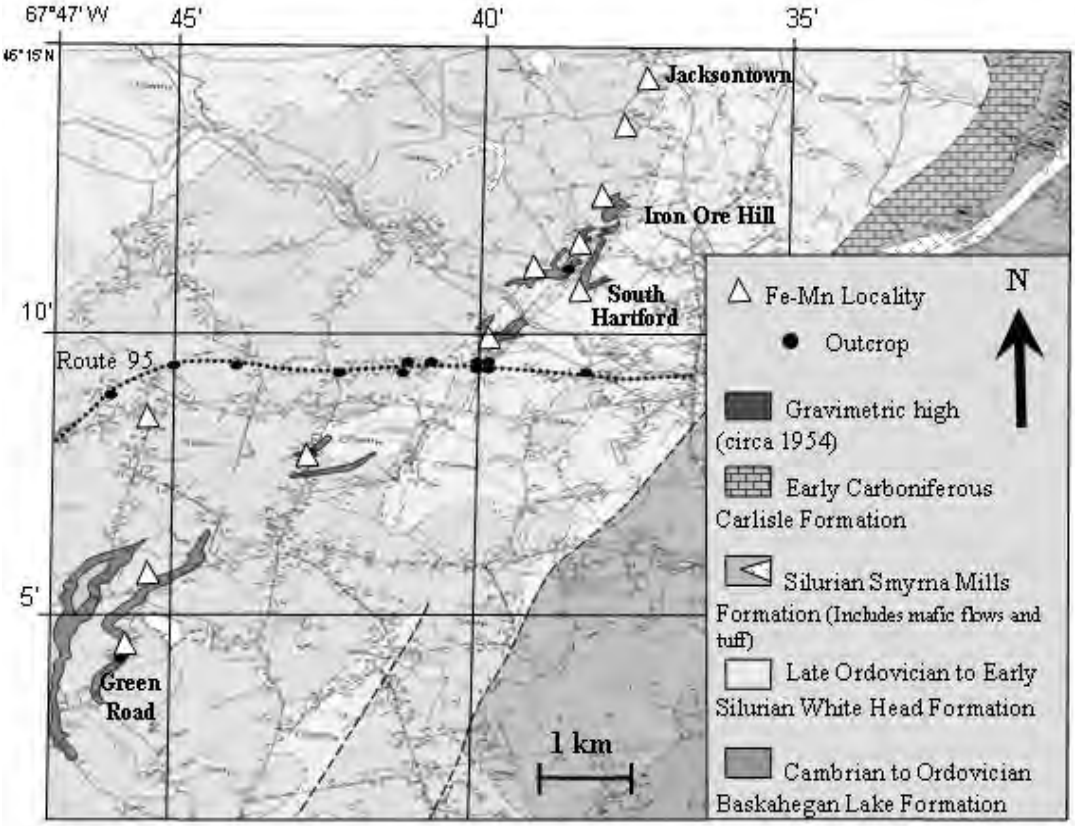

Fig. 1 Geologic map of the Woodstock area in western New Brunswick adapted from Smith and Fyffe (2006) displaying Fe-Mn deposits from Jacksontown to Green Road, NB.

within a shallow marine environment. The distribution of bedrock units is controlled by F1 and F2 folds that have northeast striking axial planes. The host sequence was metamorphosed to greenschist facies during the Acadian Orogeny (middle Devonian).

SEDIMENTOLOGY

The strata hosting the ferromanganese deposits were assigned by Roberts and Prince (1990) to the Late Ordovician–Early Silurian Cary Mills Formation and Silurian Smyrna Mills Formation in Maine and New Brunswick. However, in New Brunswick the sequence hosting the BIFs has been assigned to the Silurian Smyrna Mills Formation of the Perham Group and lies conformably on top of the Late Ordovician–Early Silurian White Head Formation associated with the Matapedia Group (Fig.1; Smith & Fyffe 2006).

The White Head Formation consists of dark grey to bluish fine-grained argillaceous limestone with interbedded calcareous shale. The Smyrna Mills Formation is composed of dark grey noncalcareous silty shale with minor layers of green and red mudstone, and associated ferromanganiferous siltstone (Smith & Fyffe 2006). The great variation in shale and/or siltstone in the Smyrna Mills Formation suggest that ocean redox conditions were highly variable during deposition of the host sequence. Manganiferous BIFs (i.e., Plymouth, Iron Ore Hill, South Hartford, Green Road) are commonly in sharp contact with units of red or green shale, or a combination of the two (Sidwell 1957). The lenticular shape and compositional variation in the Woodstock BIFs (Roberts & Prince 1990) indicates that these are stratigraphically separate Mn deposits.

The Fe-Mn zone within the Plymouth ore body was described as an assemblage of manganese oxide and manganese carbonate-silicate-oxide that formed within a shallow marine basin, an interpretation supported by the presence of asymmetrical ripple marks within the surrounding strata (Roberts & Prince 1990). Gross (1996) initially described the Plymouth Fe-Mn BIF as a series of sedimentary-volcanic ferromanganese units; however, alternative hypotheses suggest the Fe-Mn could possibly have originated from a variety of sources including oceanic Fe-Mn hydroxides and (or) the weathering of terrestrial bedrock.

GEOCHEMICAL COMPOSITION

Archived lithogeochemical data was obtained from four diamond drill holes (DDH) in the Plymouth Fe-Mn deposit. The Fe/Mn ratios from these cores were found to decrease sharply at the lower contacts between the Mn siltstone and surrounding strata. A strong inverse correlation between Al_2O_3 and Fe_2O_3 + MnO occurs within the manganiferous siltstone (Fig. 2).

Rare earth elements (REEs) displayed an average value of 140 ± 23 ppm for ∑REEs within the Mn-BIFs (Roberts & Prince 1990). REE data displayed a negative Eu anomaly within the Mn-BIF and the barren host rocks DDH 87-2 suggestive of no volcanic input associated with the Mn-BIFs (Fig. 3). Positive Eu anomalies commonly occur with Fe-Mn-bearing sediments associated with igneous systems (Mishra *et al*. 2007). If low ratios of Cerium and Lanthanum (i.e., Ce/La ratios of ≤ 0.12) occur in manganiferous BIF then the Fe and Mn are likely derived from ocean water. In Mn-BIFs the Ce/La ratio increases with an increase in carbonate, biogenic, and with increasing terrigenous Fe and Mn (Jiancheng *et al*. 2006). The high Ce/La ratios (2.5 ± 0.2) returned from in DDH 87-2 of at the Plymouth deposit suggests that the Fe and Mn may not be entirely sourced from marine Fe-Mn hydroxides.

CONCLUSIONS

The presence of Silurian mafic volcanic rocks in the Smyrna Mills Formation suggests the possibility that the Mn-BIFs might be sedimentary-volcanic in origin. However, the negative Eu anomalies associated with the host rocks suggest that there was no volcanic and (or) hydrothermal input associated with the formation of the manganiferous BIFs. High average Ce/La ratios of (2.5 ±0.2) associated within DDH 87-2 suggests the Fe and Mn within the Woodstock are not purely from oceanic Fe-Mn hydroxides. It is probable that the Fe and Mn are derived from multiple sources contributing to the overall composition of the deposit.

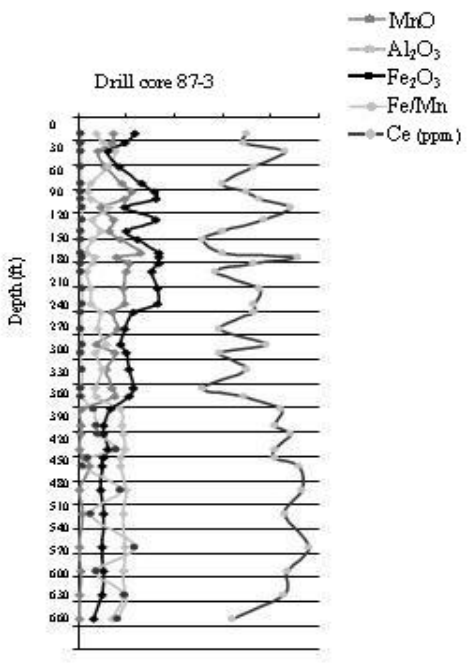

Fig. 2. Displaying the correlation between MnO, Fe_2O_3, Al_2O_3, Fe/Mn, and Ce contents within DDH 87-3

ACKNOWLEDGEMENTS

Funding is from the New Brunswick Department of Natural Resources-Minerals. Thanks also to Chris Roberts (GEODAT).

REFERENCES

FORCE, E.R. & MAYNARD, J.B. 1991. Manganese: Syngenetic Deposits on the Margins of Anoxic Basins. In: FORCE, E.R., EIDEL, J.J., & MAYNARD, J. B. (eds.), *Sedimentary and Diagenetic Mineral*

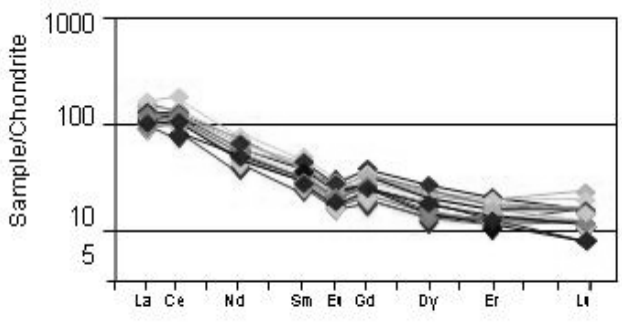

Fig. 3. Chondrite-normalized REE data from DDH-87-2 displaying depletions and anomalies of Ce. There is also a strong depletion in Eu within the drill core.

Deposits: A Basin Analysis Approach to Exploration, Society of Economic Geologists, Reviews in Economic Geology, **5**, 147-157.

GROSS, G.A. 1996. Stratiform iron. In: ECKSTRAND, O.R., SINCLAIR, W.D., & THORPE, R.I. (eds.), *Geology of Canadian Mineral Deposit Types*. Geological Survey of Canada, **8**, 41-54.

JIANCHENG, X., YANG, X., JIANGUO, D., & WEI, X. 2006. Geochemical Characteristics of Sedimentary Manganese Deposit of Guichi, Anhui Province, China. *Journal of Rare Earths*, **24**, 374-380.

MISHIRA, P.P., MOHAPATRA, B.K., & SINGH, P.P. 2007. Contrasting REE Signatures on Manganese Ores of Iron Ore Group in North Orissa, India. *Journal of Rare Earths*, **25**, 749-758.

ROBERTS, C.G. & PRINCE, J.D. 1990. Further Characterization of Plymouth Mn Deposit, New Brunswick. Department of Natural Resources and Energy Division, *Open File Report* **90-4**.

SIDWELL, K.O.J. 1957. The Woodstock, N.B., Iron – Manganese Deposits. Transactions: *Canadian Institute of Mining & Metallurgy*, **50**, 411-416.

SMITH, E.A. & FYFFE L. R. (Compilers) 2006. Bedrock Geology of the Woodstock Area (NTS 21J/04) Carleton county, New Brunswick, New Brunswick *Department of Natural Resources, Minerals, Policy and Planning Division, Plate* **2006-5**.

Lithogeochemistry of the Meguma Supergroup, Nova Scotia, Canada: petrographic constraints, depositional environments and alteration haloes about sediment hosted hydrothermal mineral deposits

Chris E. White[1] & Clifford R. Stanley[2]

[1]*Mineral Resources Branch, Dept. of Natural Resources, 1701 Hollis Street, Halifax, NS, B3J 3M8 CANADA (email: whitece@gov.ns.ca)*

[2]*Dept. of Earth & Environmental Science, Acadia University, Wolfville, NS, B4P 2R6 CANADA*

ABSTRACT: A lithogeochemical evaluation of Meguma Supergroup metasedimentary rocks from Nova Scotia has: (*i*) identified mineral suites that control the various rock compositions, (*ii*) provided clues about the paleo-environmental seafloor and basin conditions during sedimentation, (*iii*) detected previously unknown alteration zones, and (*iv*) established element concentration backgrounds. Variations in the amounts of quartz, albite, illite, smectite, chlorite and kaolinite control the sedimentary rock compositions and allow identification of cryptic stratigraphic boundaries that assist in establishing stratigraphic level within the basin. In addition, Mn, Fe, and P concentration patterns indicate that the basin became progressively more reducing with time, allowing identification of strata that could host sediment-hosted massive sulfide mineralization. Finally, alteration halos about saddle reef gold deposits and primary dispersion haloes in sedimentary rocks adjacent to Sn greisen deposits can be readily identified, providing useful exploration criteria.

KEYWORDS: *Meguma Supergroup, lithogeochemistry, stratigraphy, alteration haloes, sedimentary environment.*

INTRODUCTION

Stratigraphic correlation in flysch sequences is difficult because these thick, monotonous piles of proximal and distal turbidites contain a range of interbedded sedimentary rocks. As a result, locating prospective strata hosting mineral deposits and identifying hydrothermally altered rocks within these sequences represents a significant challenge.

Nevertheless, thorough evaluation of lithogeochemical data collected from such flysch successions, when coupled with careful mapping and correlation, can provide valuable information that benefits mineral exploration programs.

STRATIGRAPHY

The Late Neoproterozoic/Cambrian Meguma Supergroup of Nova Scotia is a flysch sequence that contains the metasandstone-dominated Goldenville Group and the overlying slate-dominated Halifax Group (White 2008a). Mapping indicates that three spatially distinct stratigraphic sequences exist in the supergroup: the Eastern, South, and French Shore stratigraphies (Fig. 1).

The South Shore Meguma stratigraphy is best known (White 2008b). The basal Goldenville Group comprises, from bottom to top: (*i*) the Moses Lake Formation, an 800 m thick package of grey metawacke, green metasiltstone, and carbonaceous pyritic and magnetitic slate; (*ii*) the Green Harbour Formation, a 4,830 m thick, thick-bedded metawacke; (*iii*) the Government Point Formation, a 1750 m thick, thin-bedded metawacke, green metasiltstone, and multicoloured slate; and (*iv*) the Moshers Island Formation, a 300 m thick sequence of green and grey, laminated Mn-rich slate and metasiltstone with minor interbedded metawacke. The overlying Halifax Group comprises: (*v*) the Cunard Formation, a 2250 m thick grey to black slate containing pyrite, pyrrhotite, and arsenopyrite beds; overlain by (*vi*) the Feltzen Formation, a 2000 m thick grey slate and metasiltstone.

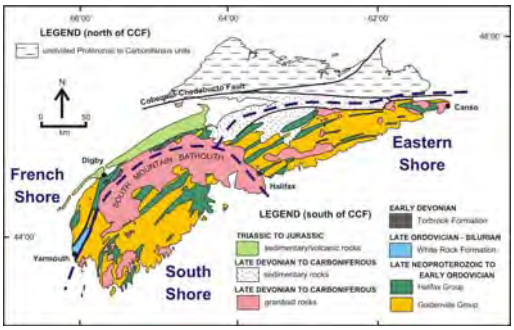

Fig. 1. Map of Nova Scotia illustrating the location of the Meguma Supergroup.

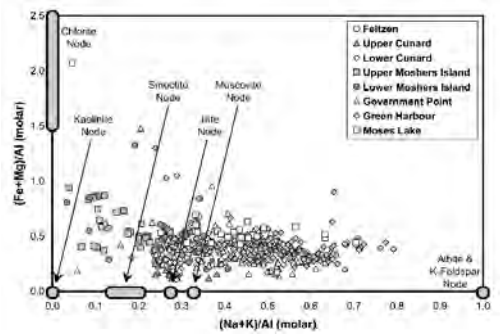

Fig. 2. Whole-rock compositions plotted on an (Na+K)/Al versus (Fe+Mg)/Al MER diagram.

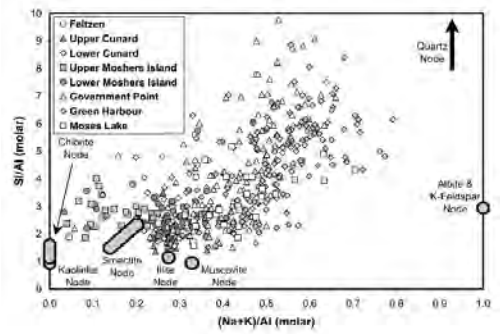

Fig. 3. Whole rock compositions plotted on an (Na+K)/Al versus Si/Al MER diagram.

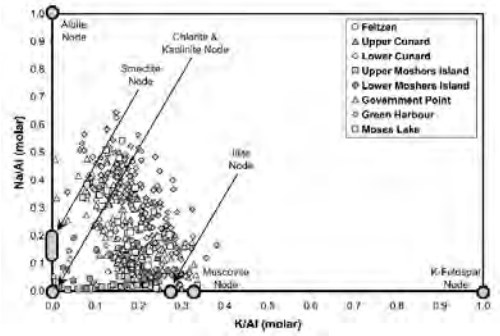

Fig. 4. Whole-rock compositions plotted on a K/Al versus Na/Al MER diagram.

LITHOGEOCHEMISTRY

A 499 sample major oxide- and trace-element lithogeochemical database was assembled from fourteen different sources to further investigate the South Shore Meguma Supergroup stratigraphy. These relatively un-weathered samples represent all formations within the Halifax (*n* = 71) and Goldenville groups (*n* = 428). After pulverization, major oxides and some trace elements were analyzed by fusion-XRF or ICP-OES, whereas other trace elements were analyzed by four acid or aqua regia digestions, with AAS or ICP-MS finish, at the St. Mary's University Regional Geochemical Laboratory, Halifax, N.S. or at ACME Analytical Laboratories Ltd., Vancouver, B.C.

A molar element ratio (MER) analysis was undertaken to gain insight into the diversity and compositional controls on these rocks, and to identify stratigraphy hosting alteration zones and potential mineral deposits.

SEDIMENT COMPOSITIONS

Three MER diagrams (Figs. 2, 3, & 4) collectively illustrate the mineralogical controls observed in each of the Meguma Supergroup formations. Because these metamorphosed rocks derive from proximal and distal flysch sediments, they likely once contained: quartz, K-feldspar, albite, muscovite, illite, smectite (montmorillonite-beidellite), chlorite (clinochlore/chamosite), Al-chlorite (sheridanite/daphnite), and (or) kaolinite. These minerals (Table 1) could be used to interpret the geochemical results on these diagrams because metamorphism rarely affects major oxides (with the exception of volatiles: H_2O, CO_2, & S_2), ensuring that the original precursor (pre-metamorphic) mineralogical controls are preserved.

Overall, Meguma Supergroup slate samples are relatively homogeneous, whereas metawackes tend to exhibit more compositional variation, probably because of their fining-upward textures.

In the Halifax Group, the Cunard

Formation has compositionally distinct upper and lower members. Both can be explained by illite-smectite mixtures, but Lower Cunard slates also contain quartz. Like the Lower Cunard rocks, the Feltzen Formation has compositions explained by mixtures of illite, smectite and quartz.

In the Goldenville Group, the Moshers Island Formation also has two compositional members: an upper one explained by mixtures of chlorite, kaolinite illite, and smectite, and a lower one explained by only illite and smectite.

In contrast, metawackes in the Government Point, Green Harbour, and Moses Lake formations (Goldenville Group) have compositions explained by mixtures of illite, albite, and quartz, but each of the these formations differ slightly in terms of the amounts of quartz and feldspar they contain, relative to illite. In addition, the Moses Lake Formation contains significant amounts of chlorite.

DEPOSITIONAL ENVIRONMENTS

Stratigraphy-MER scatterplots illustrate that background Mn/Ti and Fe/Ti ratios (Figs. 5 & 6) are elevated throughout the Moshers Island Formation. Very anomalous Mn/Ti ratios also occur sporadically in this formation, and the upper part of the Government Point Formation. These anomalies are associated with pink or black spessartine-bearing coticules possibly related to hydrothermal brine expulsion onto the seafloor that might be associated with sediment-hosted massive sulfide (SHMS) mineralization. In contrast, the elevated background Mn/Ti and Fe/Ti ratios are likely products of redox cycling associated with a change from suboxic pore water chemistry during deposition of the Moses Lake, Green Harbour, and Government Point metawackes, to anoxic pore water

Table 1. Ideal clay mineral formulae controlling Meguma Supergroup rock compositions.

Chlorite	$(Fe,Mg)_{10}Al_4Si_6O_{20}(OH)_{16}$
Al-Chlorite	$(Fe,Mg)_9Al_6Si_5O_{20}(OH)_{16}$
Montmorillonite	$Na_{2/3}(Fe,Mg)_{2/3}Al_{10/3}Si_8O_{20}(OH)_4$
Beidellite	$Na_{2/3}Al_{14/3}Si_{22/3}O_{20}(OH)_4$
Illite	$K_{3/2}Al_{11/2}Si_{13/2}O_{20}(OH)_4$
Kaolinite	$Al_2Si_2O_5(OH)_4$

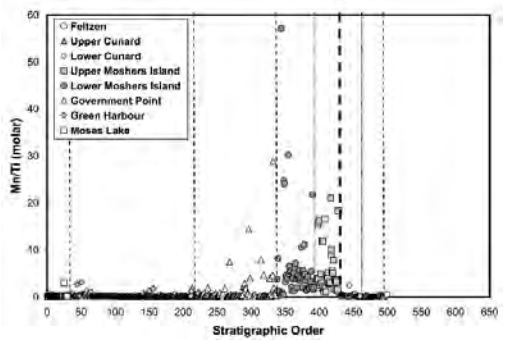

Fig. 5. Molar Mn/Ti ratios plotted versus stratigraphic order.

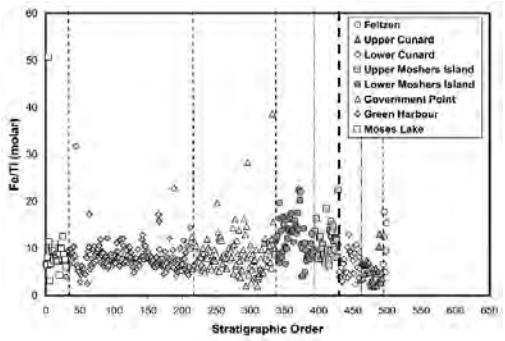

Fig. 6. Molar Fe/Ti ratios plotted versus stratigraphic order.

chemistry during deposition of the Moshers Island slates.

Subtlely low Fe/Ti (Fig. 6) and P/Ti (not pictured) MER's in the overlying Cunard Formation are thus likely a result of the absence of pelagic sedimentation of Fe-oxy-hydroxides, with adsorbed seawater phosphate, as redox conditions became even more anoxic (low enough to reduce Fe^{+3} to Fe^{+2}). Thus, evidence for a significant drop in the redox state of pore waters exists in the lower part of the Halifax Group and the upper part of the Goldenville Group, indicating that these sedimentary rocks are likely prospective for SHMS mineralization that may be responsible for the high Pb concentrations (> 700 ppm) observed in the Moshers Island Formation (Fig. 7).

HYDROTHERMAL ALTERATION

Stratigraphy-element concentration scatterplots illustrate that anomalous Zn (Fig. 8), Cu, and Rb (not pictured) exist in the lower part of the Green Harbour

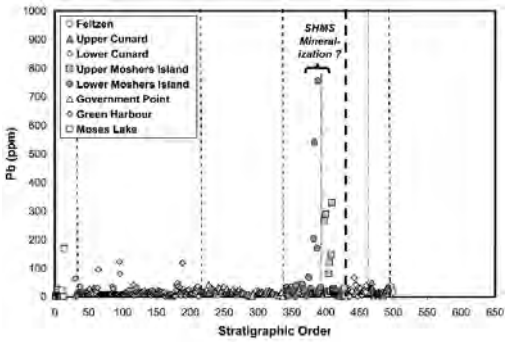

Fig. 7. Pb concentrations (ppm) plotted versus stratigraphic order.

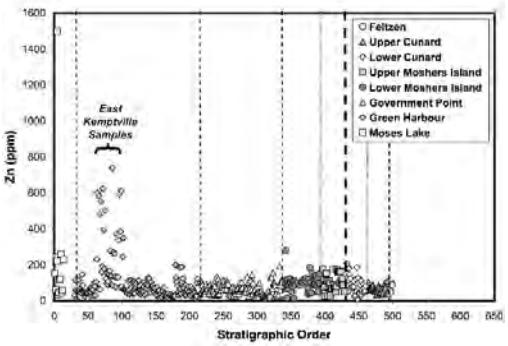

Fig. 8. Zn concentrations (ppm) plotted versus stratigraphic order.

Formation, proximal to the East Kemptville Sn greisen deposit. Given that this deposit contains accessory sphalerite and chalcopyrite, and has significant amounts of muscovite gangue, these anomalous concentrations, observed in rocks that are not visibly altered, likely comprise the geochemical expression of a cryptic primary dispersion halo about the deposit.

The stratigraphy-MER scatterplot of Figure 9 illustrates that a bimodal distribution of (Na+K)/Ti ratios (two circles) exist in metawackes that are not visibly altered near the North Brookfield saddle reef gold deposit. These low (Na+K)/Al ratios are likely the result of hydrothermal alteration of feldspar to muscovite by hydrothermal fluids associated with auriferous quartz vein precipitation via reaction involving a net Na+K loss:

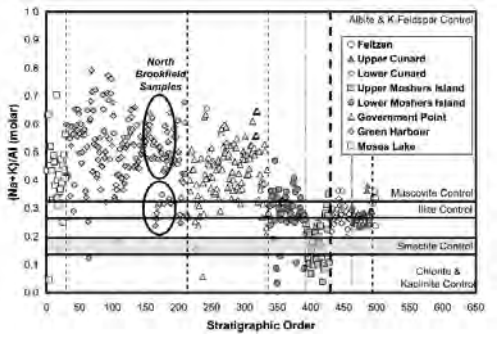

Fig. 9. Molar (Na+K)/Al ratios plotted versus stratigraphic order.

$$3\ NaAlSi_3O_8 + K^+ + 2\ H^+$$
$$\Leftrightarrow$$
$$KAl_3Si_3O_{10}(OH)_2 + 6\ SiO_2 + 3\ Na^+.$$

CONCLUSIONS

Major oxide- and trace-element geochemistry of sedimentary rocks can provide significant information critical to exploration for sediment hosted mineral deposits. Lithogeochemical evaluation of the Meguma Supergroup has facilitated stratigraphic correlation, contributed to an understanding of the marine environment of deposition, and detected the presence of hydrothermal alteration zones associated with sediment hosted massive sulfide mineralization, saddle reef Au, and greisen Sn deposits.

REFERENCES

WHITE, C.E. 2008a. Defining the stratigraphy of the Meguma Supergroup in southern Nova Scotia: where do we go from here? In: *Atlantic Geoscience Society 34th Colloquium and Annual Meeting, Program and Abstracts, February 1-2, 2008, Dartmouth, Nova Scotia*, 58 p.

WHITE, C.E. 2008b. Preliminary bedrock geology of the New Germany map sheet (NTS 21A/10), southern Nova Scotia. In: D.R. MACDONALD (ed.), *Mineral Resources Branch, Report of Activities 2007. Nova Scotia Department of Natural Resources, Report ME* **2008-1**, 113-124.

Sponsors

Symposium bags sponsor

ACME Analytical Laboratories Ltd.

Platinum sponsors

SGS

Anglo American

Gold sponsors

AREVA

Newmont – The Gold Company

Barrick

TGI3 Canada

Geological Survey Commission Canada

Silver Standard

maxwell DATASHED

Actlabs

FREEWEST – Freewest Resources Canada Inc.

Silver sponsors

ODM – Exploring Heavy Minerals

Thermo Scientific

Innov-X Systems – Innovative XRF Technologies

APEGNB / AIGNB

OZ

xstrata zinc

Adex

Bronze sponsors

PotashCorp – Helping Nature Provide

International Association of Geochemistry – IAGC – Est. 1962

New Nouveau Brunswick – Natural Resources and Energy / Ressources naturelles et Énergie

Department of Geology – University of New Brunswick

IAG